Microchim Acta (2014) 181:263–294
DOI 10.1007/s00604-013-1139-8

REVIEW ARTICLE

Upconversion nanophosphors for use in bioimaging, therapy, drug delivery and bioassays

Yuming Yang

Received: 15 August 2013 / Accepted: 30 November 2013 / Published online: 19 December 2013

Abstract Upconversion nanoparticles (UCNPs) represent a new class of fluorophores. Both the excitation and (anti-Stokes) emission wavelengths are in the long wave part of the spectrum so that their luminescence can deeply penetrate tissues and cause low photodamage in biological samples. Their large anti-Stokes shifts, sharp emission bands, zero auto-fluorescence from biological samples and high photostability renders them an ideal kind of fluorescent labels for a variety of analytical formats, for bioimaging in cancer therapy. This review covers the basic mechanisms of upconversion luminescence, the methods for the synthesis and surface modification of biocompatible UCNPs, and aspects of the in vivo delivery of UCNPs. More specifically, we discuss (a) recent progress regarding UCNPs for multimodal targeted tumor imaging, (b) UCNP-based methods of biological detection and sensing, (c) the use of UCNPs in drug delivery, (d) applications in photodynamic therapy, photothermal therapy and radiotherapy. Finally, we are addressing challenges and opportunities of this quickly emerging field. Contains 362 references.

Keywords Upconversion · Nanoparticle · Cancer therapy · Imaging · Drug delivery · Detection

Introduction

The field of nanoscience has witnessed a rapid growth in the last decade. Recently, the attention of the nanoscientists has been focusing more and more on biological applications. The development of upconversion nanophosphors over the past decade has facilitated the translation of fluorescence imaging from the microscopic to macroscopic imaging. Although the uses of other conventional fluorescent materials, including organic dyes, fluorescent proteins, metal complexes, or semiconductor quantum dot as based biomarker have achieved significant progress in real-time detection and bioimaging, they still have some drawbacks. These fluorescent materials are generally excited by ultraviolet (UV) or visible light, which may induce autofluorescence from the biological tissues, DNA damage and cell death to biological samples, resulting in low signal-to-noise ratio and limited sensitivity. In addition, the broad emission spectra of these fluorescent materials make them unsuitable for multiplex biolabeling and often suffer from low photostability when exposure to external illumination. Quantum dots (QDs) that feature a large molar extinction coefficient, high quantum yield, narrow emission bandwidth, large Stokes' shift, size-dependent tunable emission and high photostability are attractive as alternative luminescent labels for imaging [1–5]. However, the potential toxicity of QDs limit their biological applications [6].

In contrast, UCNPs have many good characteristics. The main difference between UCNPs and other luminescent imaging materials is that they can emit visible or near infrared (NIR) light under NIR irradiation. The NIR irradiation leads to absence of photo-damage to living organisms, very low autofluorescence, high detection sensitivity, and high light penetration depth in biological tissues [7, 8]. In addition, these UCNPs show a sharp emission bandwidth, high photostability, tunable emission, long lifetime, and low cytotoxicity. All these benefits make the UCNPs can be used as probes for intravital imaging which enables the investigation of physiological processes within the context of a living organism, and provides a more complete picture of disease pathology and development.

To date, much effort has been put into the design of novel upconversion nanophosphors. Surface functionalized and

Y. Yang (✉)
Regenerative Medicine and Cell Biology, Medical University of South Carolina, 68 President St., Charleston, SC 29425, USA
e-mail: ymyang1981@163.com

multifunctional UCNPs have been synthesized. Great advances on the improvement of probe targeting, pharmacokinetics, biocompatibility, photophysics, and the maturation of multimodal techniques are also made. However, multiple factors must be considered to predict how specific nanoparticles will react with living biological tissues in bioimaging process. This review presents some of the basic concepts and summarizes recent progress on the upconversion nanophosphors for bioimaging and cancer therapy. In particular, the toxicity of UCNPs toward biological cells and organisms are also discussed which supplied a specific and rational approach to design suitable UCNPs for biological applications.

Upconversion nanophosphors for bioimaging

Types of UCNPs

Over the past decade, a large number of scientists have investigated the potential applications of UCNPs in bioimaging. Lim et al. firstly reported the use of UCNPs as in vivo Caenorhabditis elegans imaging agent [9]. Along with the fast development of UCNPs for biological applications, UCNPs have also been applied as contrasts agents in positron emission tomography (PET), magnetic resonance imaging (MRI), and X-ray computer tomography (CT) for in vitro and in vivo multimodal imaging [10–12]. Furthermore, UCNPs could also be combined with anti-cancer drugs [13], photosensitizers [14, 15] or gold nanostructures [16] for potential therapeutic applications.

Up to now, a variety of upconversion nanophosphors have been developed for bioimaging, and most of them are based on rare earth (RE) doped $NaYF_4$ [17]. Other kinds of RE doped nanoparticles, such as $NaGdF_4$, $NaLaF_4$, Y_2O_3, LaF_3, GdF_3, CeO_2, $LiNaF_4$, $Ca_3(PO_4)_2$,ZrO_2 and GdOF etc. have also been considered as excellent UCNPs in recent years due to their strong upconversion luminescence intensity and good photostability. Fully understand the principles and constructions of upconversion nanophosphors is a marvelous way to develop excellent upconversion nanophosphors for bioimaging.

Principles of RE based up-conversion luminescence (UCL)

Upconversion refers to non-linear optical processes that convert two or more low-energy pump photons to a higher-energy output photon. The upconversion process is basically based on three UCL mechanisms: excited state absorption (**ESA**), photon avalanche (**PA**), and energy transfer upconversion (**ETU**). **ESA** involves multistep excitation by sequentially absorbing one or more photons from the ground state to intermediate reservoir stage, and finally populates at excited state to form the upconversion luminescence, which is illustrated in Fig. 1a for the Er^{3+} ion. The **PA** process basically involves resonant excited-state absorption, efficient cross relaxation and substantial population of the reservoir level, finally leads to strong upconversion emission. It is an unconventional pumping mechanism because it may lead to strong upconverted emission from level $^1D_2$ without any resonant ground state absorption (Fig. 1c). In the process of **ETU**, there is resonant non-radiative energy transfer or phonon-assisted non-radiative

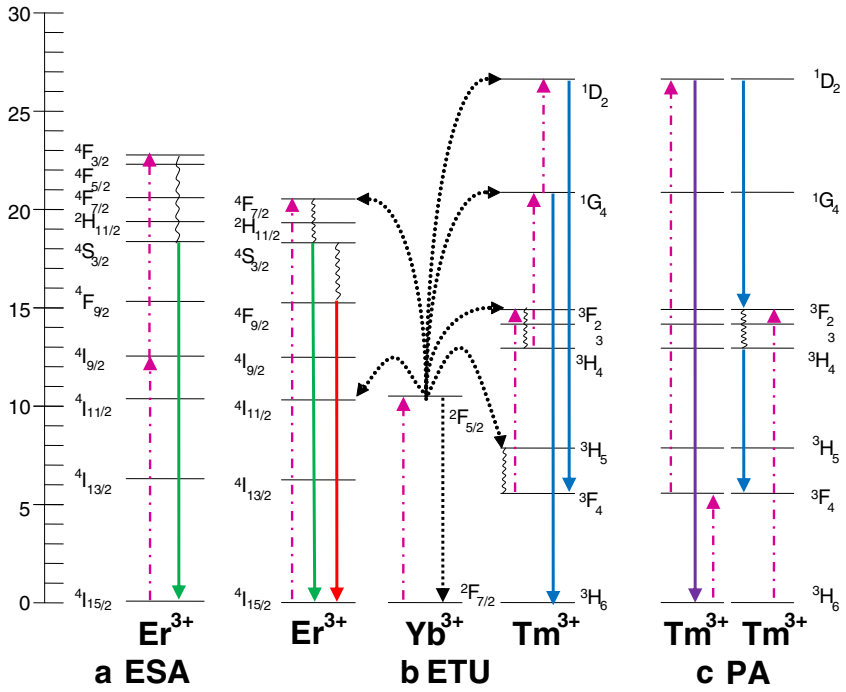

Fig. 1 Schematic illustrations of various upconversion processes: **a** excited state absorption (ESA); **b** energy transfer upconversion (ETU); **c** photon avalanche (PA)

energy transfer from sensitizer to activator. As shown in Fig. 1b, the green emission at 550 nm is generated as a result of two successive resonant energy transfers from Yb^{3+} to Er^{3+} ions, followed by non-radiative decay to the green-emitting level of $^4S_{3/2}$. In the Yb^{3+}, Tm^{3+} codoped system, the blue emission from the $^1G_4$ level is accompanied by red emission, which arises from an intermediate transition terminating at the $^3F_4$ level. The **ETU** is by far the most efficient upconversion process and is suitable for the RE doped nanophosphors.

Optical and composition characteristics of RE based upconversion nanophosphors

An inorganic UCNP consists of an inorganic host and dopant (activator). The dopant acts as luminescent centers, and the host provides a matrix to bring these centers into optimal position. One of the most substantial ways in which the upconversion nanophosphors differ from ordinary Stokes-type photoluminescent phosphors is that upconversion nanophosphors tends to be more sensitive to vibronic coupling between host and activator ion.

A large number of suitable hosts doped with actinide [18, 19] and transition metal ions have been reported to show up conversion luminescence, such as Cm^{3+}, U^{3+}, Mo^{3+}, Os^{4+}, Ni^{2+}, Ti^{2+} and Re^{4+} [20]. But mainly in the RE elements due to its special $4f^n5d^{0\text{-}1}$ inner shell configurations that are well-shielded by outer shells and have abundant and unique energy level structures. Er^{3+}, Tm^{3+} and Ho^{3+} are currently the most common activators in upconversion phosphors. Yb^{3+} is usually codoped in the inorganic host as a sensitizer due to the larger absorption cross section of Yb^{3+} in the NIR spectral region to improve UCL efficiency. In the case of Yb^{3+}, Er^{3+} codoped system, the energy interval of the ground state $^2F_{7/2}$ and the $^2F_{5/2}$ excited state of Yb^{3+} matches well with the transition energy between the $^4I_{11/2}$ and $^4I_{15/2}$ states and also the $^4F_{7/2}$ and $^4I_{11/2}$ states of Er^{3+}, thus allowing for efficient resonant energy transfer from Yb^{3+} to Er^{3+} ions. Yb^{3+} is not only a common sensitizer for Er^{3+} systems but also for Tm^{3+}, Ho^{3+} and Pr^{3+} ions. In order to minimize the cross-relaxation energy loss, the content of activators is usually less than 2 mol%.

It is also very critical to choose an appropriate host material, which plays vital roles in the upconversion luminescent process. The choice of the host lattice determines the distance between the dopant ions, the coordination numbers, the relative spatial position, and the type of anions around the dopant, resulting in different optical properties of the UCNPs [21–24]. Desirable host materials should have adequate transparency within a certain wavelength range, low phonon energy and high optical damage threshold. In addition, lattice impurities may increase the multiphonon relaxation rates between the metastable states, thereby reducing the overall visible emission intensity. Up to now, various host materials have been studied, including fluoride, oxide, chloride, bromide, iodide, oxysulfide, phosphate and vanadate etc. The hexagonal phase $NaYF_4$ crystal in bulky state has been reported to be the most efficient matrix for upconversion nanophosphors [25, 26]. Other kinds of fluorides and alkali fluorides, such as $NaGdF_4$, $NaLaF_4$, LaF_3, GdF_3, CeO_2, $LiNaF_4$, $Ca_3(PO_4)_2$,ZrO_2 and GdOF etc. have also been considered as excellent host materials in recent years due to their high refractive index and high transparency arising from low-energy phonons [27–30]. As low lattice phonon energy could minimize non-radiative losses and increase the luminescence quantum yield. While most of chlorides, bromides and iodides are sensitive to moisture, and thus are not suitable for bioimaging.

Triplet-triplet annihilation (TTA) based upconversion nanophosphors

TTA-based UCL mechanism involves the transfer of energy between a sensitizer molecule and an annihilator. Compared with rare-earth doped UCNPs, TTA based upconversion nanophosphors exhibit high quantum yield,tunable excitation and emission wavelengths by reasonable selection of the sensitizer and the acceptor. To date, a series of TTA-based upconversion systems have been successfully developed. However, most of the reported TTA-based upconversion nanophosphors are operated in organic solution, which is not suitable for the applications for bioimaging [31–35]. In order to conquer this problem, SiO_2 based and polymer enclosing strategies have been developed for the synthesis of water soluble TTA-based upconversion nanophosphors [36, 37]. For example, Li's group reported the water-soluble TTA-based UCNPs by coloading sensitizer (octaethylporphyrin Pd complex) and annihilator (9,10-diphenylanthracene) into silica nanoparticles. The TTA-based```` UCNPs show as high as 4.5 % quantum yield, low cytotoxicity and were successfully used to label living cells and for lymph node in vivo imaging with very high signal-to-noise ratio [38]. In particular, Li's group also reported a general strategy for constructing high-effective TTA-based upconversion nanocapsules by loading both sensitizer and annihilator into BSA−dextran stabilized oil droplets. Pt(II)-tetraphenyl-tetrabenzoporphyrin and BODIPY dyes (BDP-G and BDP-Y) are chosen as sensitizer/annihilator couples to fabricate green and yellow upconversion luminescent nanocapsules respectively [39]. These two kinds of TTA-based upconversion nanocapsules exhibit much stronger luminescence intensity than that of the previous SiO_2 based TTA-based UCNPs due to the aggregation-induced fluorescence quenching of annihilators. Although so much good characteristics that the TTA-based upconversion nanophosphors possess, their biological applications are still at its infancy stage. This review will focus on the progress of RE based UCNPs for bioimaging, and all the other parts of this paper are refer to the RE based UCNPs.

Properties of UCNPs for bioimaging

Firstly, compared to conventional luminescent materials, UCNPs have relatively longer lifetime. This feature makes the time-resolved luminescence detection [40, 41] feasible to minimize the interference of the undesired short lived back ground fluorescence which originates from biological tissues or other dopants under multiple-photon excitation. This property also greatly improved the signal-to-noise ratio and the detection sensitivity, which makes the UCNPs more feasible for the bioimaging applications. Most recently, Zvyagin and coworkers reported on single UCNP imaging through a layer of hemolyzed blood, and predicted that a single 70 nm UCNP would be detectable at skin depths up to 400 mm [42].

Moreover, several groups have reported that UCNPs exhibit high photostability and no optical blinking [43–45] The UCL intensity is not weakened even under a few hours continuous irradiation of UV or NIR laser. As the UCL originates from the intra-4f electron transitions of the lanthanide ions, which doesn't contain the breaking of chemical bonds.

Secondly, the lanthanide doped UCNPs show a distinct set of sharp emission bands with 10-20 nm full width at half maximum under a certain wavelength of 980 nm light excitation. This characteristic provides distinguishable spectroscopic fingerprints for accurate interpretation of the emission spectra in the environment of overlapping emission spectra. The emission colors are decided by the kind of codoped lanthanide ions. The relative emission intensities are controlled by changing the kinds of the host, the dopant concentration or morphology of the nanoparticles.

Thirdly, the near-infrared light excitation provides deep penetration and low tissue damage for in vivo imaging. Recently more and more NIR-to-visible and NIR-to-NIR UCNPs were developed, as the wavelength of 650-1,000 nm light provides higher biological tissues penetration depth.

Finally, in contrast to the conventional anti-Stokes probes such as the two phonon absorption or second harmonic generation, upconversion nanophosphors exhibit higher emission efficiency and can be excited by continuous wave laser rather than the costly femtosecond pulsed laser.Although so much good characteristics that UCNPs possess, the relatively lower quantum yield is still a defect for the UCNPs. The quantum yields of the most UCNPs is usually a little more than 0.005 % but no more than 0.3 %, which is far less than that of 5~85 % of the QDs. Up to now, a great deal of efforts are being focused on it by changing the UCNPs lattice or modifying the surface of the UCNPs [46].

Synthesis and surface functionalization of biocompatible UCNPs

Synthesis of UCNPs

For UCNPs used for bioimaging, it is very important to make biocompatible UCNPs, which have strong emission intensity, uniform size, homogeneous shape, good water solubility, and functional ligands for further bioconjugation. Up to now, different methods have been developed to get upconversion nanophosphors with desirable characteristics for bioimaging, such as sol–gel, hydrothermal, co-precipitation, and thermal decomposition methods etc. Hydrophilic molecules such as polyvinylpyrrolidone (PVP), polyacrylic acid (PAA), polyethylenimine (PEI), aminohexanoic acid (AA) and polyol are used as ligands to control particles growth, and also act as functional groups for bioconjugation.

Sol–gel method

The sol–gel process could be described as the formation of an oxide network through polycondensation reactions of a molecular precursor in a liquid. In the first stage of sol–gel method, all raw materials should be mixed and dispersed in a solvent, which enables mixing at an atomic level and get homogeneous products. In order to get luminescent materials with strong luminescence intensity, a high temperature calcination process is usually needed to improve the crystallinity. Based on this method, a series of UCNPs have been developed, such as ZrO_2:Er^{3+}, $BaTiO_3$:Er^{3+} [23, 47], ZnO:Er^{3+} [48], $Lu_3Gd_5O_{12}$:Er^{3+} [49, 50], $NaYF_4$:Er^{3+}/Yb^{3+}, $NaNbO_3$:Tm^{3+}/Er^{3+}/Yb^{3+} [51], Gd_2O_3:Er^{3+}/Tm^{3+}/Yb^{3+} [52], Y_2O_3: Ho^{3+}/Yb^{3+}[53] and $SrMoO_4$:Yb^{3+}/Tm^{3+}/Ho^{3+} [54] etc. upconversion nanophosphors. However, the particles synthesized by the sol–gel method are not suitable for biological applications. As the particle aggregation may occur when dispersed in aqueous solutions and also in the high temperature calcination procedure.

Co-precipitation method

The co-precipitation method is carrying on by a precipitate of substances normally soluble under the conditions employed. Co-precipitation is one of the successful methods for synthesizing ultrafine nanoparticles with narrow particle size distribution. Van Veggel is one of the pioneers who developed Er^{3+}, Nd^{3+}, and Ho^{3+} doped LaF_3 nanoparticles using the co-precipitation method. Ammonium di-*n*-octadecyldithiophosphate was used as the ligand to control particle growth and to stabilize the particles against aggregation [55]. Chow's group further developed Yb–Er, Yb–Ho and Yb–Tm co-doped LaF_3 UCNPs using the same method [56]. In most cases, a heat treatment procedure is needed to increase the

luminescence intensity. For example, lanthanide doped $NaYF_4$, $LuPO_4$ and $YbPO_4$ UCNPs were synthesized by Haase group using the co-precipitation method coupling with a heat treatment process [57, 58]. Spherical $NaYF_4$:Yb,Er particles with narrow size distribution were also prepared by Yi et al. in the presence of ethylenediaminetetraacetic acid (EDTA). Particles with controllable size in the range of 37 to 166 nm diameter were obtained by adjusting the molar ratio of EDTA to total lanthanides [59]. In addition to the EDTA acting as chelating agent to control the size of nanoparticles, PVP is also chosen as a good kind of chelating agent to improve the solubility and surface functionality of the nanoparticles. Zhang et al. developed $NaYF_4$ nanocrystals coated with monodisperse silica using PVP as the chelating agent. The PVP stabilized $NaYF_4$ nanocrystals could be directly coated with a uniform layer of silica to produce a surface for further conjugation of biomolecules.

Thermal decomposition method

Thermal decomposition, also called thermolysis, is defined as a chemical reaction whereby the precursors are dissolved and heated in high boiling point solvents. The precursors decompose to form nucleates when temperature goes up, following with the growth of the nucleates into the target nanoparticles. This method was firstly developed by Yan's group to synthesize single crystalline monodisperse LaF_3 nanocrystals via the thermal decomposition of lanthanum trifluoroacetate ($La(CF_3COO)_3$) precursor in the presence of oleic acid (OA) and octadecene (ODE) [60]. Uniform LaF_3 nanocrystals with good crystallinity could be obtained by controllable release of the fluoride anions into the solution. The OA molecules act not only as a solvent but also as surfactants that prevent the nanocrystals from agglomeration. Yan's group further extended this method to the synthesis of other high quality sodium rare-earth fluoride nanocrystals, such as $NaYF_4$:Yb,Tm [61], $NaREF_4$ (RE: Pr to Lu,Y) [62] (Fig. 2), $NaYF_4$:Yb,Er core (α- and β-$NaYF_4$:Yb,Er) and core/shell (α-$NaYF_4$:Yb,Er@α-$NaYF_4$ and β-NaYF4:Yb,Er@α-$NaYF_4$) [63] nanocrystals with controllable size and morphology. The ratio of the Na/RE, composition of the solvents, reaction temperature and time played important roles in controlling the morphology and the phase of the nanoparticles. There are also many other groups further used and developed this method to synthesize a series of high quality nanoparticles. For example, Li's group successfully synthesized sub-10 nm β-$NaLuF_4$:24 mol% Gd^{3+}, 20 mol% Yb^{3+}, 1 mol% Tm^{3+} nanocrystals, which display bright UCL with a quantum yield of 0.47±0.06 % under continuous-wave excitation at 980 nm [64]. In particular, Capobianco group reported the synthesis of $NaYF_4$:Yb,Er and $NaYF_4$:Yb, Tm using the thermolysis method [65]. They further made a modification to this method by introducing the lanthanide precursors slowly into the high-temperature reaction mixture through a stainless steel canula. Nanoparticles with a regular shape and a monodisperse particle size distribution were obtained by this modified method [66]. In recent years, Capobianco and co-workers have also extended this method to the synthesis other kinds of UCNPs, such as $NaGdF_4$:Ho,Yb [67], $NaGdF_4$:Yb, Er and $BaYF_5$:Yb,Tm [68, 69]. Now, the thermal decomposition method has come to be a common route to synthesize high quality upconversion monodisperse nanoparticles, and a great deal of excellent research results were subsequently reported [70–76].

Hydro(solvo)thermal method

The hydrothermal/solvothermal method refers to the utilization of a solvent under pressures and temperatures above the critical point to increase the solubility of precursors and speed up the reactions between the precursors. In contrast to the other kinds of synthetic methods, the hydrothermal method allows for the preparation of highly crystalline nanoparticles with controlled size and good dispersibility at much lower temperature. The particle size, morphology and optical properties could be controlled by the pH of the solution, doped ion concentration, precursors ratio, reaction temperature and time etc. Polyols (glycol, diethylene glycol and glycerol) [77], OA [78, 79], PEI [80–82], citric acid [83] and PVP [80] are usually added as important reagents for particle size, water solubility and morphology control. Nevertheless, the main disadvantage of the hydrothermal method is the impossibility of observing the nanocrystals growth process.

One step method

In order to get UCNPs that are compatible with biomolecules, one-step method was developed on the basis of the methods listed above. Water soluble UCNPs could be synthesized through the one step hydro(solvo)thermal [84–86] or co-precipitation method in the presence of hydrophilic or binary cooperative ligands, such as polyols [77, 87, 88], EDTA [89–92], citrate [93–97], sodium dodecyl sulfate (SDS) [98], PVP [99], small-molecule binary acid [100], polyethylene glycol (PEG) [101], PVP [102], PAA [103, 104], PEI [103], 3-mercaptopropionic acid (3MA) and 6-aminocaproic acid (6AA) [105] together with sodium bis(2-ethylhexyl)sulfosuccinate or OA etc. [87, 101]. There are also methods that use ionic liquid and 1-butyl-3-methylimidazolium tetrafluoroborate as co-solvent, template and reactant to synthesize UCNPs. This one step ionic liquid assisted method is efficient and environmentally mild due to the chemical stability, low vapor pressure and non-flammability characteristics of the ionic liquids [106, 107]. Although the one step method simplifies the reaction procedure, uniform hydrophilic UCNPs with small size are hardly obtained by this method. So the hydrophobic UCNPs that

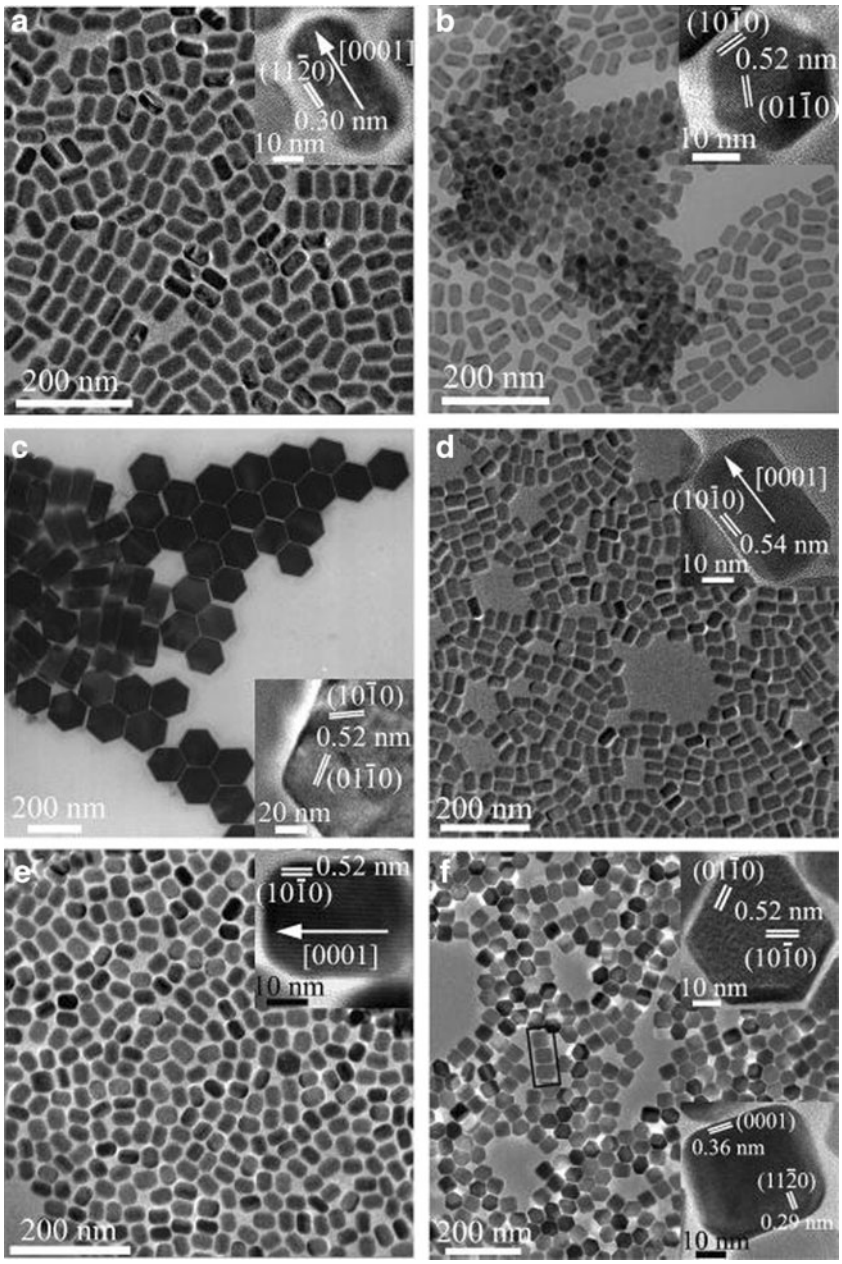

Fig. 2 TEM and HRTEM (inset) images of β-$NaYF_4$ nanorods redispersed in toluene/hexane (1:1) (**a**) and in toluene/hexane/ethanol (1:1:0.48) (**b**), of β-$NaYF_4$ nanoplates (**c**), of β-$NaNdF_4$ nanorods (**d**), and of β-$NaEuF_4$ nanorods (**e**). TEM and HRTEM (inset, upper: lying flat on the face; lower: standing on the side face from the *highlighted square*) images of β-$NaHoF_4$ hexagonal plates (**f**). (Reprinted with permission from ref. [62]. Copyright 2006 American Chemical Society)

synthesized by the other methods are still indispensable, and the strategies for the conversion of hydrophobic UCNPs to hydrophilic ones are also essential and will be discussed in detail in the following contents.

Surface modification

For UCNPs used for bioimaging, surface modification is required to obtain biocompatible nanoparticles with excellent water dispersity, physiologic stability and functional anchors for further bioconjugation. The methods of ligand exchange, ligand oxidation [108, 109], ligand attraction [110–113], layer by layer assembly [114–118] and silanization [112, 119–122] are well known methods to convert the hydrophobic nanoparticles to the hydrophilic ones.

For the ligand exchange method, the original hydrophobic ligands are displaced by other polymeric molecules, which could provide a hydrophilic surface and anchors for further bioconjugation. Most of the hydrophobic UCNPs are coated by OA and oleylamine (OM) surfactants using -COOH and -NH_2 as chelating ligands respectively. The -COOH ligands have stronger coordination ability to the lanthanide ions than the -NH_2 ligands. For the UCNPs using -COOH as the chelating ligands, an excess of chelating ligands are required to displace the original -COOH ligands due to its strong interactions with lanthanide ions. A typical example based on the

ligand exchange method is reported by Capobianco group in 2009. PAA was chosen as the surface modification ligands. A complete ligand exchange with PAA was realized and resulted in moderate UCL intensity as well as physical stability of the dispersed nanoparticles in solution for up to 3 months [67]. Van Veggel group also reported a technique for the replacement of oleate with PEG-phosphate ligand as an efficient method for the generation of water-dispersible $NaYF_4$ nanoparticles. Many other kinds of molecules were also chosen as surfactants to displace the OA or OM in the ligand exchange process, such as hexanedioic acid [123, 124], 3MA [125, 126], dimercaptosuccinic acid (DMSA) [127], pluronic F127 [128], mercaptosuccinic acid (MSA) [129], citrate [12, 130, 131], poly(amidoamine) (PAMAM) [132], PEG-diacid (MW 600) [24], PEI [133] and thioglycollic acid (TGA) [134, 135], maleimide-PEG-COOH [136] and nitrosonium tetrafluoroborate ($NOBF_4$) [137, 138] etc. Among these surfactants, the PEGylation could shield the UCNPs from quick immune-mediated removal when the UCNPs are to be used intravenously. However, the luminescence intensity of the UCNPs in aqueous environments was found to be severely quenched when compared to the original NPs in organic solvents. This is attributed to an increase in the multiphonon relaxations of the lanthanide excited state in aqueous environments due to high energy vibrational modes of water molecules.

Ligand oxidation is another method used for the hydrophobic UCNPs modifications. This method has no obvious effects on the particle morphology or luminescence properties of the UCNPs, but is only applicable to a few specific kinds of ligands. A specific example is the carbon-carbon double bond of the OA oxidized by Lemieux-von Rudloff reagent [108] or ozone [139] to generate water soluble carboxylic ligands. The carbon-carbon double bond of the OA was also reported undergoing epoxidation in the first step and further coupling with PEG monomethyl ether (mPEG-OH) to realize the hydrophilic modification [109].

Self assembly method is based on the electrostatic attraction between the oppositely charged species deposited [114–118, 129, 140] or with some special host and guest molecules [141]. The major advantage is that it permits the preparation of coated colloids of different shapes and sizes, with uniform layers of diverse composition as well as controllable thickness. Li's group firstly applied this method on the synthesis of hydrophilic UCNPs [117]. The zeta potential of the UCNPs alternated from negative to positive values along with the alternative absorption of poly(allylamine hydrochloride) PAH and poly(sodium 4-styrenesulfonate) (PSS), resulted in the successful modification of $NaYF_4$:Yb,Er/Tm nanoparticles with rich amino ligands on their surfaces. There are also methods that use excess organic solvents under ultrasonic condition [142] or by changing the pH value of the solution [143] to make ligand-free UCNPs, then hydrophilic and biocompatible molecules could be conjugated on the surface through electronic attraction process.

Ligand attraction approach involves the absorption of an amphiphilic copolymer onto the surface of the UCNPs through the hydrophobic-hydrophobic attraction between the original ligands and the hydrophobic ligands of the surfactant. One typical example is the coating of 25 % octylamine and 40 % isopropylamine modified PAA on the surface of $NaYF_4$:Yb,Er(Tm)/$NaYF_4$ core/shell nanoparticles [144]. The coating of PAA was from the hydrophobic interactions between the octyl and isopropyl groups of PAA and the octadecyl groups of OM on the UCNPs surface. After coating, the hydrophilic carboxyl groups of PAA extended outward, making nanoparticles water soluble and allowing further attachment of biomolecules. PEG-block-poly(caprolactone) (PEG-b-PCL), PEG-block-poly(lactic-coglycolic acid) (PEG-b-PLGA), and (PEG-block-lactic acid) (PEG-b-PLA) [145, 146], octylamine–PAA–PEG (OA–PAA–PEG) [147], PEG [15, 45], hexadecyltrimethylammonium bromide (CTAB) [148], octylamine-modified PAA (OPA) [131], PEG–phospholipids[44] etc. were also used as the hydrophilic polymers coating on the surface of hydrophobic UCNPs to improve the UCNPs water solubility.

Surface silanization is one of the most important methods for the UCNPs surface modification. An amorphous silica shell is coating on the surface of the UCNPs by hydrolysis and condensation of siloxane monomers [149]. This method is applicable for coating the silica on both hydrophilic and hydrophobic metals, metal oxides, and QDs nanoparticles with controllable thickness of the shell by Stöber method or reverse microemulsion method. In order to make the UCNPs to be water soluble and be able to conjugated by biological molecules, modified silanes (aminosilanes), such as aminopropyltrimethoxysilane (APTES) [150], (3-aminopropyl) triethoxysilane (APS) [151] are directly (one step) or indirectly (two steps) reacted with the UCNPs to generate functional amino groups on the surface of the UCNPs. Wolfbeis's group reported the preparation of lanthanide-doped UCNPs for protein conjugation. The core of $NaYF_4$:Yb, Er/Tm was coated with a silica shell which then was modified with a PEG spacer and N-hydroxysuccinimide ester groups. The N-hydroxysuccinimide ester renders them highly reactive towards amine nucleophiles such as proteins [152]. After coating with silanes, the silanized UCNPs are more stable in physiologic solutions than polymeric coats. The stability of the coating also reduces the risk of toxic effect from leaching of lanthanide ions into the biology tissues. Moreover, a subsequent coating of a mesoporous silica layer onto the UCNPs @ silica nanoparticles makes the UCNPs could be used as drug carriers [14].

In addition to the synthesis methods listed above, many other methods have also been developed for the synthesis of UCNPs, such as microwave synthesis [153–155], combustion synthesis [126–128] and flame synthesis [156]. Although

these methods exhibit time saving or energy saving advantages, considerable aggregation, lack of particle size control or low purity problems are still need to be solved.

Optimization of UCNPs for bioimaging

Emission color control of UCNPs

There are different ways to provide UCNPs with multicolor. The controlling of dopant-host combination is one of the most straightforward approaches to get multicolor UCNPs. The wavelength of the emission peaks can be controlled by adjusting the combinations of dopant ions and the host materials, which further controls the emission color of the UCNPs. Markus Haase and co-workers originally demonstrated the upconversion emission of lanthanide doped phosphate nanocrystals in transparent colloidal solution [58]. Multicolor could be seen from a single kind of Yb/Er or Yb/Tm codoped $NaYF_4$ nanocrystals with the use of color filters. Different emission colors could also be seen by changing the dopant ions without using any color filter [157]. In addition, the concentration of the dopant ions has strong impact on the emission color of the UCNPs [158, 159]. The emission color of the UCNPs varies with the concentration of the dopant ions. Take Y_2O_3:Yb/Er as an example, an increase dopant concentration of Yb^{3+} induces enhanced back energy transfer from Er^{3+} to Yb^{3+}, resulting in a relative increase in intensity of red emission of Er^{3+} [160]. Another typical example is reported by Liu's group. The Yb/Er codoped $NaYF_4$ nanocrystals exhibit sharp emission peaks in blue, green and red region. Upon excitation at 980 nm, the $NaYF_4$:Yb,Er nanoparticles exhibit yellow to red emission by increasing the concentrations of Yb^{3+} (25-60 %) [161] (Fig. 3). It was also reported by Wolfbeis et al. that the two emission ratio bands could be modified by covering the UCNPs with a screen layer containing different amounts of an organic dye such that one of the two emission bands is re-absorbed to various degrees. The second emission band is not absorbed by the dye on the surface and serves as a ratiometric reference to the emission of the first band [162]. Nanocrystal size is another important factor in the UCNPs emission color control. As along with nanoparticle decrease, the surface concentration of the dopant ions are increased, leading to a gradual variation of the emission color. Xue etc. reported that the relative intensity of the blue as well as the red to the green increased gradually with

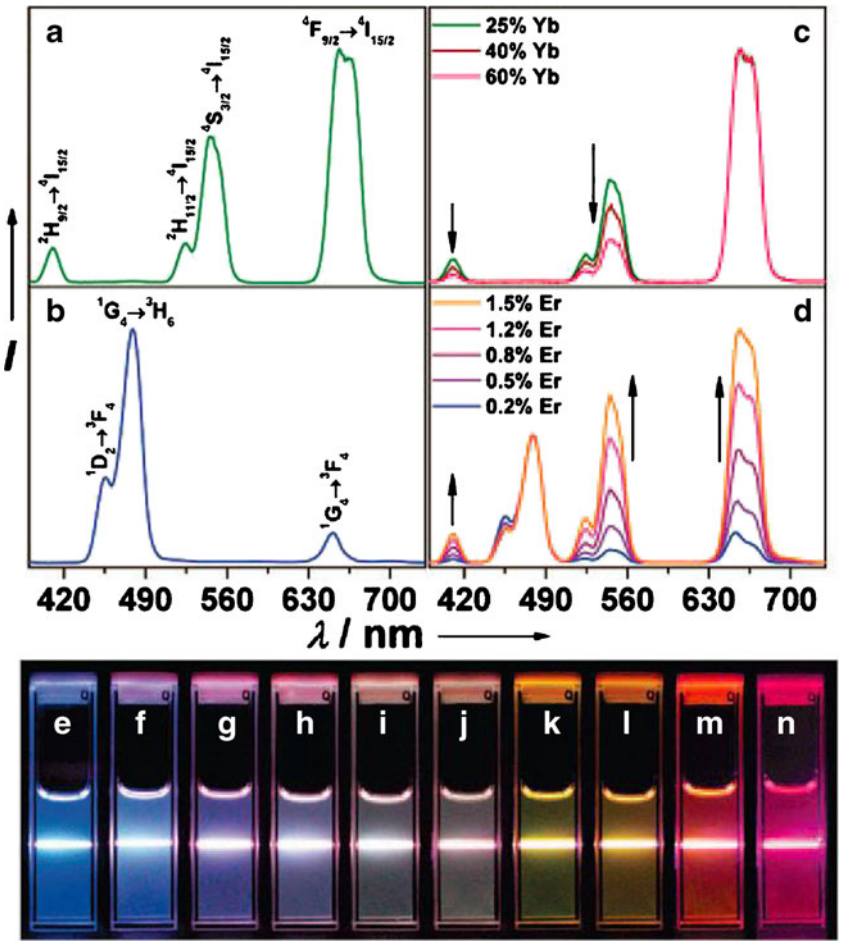

Fig. 3 Room temperature upconversion emission spectra of **a** $NaYF_4$:Yb/Er (18/2 mol%), **b** $NaYF_4$:Yb/Tm (20/0.2 mol%), **c** $NaYF_4$:Yb/Er (25-60/2 mol%), and **d** $NaYF_4$:Yb/Tm/Er (20/0.2/0.2-1.5 mol%) particles in ethanol solutions (10 mM). The spectra in (**c**) and (**d**) were normalized to Er^{3+} 650 nm and Tm^{3+} 480 nm emissions, respectively. Compiled luminescent photos showing corresponding colloidal solutions of **e** $NaYF_4$:Yb/Tm (20/0.2 mol%), **f**–**j** $NaYF_4$:Yb/Tm/Er (20/0.2/0.2-1.5 mol%), and **k**–**n** $NaYF_4$:Yb/Er (18-60/2 mol%). The samples were excited at 980 nm with a 600 mW diode laser. The photographs were taken with exposure times of 3.2 s for **e**–**l** and 10 s for m and n. (Reprinted with permission from ref. [161]. Copyright 2008 American Chemical Society)

decreasing particle size [163]. Yan etc. also reported that as the size of α-$NaYF_4$:Yb,Er nanopolyhedra decreases from 13.7 to 5.1 nm, the intensity ratio of green to red emission($f_{g/r}$) significantly diminishes from 0.63 to 0.13. An intense red emission is observable with the naked eye [63]. The highly efficient multicolor upconversion emissions are also related with the crystallite phase and associated defect state. It was reported by Yan's group that the formation of core/shell-structured α-$NaYF_4$:Yb,Er@α-$NaYF_4$ enhances both the intensity of green emission by 200 % and $f_{g/r}$ from 0.4 to 2.0. Therefore, 8.0 nm α-$NaYF_4$:Yb,Er and the α-$NaYF_4$:Yb,Er @ α-$NaYF_4$ nanopolyhedra exhibit an intense yellow and yellowish-green emission respectively [63]. Zhang's group also reported on fabricating sandwich-structured UCNPs with a $NaYbF_4$ matrix sandwiched between two $NaYF_4$ layers. By doping different emitters into each of the shells and adjusting their thickness, different color output tunable based on the RGB color model were obtained [164]. It was also reported that the relative intensity of green and red emission bands in $NaYF_4$:Yb^{3+},Er^{3+} nanoparticles could be controlled by changing the excitation pulse repetition rate [165].

UCNPs luminescence efficiency improvement

UCNPs have attracted considerable attention for their potential biological applications due to their excellent optical characteristics, such as large anti-Stokes shift, high photostability, fine tuning multicolor emission and narrow emission bandwidth etc. However, limited UCL efficiency is still far from perfect for such applications. To achieve high upconversion efficiency, considerable efforts have been devoted [166]. The most direct method is by suitable choosing of the host and controlling the concentration or kind of the dopant ions [167–169]. For example, the intensity of the upconversion emission was demonstrated by Prasad group to increase by up to 43 times along with an increase in the relative content of Yb^{3+} ions from 20 to 100 %, with a corresponding decrease in the Y^{3+} content from 80 to 0 % [21]. Generally, the relative low emission efficiency of doped nanoparticles is usually due to the energy transfer processes to the surface through adjacent dopant ions or because the luminescence of surface dopant ions is quenched. Facing this problem, increasing the size of UCNPs is one of the most effective way to increase the upconversion luminescence efficiency [170]. As bigger UCNPs have relative smaller surface area, less surface defects and less surface ligands. However, too large UCNPs are usually not suitable for in vitro or in vivo bioimaging. In addition, coating a shell made up of a material through which energy cannot be transferred around the doped nanoparticles can also suppress these quenched processes and enhance the upconversion emission intensity of the phosphors greatly. Different kinds of core/shell nanoparticles with lanthanide doped or undoped in the core or shell were synthesized to increase the luminescence intensity [63, 144, 170–177]. For example, Prasad and coworkers demonstrated that the luminescence intensity of the previously designed NIR-to-NIR α-$NaYbF_4$:Tm^{3+} UCNPs is enhanced 35 times by encapsulating them in a hetero shell of CaF_2, yielding a quantum yield as high as 0.6±0.1 % under excitation with a low power density of~0.3 $W \cdot cm^2$-1 [178]. Coupling Ag or Au shells onto the $NaYF_4$ nanocrystals is also a good way to increase the upconversion luminescence intensity due to the plasmon resonance phenomenon, which can be an effective promoter of fluorescence when optimized to provide an electric field enhancement that arises from the collective oscillations of the electrons due to resonance [179–182]. The research results show that the core-active/shell nanoparticles luminescence intensity is stronger than the uncoated nanoparticles, while the core-active/shell-active nanoparticles have the strongest luminescence intensity.

Different from the core/shell nanoparticles listed above that use UCNPs as the core, Stucky and coworkers presented a kind of nanoparticles that comprise silver cores and dense layers of Y_2O_3:Er separated by a silica shell materials and metals in nanoscale. With increasing spacer thickness the average luminescence intensity reaches a maximum value of 4 times that from the pure Y_2O_3:Er shell at an optimal spacer thickness of 30 nm [183].

Formation of NIR-to-NIR UCNPs

The NIR-to-NIR upconversion process provides deeper light penetration into biological specimen and results in high contrast optical imaging due to absence of an autofluorescence background and decreased light scattering [21, 126]. Among UCNPs, the NIR-to-NIR UCNPs are of particular important for bioimaging [184, 185]. This is because the excitation (~ 980 nm) and photoluminescence emission peaks (~ 800 nm) are both within the spectral range of 750~1,000 nm, which is considered as "biological transparency window". It was reported that the fluorescence emission wavelengths of cubic-phase $NaYF_4$ nanocrystals doped with Yb^{3+}, Tm^{3+}, and Er^{3+} were tuned from the visible to NIR regions through changing the Er/Tm ratio [181]. In addition, YOF:Yb,Er@YOF also emitted strong red upconversion fluorescence. The YOF shell greatly enhanced the red emission at~669 nm (~18 times) and suppressed the green emission of erbium at~530 nm [133].

Optimization of the excitation light

Due to the strong absorption of water and biological specimens at 980 nm, optimization the excitation laser is needed to be considered the severe overheating effect. He and coworkers originally reported a promising excitation approach for better NIR-to-NIR UCL in vitro or in vivo imaging by using a cost-effective 915 nm laser, which provides drastically less heating

of the biological specimen and larger imaging depth in tissues due to quite low water absorption at 915 nm wavelength [129]. Most recently, Yan and coworkers reported the extension of the UC excitation spectrum to 808 nm wavelengths, where water has much lower absorption. A core/shell structure was constructed to ensure successive Nd^{3+} to Yb^{3+} activator energy transfer (Fig. 4). The in vivo imaging experiment confirmed that the 808 nm laser-induced local overheating effect is greatly minimized compared with the 980 nm laser with a power density of 130 $mW \cdot cm^{2}$-1 for the lasers [186].

Optimal design for UCNPs in vivo delivery

Therapeutic UCNPs technologies have the potential to revolutionize the drug development process and change the landscape of the pharmaceutical industry. As UCNPs have many advantages over the other nanoparticles for drug delivery, such as controllable particle size (from<10 nm to hundreds of nanometers), adjustable particle surface charge, low cytotoxicity, and high physiologic stability. Especially the UCNPs have shown promise in delivering molecules to desired sites in the body and imaging the site of drug delivery or monitor the in vivo efficacy of the therapeutic agent at the meantime. One significant challenge for the successful development of therapeutic UCNPs is rapid clearance during the process of systemic delivery. When UCNPs enter the blood-vessel, the particle surface may experience nonspecific protein adsorption, thereby making them to be more rapidly cleared from the bloodstream through phagocytosis by the mononuclear phagocyte system in the liver and by spleen filtration. Therefore, the factors that could affect the clearance and biodistribution of nanoparticles should be carefully considered for the optimal design of therapeutic nanoparticles.

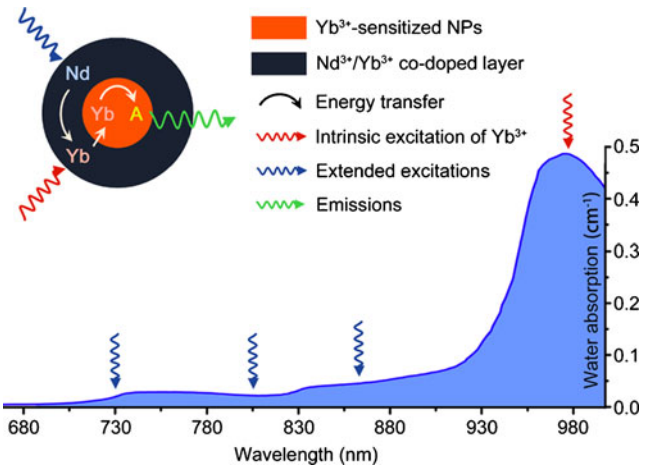

Fig. 4 Absorption of water in the NIR and the integration scheme of $Nd^{3+} \rightarrow Yb^{3+}$ ET process by introducing Nd^{3+}/Yb^{3+} co-doped shell. The resulting $Nd^{3+} \rightarrow Yb^{3+} \rightarrow$activator ET could extend the effective excitation bands for conventional Yb^{3+}-sensitized UCNPs. Featuring lower water absorptions, these alternative excitation bands are expected to minimize the tissue overheating effect caused by NIR laser exposure (*blue line* represents absorption spectrum of water). (Reprinted with permission from ref. [186]. Copyright 2013 American Chemical Society)

Particle size range

On the basis of physiological parameters such as tissue extravasation, hepatic filtration and kidney excretion, nanoparticles smaller than 10 nm can be rapidly cleared by the kidney or through extravasation, while larger nanoparticles of more than 100 nm may have higher tendency to be cleared by the mononuclear phagocyte system and hepatic filtration [187]. For nanoparticles used for tumor imaging, nanoparticle size also plays a key role in tumor accumulation through the enhanced permeability and retention effect (EPR). EPR is a unique feature which allows macromolecules or drug delivery nanoparticles (cutoff size of>400 nm) to preferentially accumulate and diffuse in tumor tissues. Fang et al. compared different sizes (80, 170 and 240 nm) of PEGylated spherical nanoparticles for protein absorption, nanoparticle uptake by murine macrophages, and blood clearance kinetics [188]. The results showed that nanoparticles with smaller particles size of less than 100 nm have a higher circulation half-time in the blood, experience reduced hepatic filtration, increase the accumulation and enhance diffusion within tissue. Jain and coworkers investigated one human and five murine tumors including mammary and colorectal carcinomas, hepatoma, glioma and sarcoma, the experiment results showed that tumors grown subcutaneously exhibited a characteristic pore cutoff size ranging from 200 nm to 1.2 μm [189]. It was also reported that the pore cutoff size was related to the temperature. The pore cutoff size was estimated to be between 7 and 100 nm at 34 °C and was increased to >400 nm at 42 °C [190]. Yin and coworkers suggested that nanoparticles with slight negative charges and particle size of 150 nm were tended to accumulate in tumor more efficiently. Therefore, to capitalize on the EPR effect and to efficiently escape from the physiological barriers, the optimal nanoparticle size was suggested to be in the range of approximately 10–100 nm [191, 192].

Surface charge

It has been demonstrated that the zeta potential of nanoparticles also affect their interaction with plasma proteins and blood components, uptake and clearance by macrophages, and hence potentially influence their biodistribution and targeted delivery of payload to the intended target sites. In vivo biodistribution studies demonstrated that undesirable liver uptake was very high for highly positively or negatively charged nanoparticles, which is likely due to active phagocytosis by macrophages (kupffer cells) in the liver. In contrast, liver uptake was very low but tumor uptake was very high when the surface charge of nanoparticles was slightly negative [193]. It was also reported that cationic particles are more

cytotoxic and more likely to induce haemolysis and platelet aggregation than are neutral or anionic particles [194], which has been confirmed in studies of the ability of cationic polystyrene beads to induce cytotoxicity, vascular leakage and inflammatory infiltrates in the lungs of exposed rats and mice [195, 196]. On the contrary, Jin et al. reported that the positively charged UCNP-PEI evinced greatly enhanced cellular uptake in comparison with its neutral or negative counterparts [80]. In another study of Zhang's group, different surface charge UCNPs were tested for cellular uptake. The results showed that the positively charged UCNPs (UCNP-NH_2, zeta potential+18.9 mV) are much easier for cellular uptake than the negatively charged UCNPs(UCNP-si, zeta potential -19.4 mV). The cellular uptake of UCNP-NH_2 with positive charge only needs 3 h of incubation time because of the opposite charge between cell membrane and particles' surface [197]. They suggested that when nanoparticles are used as in vivo imaging probes, it's better to use particles with positive charge to avoid the long-time circulation period in the body and reduce the cost of particles due to the metabolism. Based on these studies, we can conclude that UCNPs with slightly negative charge may reduce the undesirable clearance by the reticuloendothelial system (RES) such as liver, improve the blood compatibility, thus deliver the anti-cancer drugs more efficiently to the tumor sites, while slightly positively charge UCNPs may increase its cellular uptake by tumor cells. So the optimal range of nanoparticle zeta potential was suggested to be between - 10 mV and+10 mV for reduced phagocytosis and minimized nonspecific interactions of UCNPs [191].

Surface PEGylation

Prior to nanoparticles applications, PEG was used as a non-toxic, water-soluble dispersant or stabilizer. Nanoparticles modified with PEG was found to reduce nanoparticles accumulation in off-target organs such as liver and spleen. A PEG shell on the nanoparticle surface shields hydrophobic or charged particles from attachment by blood proteins, leading to prolonged circulation half-life compared to non-PEGylated nanoparticles [198–202]. One typical PEG modified UCNPs used for drug delivery were reported by Liu and coworkers. UCNPs functionalized with a PEG grafted amphiphilic polymer are loaded with doxorubicin (DOX) by simple physical adsorption via a supramolecular chemistry approach for intracellular drug delivery. The loading and releasing of DOX from UCNPs are controlled by varying pH. UCL imaging by a modified laser scanning confocal microscope reveals the time course of intracellular delivery of DOX by UCNPs. Subsequently, they further reported the use of PEG coated UCNPs as an exogenous contrast agent to track mouse MSCs (mMSCs) in vivo. To improve the labeling efficiency, oligo-arginine is conjugated to the surface of the UCNPs@PEG to enhance the nanoparticles uptake by mMSCs [203]. Another typical example is a kind of trimodal imaging probe of PEGylated NaY/GdF_4: Yb, Er, Tm @SiO_2-Au@PEG_{5000} nanoparticles with uniform size of less than 50 nm. The as-designed nanoprobes showed strong emissions ranging from the visible to NIR for fluorescent imaging, T_1-weighted MRI by shorting T_1 relaxation time and enhanced Hounsfield units (HU) value as a CT contrast agent [11]. Van Veggel and coworkers selected a ligand exchange approach where the oleate ligands on the surface of the nanoparticles are displaced by PEG-phosphate ligands, resulting in water-dispersible UCNPs. The PEG-phosphate coated UCNPs were used to image a line of ovarian cancer cells ($CaOV_3$) to demonstrate their promise in biological application [204]. In addition to PEG [205–209], some other promising hydrophilic polymers are also under investigation for the same purpose, including PAA [210], PEI [80, 211], polyphosphazene [110], poly (styrene-block-allyl alcohol) (PS(16)-b-PAA(10)) et al. [212].

UCNP Targeting

The targeting and accumulation of drugs to specific sites where the agent is released provides a mean to reach high drug concentration at a designated area with far less systemic side effects. Two general approaches have been utilized to accomplish this process: passive targeting and active targeting.

Passive targeting For the nanoparticles used for cancer therapeutic, the process of nanoparticles passive targeting takes place in a non-specific way through extravasating into the gaps of the tumor interstitial space. These gaps between adjacent endothelial cells with a diameter up till 800 nm exist in neo-angiogenic blood vessels which serve to supply the tumor with nutrients. But larger tumors show poor vascularization, especially inside the necrotic areas, which prevents the localization of the nanoparticles and makes local drug deposition impossible.

Active targeting Because of these inherent limitations of the passive targeting, the next generation of active targeting nanoparticle delivery systems are being investigated. The ultimate goal is to deliver therapeutic agents and contrast agents to the single target cell. This can be achieved by conjugating the nanoparticles with biological recognition moieties which recognize cell surface antigens or receptors. The target recognition moiety can be any chemical or biological entity, such as aptamers, peptides, sugars, small molecules, antibodies and antibody fragments. However, the choice of targeting ligand is still a challenging task. As the ligand should have high affinity, high specificity, wide dynamic range, good stability and fast response time. One of the most often used targeting ligand is the cyclic RGD peptide. In vivo tumor recognition and drug delivery were realized by using the cyclic RGD peptide

conjugated UCNPs [150, 213–216]. In addition to the RGD, other kind of peptides[199, 203] and antibodies[133, 205, 206, 217–231], such as HIV transactivator protein (TAT) peptide [232], anti-carcinoembryonic (CEA) 8 antibody [223, 231], Neurotoxin [233], (immunoglobulin G) IgG antibody [227–229], anticonnexin 43 [224], anti-MUC-1 [218], anti-PSA MabH50, anti-TSH Mab5409, anti-LH Mab8D10 [225], heparin and basic fibroblast growth factor (bFGF)[217] also showed excellent targeting properties when binding to the surface of nanoparticles for bioimaging.

Nucleic acid aptamers are single-stranded DNA or RNA oligonucleotides with well-defined, three dimensional structures. With a combinatorial method called in vitro selection or systematic evolution of ligands by exponential enrichment (SELEX), aptamers can recognize a wide variety of molecules, such as proteins, phospholipids, sugars and nucleic acids. Compare with antibodies, aptamers exhibit lower immunogenicity, more cost effective and relatively smaller size compared with ~150 kD for antibodies, which enables better tissue penetration. Recent years, more and more aptamers/oligonucleotides were selected as the surface targeting ligands of UCNPs [211, 234–243].

Small molecules have also attracted considerable attention as potential targeting ligands due to their low molecular weights, low production costs and easy conjugation with UCNPs. Folic acid (FA) coupled UCNPs have been demonstrated to be effective in targeting folate receptor overexpression cells in vitro and tumors in vivo and in vitro [81, 127, 151, 244–247]. However, immunochemistry studies have shown over expression of folate receptors in normal tissues, which leads to some concerns for its further clinical application. There are also many other kinds of small molecules have been developed as targeting ligands, which show high specificity for specific molecules [248, 249], pH [250], ions [251–254], endothelial cells, human macrophages or cancer cells et al. [255, 256]. For example, most recently Li's group developed a cyanine-modified nanocomposite (hCy7-UCNPs), which is capable of monitoring $MeHg^+$ ex vivo and in vivo by UCL bioimaging with a detection limit of as low as 0.18 ppb [257] (Fig. 5).

In addition to loading with targeting ligands to improve its drug delivery efficiency, the UCNPs were also loaded with some other kind of agents simultaneously to further improve the local delivery of particles. A typical example is reported by loading the FA and microtubule inhibitor CA4P on to the surface of UCNPs. The loading of CA4P further helps UCNPs to cross blood vessel walls to reach tumor cells by depolymerizing the microtubules of endothelial cells [258].

UCNPs for bioimaging

For in vitro and in vivo imaging

As a new imaging technique, UCNPs imaging offers a unique approach for visualizing morphological details in tissue with sub cellular resolution, and has comes to be a powerful non-invasive tool for visualizing the full range of bio-species from living cells to animals. Exploitation in general internalization studies was performed using bare or modified UCNPs [43]. They have been widely used for in vitro or in vivo imaging to demonstrate their promise in biological in vivo applications [204, 230, 259–264]. Kobayashi et al. demonstrated in vivo multiple color lymphatic imaging using upconverting nanocrystals in 2009 [148]. Multicolor in vivo lymph node mapping UCL imaging was further demonstrated by Liu's group in the following year, and found the in vivo detection limit of UCNPs to be at least one order of magnitude lower than that of QDs [147]. Li's group reported a series of articles related the UCNPs for lymphatic imaging [102, 265, 266]. In

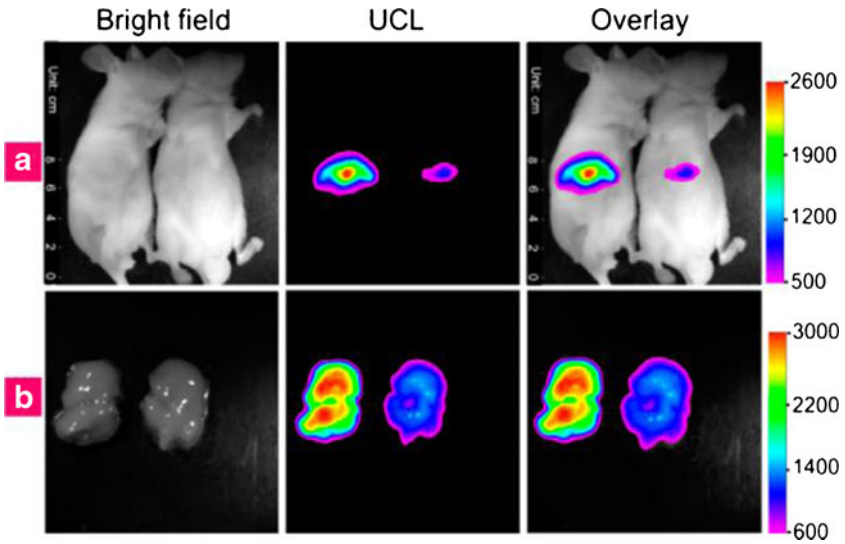

Fig. 5 **a** In vivo UCL images of 40 μg hCy7-UCNPs-pretreated living mice injected intravenously with 0.2 mL normal saline (*left mouse*) or 0.1 mM $MeHg^+$ solution (*right mouse*). **b** The corresponding UCL images of the livers which were isolated from the above dissected mice. The UCL emission was collected at 800±12 nm upon irradiation at 980 nm. (Reprinted with permission from ref. [257]. Copyright 2013 American Chemical Society)

particular, they reported a multifunctional $NaLuF_4$-based UCNPs, which have been successfully applied to the trimodal CT/magnetic resonance (MR)/UCL lymphatic imaging on small animals. The doping of lanthanide ions endows the $NaLuF_4$-based UCNPs with high T_1-enhancement, bright UCL emissions, and excellent X-ray absorption coefficient [267]. Niagara et al. applied silica/$NaYF_4$:Yb,Er to dynamically track live myoblast cells in vitro and in a living mouse model of cryo-injured hind limb [268]. In vivo confocal imaging of nanoparticle-loaded cells intravenously injected into a mouse tail vein showed them flowing in the ear blood vessels. Nanoparticle-loaded cells were also unambiguously identified with superior contrast against a negligible background at least 1,300 μm deep in a fully vascularized living tissue upon intramuscular injection.

For in vitro and in vivo targeted imaging

From general internalization studies, the potential of UCNPs were further developed to the next stage of targeted imaging. Different kinds of antibodies, aptamers, small molecules and peptides were conjugated on the surface of the UCNPs for targeted imaging of specific kinds of cells or biological molecules. Zako originally reported the tumor cell-targeted upconversion imaging using UCNPs modified with cyclic RGD peptide (RGD-Y_2O_3). The non-invasive imaging of integrin $\alpha_v\beta_3$ expression using UCNPs probes demonstrated their great potential for cancer imaging in living subjects [150]. FA is also widely chosen as targeting ligands for specific targeting and imaging of cancer cells [127, 269]. Xiong et al. synthesized the RGD peptide [215] and FA [247] labeled UCNPs for in vivo targeted imaging of subcutaneous U87MG tumor and HeLa tumor respectively borne by athymic nude mice. The RGD and FA labeled UCNPs were operated through intravenous injection. The results indicated that UCNPs could be used as whole-body targeted UCL imaging agents. Yu et al. reported the development of neurotoxin-mediated upconversion nanoprobes for tumor targeting and visualization in living Balb-c nude mice bearing xenograft glioma tumors. The obtained high-contrast images demonstrated highly specific tumor binding and direct tumor visualization with bright red fluorescence under 980 nm NIR irradiation [233]. Gap junctions have gained interest in recent years due to their involvement in cancer progression and cardiac disorders. Zhang's group developed anti-Cx43 conjugated NIR-UCNs for gap junctions imaging of H9c2 cardiomyocyte cells (CRL-1446). As these gap junctions formed between cardiac cells have a higher concentration of the protein connexin 43 [270].

Multimodal UCNPs for bioimaging

Currently, biomedical imaging techniques including MRI, PET and CT play vital roles in the diagnosis of various diseases. Each imaging modality has its own merits and disadvantages, and a single technique does not possess all the required capabilities for comprehensive imaging. Therefore, multimodal UCNPs for bioimaging are quickly becoming important tools for biomedical research and clinical diagnostics.

MRI-Optical imaging

Optical imaging as an inexpensive, robust and portable method provides the highest sensitivity and spatial resolution for in vitro imaging, but still lacks the full capability to obtain anatomical and physiological details in vivo. On the other hand, MRI technique has excellent spatial resolution, good depth for in vivo imaging and exceptional anatomic information, but suffers from limited sensitivity and lacks resolution for imaging at the cellular level. Combination of MRI and optical imaging can lead to the development of new approaches to bridge gaps in resolution and depth of imaging between these two modalities. Potential benefits of combined UCNPs and MRI have stimulated a development of hybrid magnetic-optical nano materials for in vitro and in vivo imaging [45, 125, 271–285]. Prasad group is one of the pioneers who originally developed Gd^{3+} and $Er^{3+}/Yb^{3+}/Eu^{3+}$ codoped $NaYF_4$ for the dual modality of optical and MR imaging [125]. In 2011, they further synthesized core/shell $NaYbF_4$: $Tm^{3+}/NaGdF_4$ nanocrystals to be used as probes for bimodal NIR-to-NIR UCL and MR imaging [286]. Owing to the large magnetic moment, superparamagnetic Fe_3O_4 nanoparticles have been combined with RE-UCNPs together for fabricating magnetic operation, T_2-enhanced MR imaging and UCL imaging [287, 288]. For example, Li's group reported core-shell $NaYF_4$:Yb, Er/Tm@SiO_2@Fe_3O_4 nanoparticles with very good superparamagnetic and luminescent properties [89]. In particular, Liu's group developed UCL/down-conversion fluorescence/MR imaging nanocomposite for in vivo cancer cell imaging. A chemotherapy drug of DOX is also loaded into the nanocomposite, which enables novel imaging-guided and magnetic targeted drug delivery [212].

CT/UCL and CT/MRI/UCL imaging

Since the $NaGdF_4$ upconversion nanocrystals were reported as an effective dual-mode UCL imaging and CT imaging nanocomposites, abundant research avalanched on the development of UCNPs as novel CT contrast agents [11, 209, 289–291]. For UCNPs used as CT contrast agents, there are two approaches to improve the X-ray attenuation coefficient. The first method is to increase the lanthanide elements content in a single particle. Liu et al. prepared the PEGylated Yb_2O_3:Er nanoparticles with high Yb content in a single particle suitable for both X-ray CT imaging and UCL imaging [292]. The second way is to choose higher atomic number

elements among RE elements for the preparation of UCNPs. For the REF_3 and $NaREF_4$ fluorides, the La content in LaF_3 is 70.9 %, much higher than other RE elements content in $NaREF_4$. Therefore, REF_3-based UCNPs can serve as excellent CT contrast agents and ideal building blocks for multimodal imaging agents. Based on this mechanism, FA-conjugated silica modified LaF_3:Yb,Tm UCNPs (UCNPs@SiO_2-FA) with high La content in a single particle were strategically designed by Cui's group for simultaneously targeted dual-modality imaging of UCL and CT [246].

Compared with CT scan, an MRI is suited for examining soft tissue, such as ligament and tendon injury, spinal cord injury, brain tumors etc. While a CT scan is better suited for bone injuries, lung and chest imaging, and detecting cancers. Make a combination of UCL, CT and MRI imaging is no doubt a good way to realize better tissue scans. Up to now, a series of multimodal CT/MRI/UCL imaging nanocomposites have been developed with high T_1-enhancement, bright UCL emissions, and excellent X-ray absorption coefficient [267, 293, 294]. Take the core-shell Fe_3O_4@$NaLuF_4$:Yb,Er/Tm nanocomposite which developed by Li's group as an typical example, it exhibits superparamagnetic property and T_2-enhanced magnetic resonance effect resulting from the Fe_3O_4 cores, and excellent X-ray attenuation and UCL under excitation at 980 nm. In vivo MR, CT and UCL images of tumor-bearing mice show that the Fe_3O_4@$NaLuF_4$:Yb,Er/Tm nanoparticles can be successfully used in multimodal imaging [295]. Most recently, Liu et al. reported a multifunctional nanoprobe based on PEGylated Gd_2O_3:Yb^{3+}, Er^{3+} nanorods for in vivo UCL, T_1-enhanced MR, and CT multi-modality imaging. The capability of PEG-UCNPs as high performance contrast agents for UCL/MR/CT imaging is evaluated successfully through small-animal experiments. Additionally, pharmacokinetics, biodistribution, and clearance route are studied after intravenous injection in a mouse model, reflecting their overall safety use for in vivo imaging [296] (Fig. 6).

PET/MRI/UCL or PET/CT/UCL imaging

PET is a nuclear medical imaging technique that produces a three-dimensional image or picture of functional processes in the body. PET scans are increasingly read alongside CT or MRI scans to provide excellent spatial resolution and high sensitivity. As CT provides exceptional anatomical information, but suffers from limited sensitivity. PET provides a visualization method with high sensitivity, but a low (~mm) spatial resolution. However, CT, PET, and MRI are all unsuitable for visualizing living cells because of low planar resolution, but this can be remedied by combining with UCNPs, which provides the highest spatial resolution and is suitable for imaging living cells.

Li's group have developed a series of nanocomposites for the multimodal PET/MRI/UCL or PET/CT/UCL imaging using ^{18}F as the radionuclide [12, 74]. For example, a simple, rapid, efficient and general synthesis strategy for ^{18}F-labeled rare-earth nanoparticles through a facile inorganic reaction between rare-earth cations and fluoride ions were developed. The ^{18}F-labeling process based on rare-earth elements was achieved efficiently in water at room temperature with an ^{18}F-labeling yield of>90 % and completed within 5 min. The as prepared ^{18}F-labeled rare-earth nanoparticles was further evaluated by UCL and PET imaging of their in vivo distribution and application in lymph monitoring [297]. In addition to the method of doping with Gd^{3+} within host material, they also developed PET/MRI/UCL nanoparticles that Gd^{3+} is distributed on the surface of the nanoparticle through cation exchange with Y^{3+}. ^{18}F is introduced on the UCNPs through interaction with the rare-earth ions for PET imaging. The versatility of the surface modification approach for incorporating functional molecules and fabricating fluorine-18-labeled magnetic-upconversion nanophosphors as multimodal bioprobes has been demonstrated by targeted cell imaging, in vivo UCL, MR imaging, and PET imaging of whole-body small animals [298].

Very recently, Lee et al. reported a RGD peptide-conjugated multimodal $NaGdF_4$:Yb^{3+}/Er^{3+} nanophosphors for UCL, MR and PET imaging of tumor angiogenesis. Their results suggest that ^{124}I-labeled RGD–functionalized UCNPs have high specificity for $\alpha_v\beta_3$ integrin–expressing U87MG tumor cells and xenografted tumor models. Multimodal UCNPs can be used as multimodal imaging probes for cancer-specific diagnoses [213].

Single-photon emission computed tomography (SPECT)/UCL imaging

As a pioneer of the magnetic-optical multifunctional imaging field, Li's group also reported a rare-earth cation-exchange-based post-labeling method to introduce ^{153}Sm into the lattice of UCNPs, providing a facile strategy of fabricating multifunctional nanoprobes for UCL and SPECT dual-modality imaging. This ^{153}Sm-postlabelling method shows rapid treatment time of less than1 min, high labeling yield of>99 %, and without usage of organic solvents. More importantly, this ^{153}Sm-postlabelling method is also suitable for most of RE nanoparticles to track their in vivo behaviors [299].

UCNPs for biological detection and therapy

UCNPs for biological detection

Apart from being used for cancer cell related bioimagings, UCNPs were selected as probes for disease related sensing or

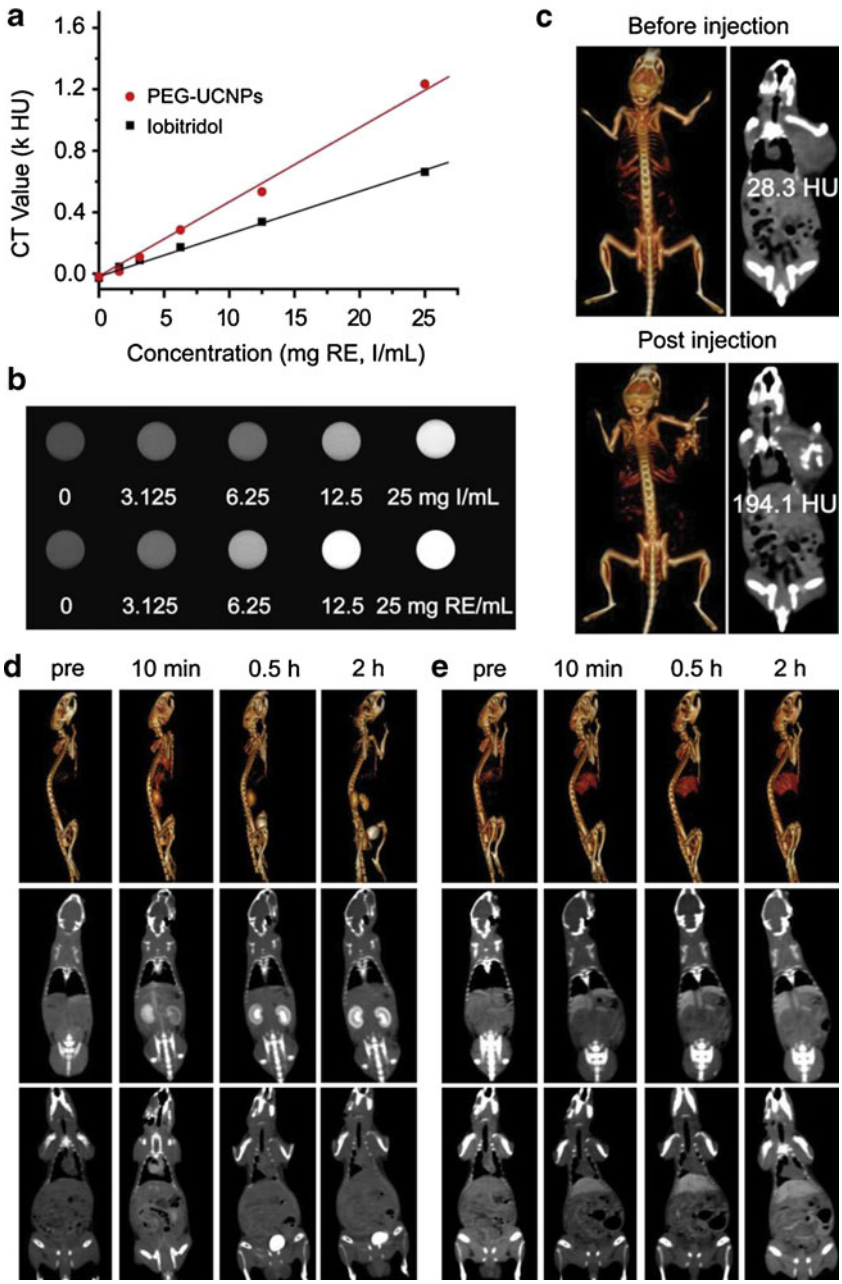

Fig. 6 CT value (HU) of PEG-UCNPs and iobitridol as function of the concentration (**a**). In vitro CT images of PEG-UCNPs and iobitridol with different concentration (**b**). CT coronal images of a female tumor-bearing C57BL/6 mouse: pre-injection and 30 min after intratumoral injection of PEG-UCNPs (**c**). In vivo serial CT view images of rats after intravenous injection of iobitridol solution (350 mg I mL-1) and PEG-UCNPs solution (50 mg RE mL-1) at timed intervals (**d**, **e**). (Reprinted with permission from ref. [296]. Copyright 2013, Elsevier)

monitoring [300]. For example, mesenchymal stem cells have shown great potential in regenerative medicine. Sensitive and reliable methods for stem cell labeling and in vivo tracking are thus of great importance. Liu's group reported the use of oligo-arginine conjugated UCNPs as an exogenous contrast agent to track mouse mesenchymal stem cells in vivo. As few as ~10 cells labeled with UCNPs are detected in vivo, which highlight the promise of using UCNPs as a new type of ultra-sensitive probes for labeling and in vivo tracking of stem cells at nearly the single cell level [203]. In another case, Liu and coworkers developed MnO_2 nanosheet modified UCNPs for rapid, selective detection of glutathione in aqueous solutions and living cells [301].

DNA/RNA analysis is of great importance in molecular biology, genetics, and molecular medicine. Zhang and co-workers have reported a few papers of UCNPs for the detection of single-stranded nucleic acids [118, 302, 303]. Liu et al. developed an UCNPs based luminescence resonance energy transfer (LRET) system for sensitive detection of methicillin-resistant staphylococcus aureus (MRSA) DNA sequence with high sensitivity and specificity, using $NaYF_4$:Yb, Er UCNPs as the energy donor and carboxytetramethylrhodamine (TAMRA) as the energy acceptor. TAMRA labeled MRSA DNA report oligonucleotides are brought close to the UCNPs upon sandwich hybridization between the capture and report oligonucleotides and a long MRSA target DNA, resulting in

an efficient LRET. Specific detection of MRSA DNA sequences with a detection limit of as low as 0.18 nM is achieved using this probe [238].

In addition to the above applications, UCNPs were developed as probes for ochratoxin A [242, 304], graphene oxide [305], DNA [118, 306–308], siRNA [309], matrix metalloproteinase-2 [310], typhimurium and staphylococcus aureus detection [236], and also used in immunoassay for estradiol [311] and goat antihuman IgG antibody detection [229]. Moreover, UCNPs have also been widely developed for disease related ions detection [252–254].

UCNPs for targeted drug delivery

In recent years, much attention has been paid to developing new drug delivery systems with enhanced bioavailability, greater efficiency, lower toxicity, controlled release advantages. In general, an efficient drug delivery system should not only deliver the therapeutic drugs to the target cells or tissues but also maintain the optimum concentration and rational toxicity of drugs in precise sites of the organs, which can improve therapeutic efficiency and reduce toxicity.

UCNPs as drug carrier

The UCNPs based delivery system can be employed for tracking and evaluating the efficiency of the drug release and mechanism of drug delivery. Up to now, most of the UCNPs drug delivery system were realized by coating PEG [13, 312], or mesoporous silica for the probes attachment or drugs loading [10, 232, 313]. Liu and coworkers functionalize UCNPs with a PEG grafted amphiphilic polymer. Then the PEGylated UCNPs are loaded with DOX molecules and conjugated with FA for targeted drug delivery and cell imaging. The loading and releasing of DOX from UCNPs are controlled by varying pH, with an increased drug dissociation rate in acidic environment, favorable for controlled drug release [13]. Zhang and coworkers reported a multifunctional "nanorattle" hollow spheres that consist of RE-doped $NaYF_4$ shells with a SiO_2-coated Fe_3O_4 inner particle. The material emits visible luminescence upon NIR excitation and can be directed by an external magnetic field to a specific target, making it an attractive system for a variety of biological applications. In vivo experiments exhibit encouraging tumor shrinkage with the DOX loading and significantly enhanced tumor targeting in the presence of an applied magnetic field [314].

Lin and coworkers also reported a series of UCNPs based drug-delivery systems. Such as the core-shell structured Gd_2O_3:Er^{3+}/$mSiO_2$ UCNPs [315], UCNP(β-$NaYF_4$:Yb^{3+}, Er^{3+}@ β-$NaGdF_4$:Yb^{3+})@$mSiO_2$-PEG [316], $NaYF_4$:Yb^{3+}, Er^{3+}@Silica [317, 318], $NaYF_4$:Yb^{3+}/Er^{3+}@$nSiO_2$@$mSiO_2$ [319], $NaYF_4$:Yb^{3+}/Er^{3+}@SiO_2@P(NIPAM-co-MAA) hybrid microspheres [320], porous $NaYF_4$:Yb^{3+}, Er^{3+}@SiO_2 [321] and the Fe_3O_4@$nSiO_2$@$mSiO_2$ @ $NaYF_4$: Yb^{3+}, Er^{3+}/Tm^{3+} nanocomposites with mesoporous, upconversion luminescent and magnetic properties [10]. Take the Fe_3O_4@$nSiO_2$@$mSiO_2$ @ $NaYF_4$: Yb^{3+}, Er^{3+}/Tm^{3+} nanocomposites as a typical example, rug release tests suggest that the nanocomposite has a controlled drug release property. The upconversion emission intensity of the bifunctional carrier increases with the released amount of model drug, thus allowing the release process to be monitored and tracked by the change of UCL intensity. Most recently, they further developed a novel drug delivery system based on FA-targeted platinum(IV)-conjugated $NaYF_4$:Yb^{3+}/Er^{3+} nanoparticles for targeted drug delivery and cell imaging. The platinum (IV) pro-drug system demonstrates the ability to release platinum (II) to exhibit anti-cancer activities in the cellular environment [322]. In addition, Liu et al. reported the design and controlled synthesis of monodisperse UCNP@$mSiO_2$ nanocomposites smaller than 50 nm, which can be used as NIR fluorescence and MRI agents and a platform for drug delivery as well [323]. In the mean time, they also synthesized TAT conjugated $NaYF_4$:Er/Yb@$NaGdF_4$-PEG UCNPs as nanoprobes for simultaneous dual modal MR/optical imaging and direct nuclear drug delivery [232]. Most recently, Lin and coworkers reported a multifunctional upconversion nanoparticle/polymer composite system UCNP@P-Pt/RhB (P: mPEGb-PCL-b-PLL), which successfully used for cisplatin (IV) drug delivery and in vitro/in vivo imaging. The anti-cancer activities of the cisplatin (IV) prodrug system have been demonstrated by releasing cisplatin in the cellular environment or tumor-bearing animal models [324].

It's well known that the hollow/mesoporous materials have been commonly used in the fields of drug delivery due to their high specific surface and cavity volumes. Most recently, Lin and coworkers further developed a series of hollow structured UCNPs for cell imaging and drug delivery. The as-prepared FA-modified hollow $NaYF_4$:Yb^{3+}, Er^{3+} UCNPs can be performed as anti-cancer drug carriers for the investigation of drug storage/release properties, which exhibit greater cytotoxicity than DOX-loaded α-$NaYF_4$ nanoparticles due to the specific cell uptake by HeLa cells via FA receptor-mediate endocytosis. Furthermore, upconversion luminescence images of $NaYF_4$-PEI-DOX and $NaYF_4$-PEI-FA-DOX nanoparticles for cell imaging indicate that these $NaYF_4$-PEI-FA-DOX composites were preferentially internalized by the HeLa cells [81] (Fig. 7). While, the hollow/mesoporous $NaREF_4$ (RE = Nd–Lu, Y) nanoparticles with small size and uniform morphology can be used as anti-cancer drug (DOX) carriers for drug storage/release investigations [98]. In addition, Lin and coworkers also developed a multifunctional PAA modified lanthanide-doped $GdVO_4$ nanocomposites [PAA@$GdVO_4$:Ln^{3+} (Ln=Yb/Er, Yb/Ho, Yb/Tm)] by filling

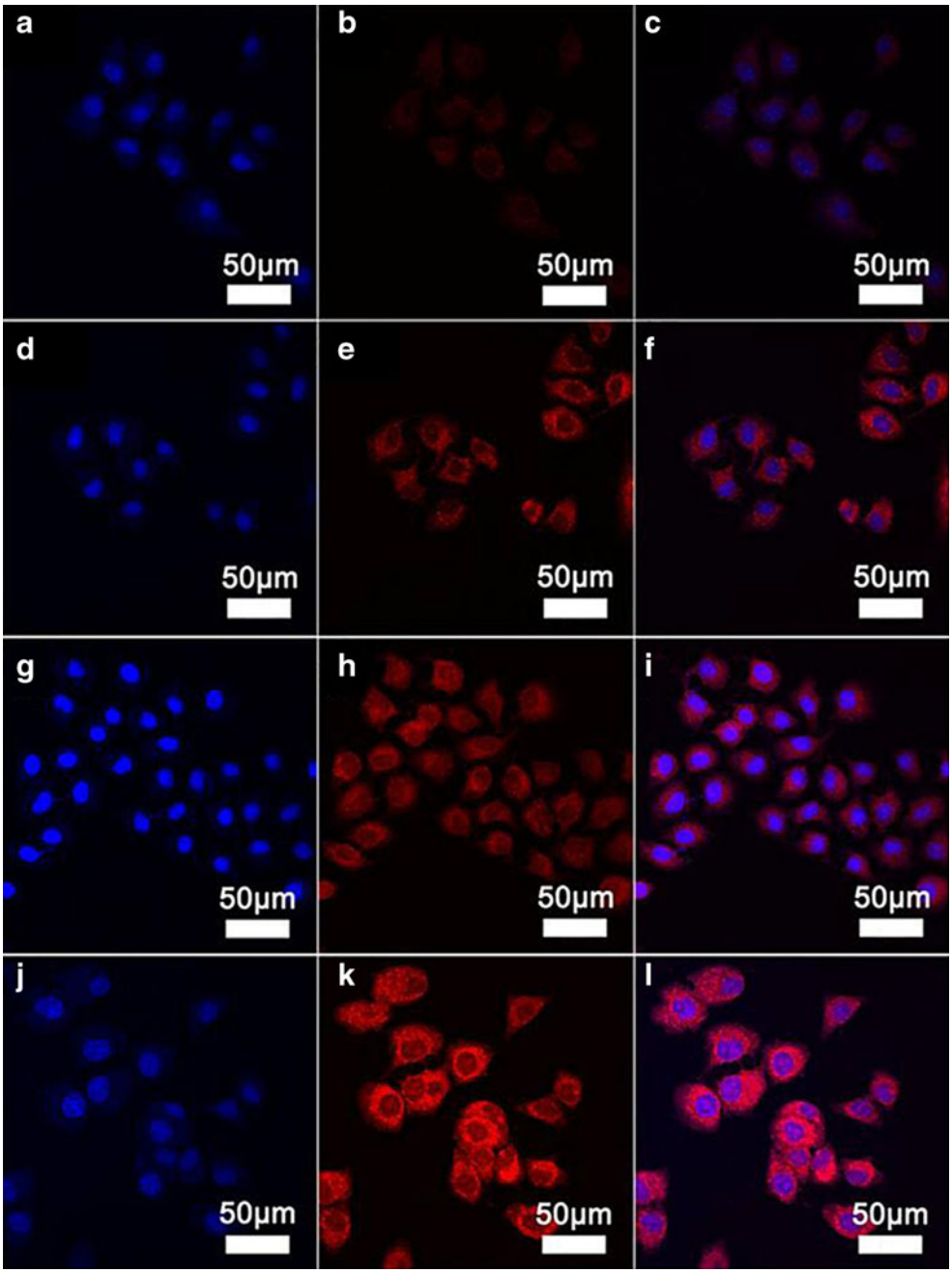

Fig. 7 Confocal laser scanning microscope images of HeLa cells incubated with $NaYF_4$-PEI-DOX ([DOX]=20 μg·mL-1) for 1 h (**a**–**c**), 6 h (**d**–**f**), and DOX-loaded $NaYF_4$-PEI-FA-DOX or 1 h (**g**–**i**), 6 h (**j**–**l**) at 37 °C, respectively. Each series can be classified to the nuclei of cells (being dyed in *blue* by Hoechst 33324 for visualization), DOX-loaded nanocarriers, and a merge of the two channels of both above, respectively. (Reprinted with permission from ref. [81]. Copyright 2013, Elsevier)

PAA hydrogel into $GdVO_4$ hollow spheres via photoinduced polymerization. In addition to the UCL imaging function, the hybrid spheres can also act as T-1 contrast agents for MRI owing to the existence of Gd^{3+} ions on the surface of composites. Moreover, DOX-loaded PAA@$GdVO_4$: Yb^{3+}/Er^{3+} system exhibits pH-dependent drug releasing kinetics due to the nature of PAA. A lower pH offers a faster drug release rate [325].

Most recently, Yu and coworkers reported an etching-free synthesis of PEGylated Y_2O_3:Yb^{3+}/Er^{3+} hollow nanospheres, which exhibit the potential as drug carrier and enable high contrast cellular and tissue imaging. The experiments on hemolysis and the circulation time in blood indicates that this kind of hollow nanospheres has potential applications in angiography [326].

For UCNPs used as drug carrier, controllable drug release is also very important to improve the therapeutic efficacy and decrease the side effects. Liu and coworkers reported an NIR-responsive mesoporous silica coated UCNP, which could be loaded with DOX for controllable drug delivery and fluorescence imaging. After surface conjugated with FA, the FA-conjugated nanocarrier allows targeted intracellular drug delivery and controlled drug release through the photocleavage of the *o*-nitrobenzyl caged linker by the converted UV

emission from UCNPs [327]. Lin and coworkers developed a bilayer thermosensitive P(NIPAm-co-AAm) hydrogel. Drug release from composite hydrogels was achieved under 980 nm NIR light irradiation by using lysozyme as a macromolecular drug, which provides a platform for simultaneous NIR luminescence imaging and NIR catalyzed drug release [328].

UCNPs for siRNA delivery

Small interfering RNA (siRNA) has emerged as a gene-based therapy due to their highly desirable roles in RNA interference and gene silencing effects in biomedical research. The key requirements for an effective siRNA therapy is that sufficient siRNA need to be introduced into cells or organs and remote control the release of siRNA inside target cells in a highly spatial and temporal precision. Up to now, a few types of UCNPs have been developed for the purpose of effective siRNA delivery. Zhang and coworkers reported a UCNPs based system for targeted delivery of siRNA to cancer cells. The siRNA was attached to anti-Her2 antibody conjugated UCNPs and the delivery of these nanoparticles to SK-BR-3 cells was studied, which certified the capability of using UCNPs as a fluorescent probe and delivery system for simultaneous imaging and delivery of biological molecules [226]. Very recently, Yang et al. reported a system of silica coated UCNPs, which were functionalized with cationic photocaged linkers through covalent bonding. Anionic siRNA could be effectively absorbed onto the linkers through electrostatic attractions and were easily internalized by living cells. Upon NIR light irradiation, the photocaged linker on the Si-UCNPs surface could be cleaved by the upconverted UV light and thus initiated the intracellular release of the siRNA [329].

UCNPs for photodynamic therapy (PDT)

PDT is a relatively new clinical therapeutic modality which involves killing of disease cells by excitation of photosensitizer chemicals with high-energy light to generate reactive oxygen species from surrounding dissolved oxygen [330–332]. However, poor tissue penetration of high-energy light and hydrophobic photosensitizers limits the effectiveness to superficial pathologies. UCNPs can be used to activates the photosensitizers in deep tissue because NIR light can penetrate a few centimeters into soft tissue due to weak absorption in the optical "transparent window".

Four main classes of photosensitizers have been approved by the U.S. Food and Drug Administration for clinical use against cancer cells, containing porphyrin derivatives, chlorins, phthalocyanines, and porphycenes [333, 334]. The second-generation photosensitizers of zinc (II)-phthalocyanine (ZnPc) have been proven highly selective for tumor targets and showed enhanced cytotoxic effects both in vitro and in vivo.

Since the first report on UCNP/Merocyanine 540 based PDT drugs in 2007 [335], different methods have been developed for construction of the UCNPs for PDT, containing directly conjugation of photosensitizers through the carboxyl ligands [336], or by coating mesoporous silica [337–339], alpha-cyclodextrin [340], PEI or PEG onto the surface of UCNPs for the attachment of photosensitizers [341]. Zhang's group reported the attachment of ZnPc photosensitizers to PEI modified $NaYF_4$ UCNPs and used them as nano-transducers for PDT of viruses [342] or cancer cells [43, 343]. However, the amount of photosensitizers attached is low and the photosensitizers are not stable attached to the UCNPs. In order to solve this problem, Zhang and coworkers further developed mesoporous silica coated UCNPs for the loading of photosensitizer [14, 344]. The photosensitizer encapsulated in mesoporous silica is protected from degradation in the harsh biological environment. In particular, they use multicolor-emission capability of the UCNPs at a single excitation wavelength for simultaneous activation of two photosensitizers for enhanced PDT, which showed a greater PDT efficacy compared with the UCNPs with a single photosensitizer. Moreover, they originally applied photosensitizer-loaded UCNPs as an in vivo-targeted PDT agent. The in vivo studies showed tumor growth inhibition in PDT-treated mice by direct injection of UCNPs into melanoma tumors or intravenous injection of UCNPs conjugated with a tumor-targeting agent into tumor-bearing mice [345].

In order to improve the biocompatibility and easier for further chemical modification, an outer layer of PEG on the core of UCNPs is usually used which acts as solubilizing agent and allows the penetration of O_2 and diffusion of singlet oxygen [346]. Prud'homme and coworkers reported the preparation of a novel biocompatible poly(ethylene glycol-block-(DL)lactic acid) block copolymers (PEG-b-PLA) coated β-$NaYF_4$:Yb^{3+}, Er^{3+} UCNPs, using meso-tetraphenyl porphine (TPP) as the photosensitizer which is stabilized by PEG-*b*-PLA. Based on in vitro studies utilizing HeLa cervical cancer cell lines, the composite nanoparticles are shown to exhibit low dark toxicity and efficient cancer cell-killing activity upon NIR excitation [146]. Liu and coworkers load photosensitizer of Chlorin e6 (Ce6) on PEG-coated UCNPs, forming a UCNP-Ce6 supramolecular complex that produces singlet oxygen to kill cancer cells under NIR light. Excellent PDT efficacy is achieved in tumor-bearing mice upon intratumoral injection of UCNP-Ce6 and the followed NIR light exposure [15].

Most recently, chitosan derivatives are also used to modify the surface of the hydrophobic UCNPs and efficiently trap the photosensitizers for PDT. In addition to good biocompatibility, chitosan is also biodegradable and provides a hydrophilic environment for solubilizing the nanoconstructs. Xing and coworkers developed a photosensitizer pyropheophorbide a (Ppa) and RGD peptide comodified chitosan-wrapped $NaYF_4$:Yb/Er upconversion nanoparticle (UCNP-Ppa-RGD)

for targeted near-infrared PDT, which exhibits high phototoxicity against cancer cells upon 980 nm laser irradiation at an appropriate dosage [216]. Gu and coworkers reported the using of FA-modified amphiphilic chitosan (FASOC) coated UCNPs (FASOC-UCNP) anchor the ZnPc close to the UCNPs, thereby facilitating resonance energy transfer from UCNPs to ZnPc. The FASOC-UCNP exhibit higher tumor targeting ability than none FA modified UCNPs (SOC-UCNP). In vivo PDT treatments for deep-seated tumors demonstrated that NIR light-triggered PDT based on the nanoconstructs possesses remarkable therapeutic efficacy with tumor inhibition ratio up to 50 % compared with conventional visible light-activated PDT with a noticeable reduced tumor inhibition ratio of 18 % [244] (Fig. 8).

Methylene blue (MB) is a widely used photosensitizer used to create singlet oxygen when exposed to both oxygen and light [347–350]. Shi et al. developed a new kind of UCNP/MB-based PDT drug, $NaYF_4$:Er/Yb/Gd@SiO_2(MB), with a particle diameter less than 50 nm, which provide a potential theranostic nanomedicine for future near-infrared laser-triggered PDT and simultaneous magnetic/optical bimodal imaging [337].

Liu's group reported a UCNP@2xCe6-DMMA-PEG nanocomposite by coating UCNP@2xCe6 with an outer layer of charge-reversible polymer containing dimethylmaleic acid (DMMA) groups and polyethylene glycol (PEG) chains using Ce6 as photosensitizer. The surface is negatively charged and PEG coated under pH 7.4, which could be converted to a

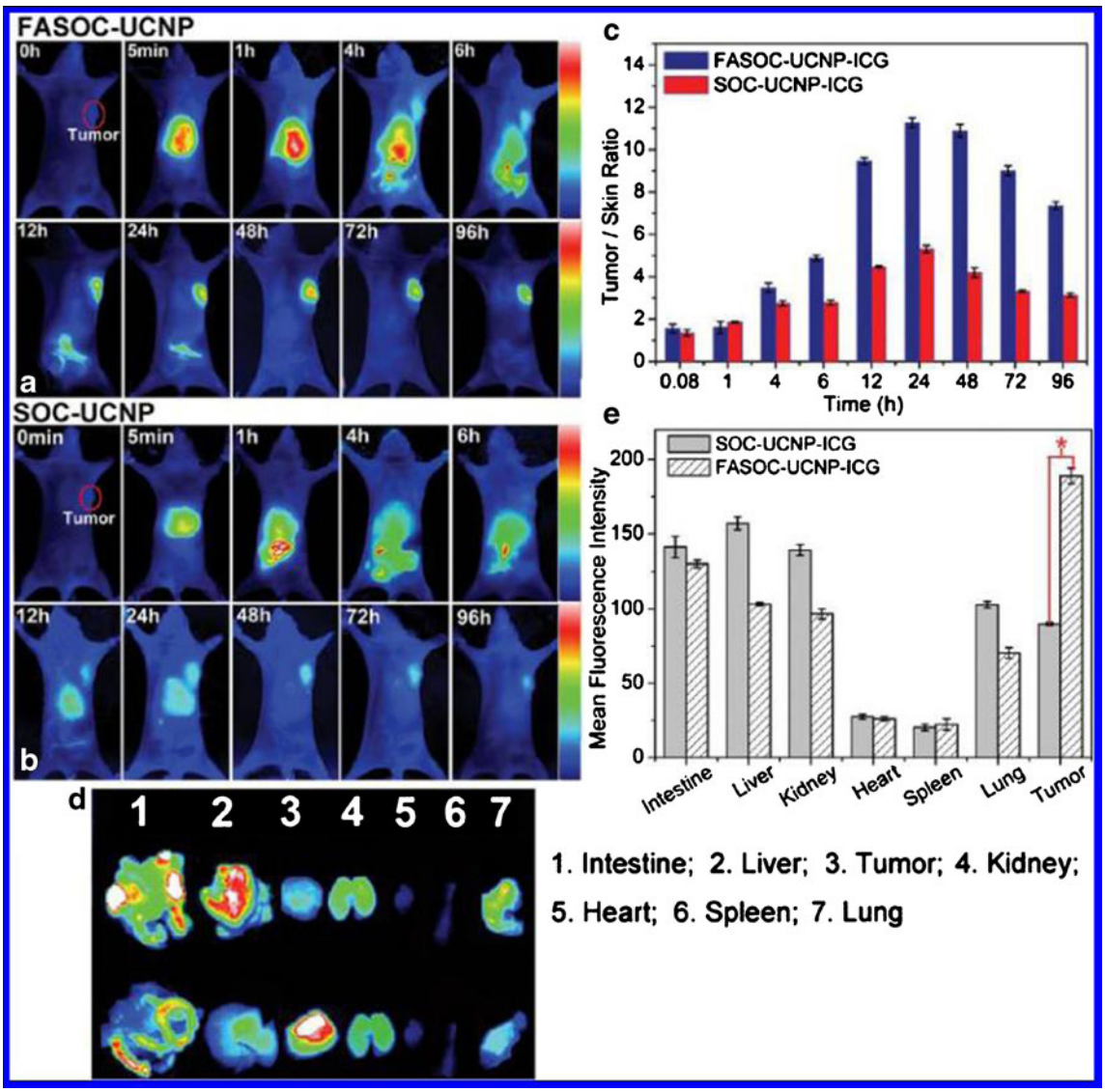

Fig. 8 In vivo tumor-targeting of the nanoconstructs. Fluorescence images of nude mice bearing Bel-7402 tumors with intravenously injection of **a** FASOC-UCNP-ICG and **b** SOC-UCNP-ICG; **c** tumor/skin ratio of tumor-bearing mice injected with different nanoconstructs; **d** fluorescence images of isolated organs separated from Bel-7402 tumor-bearing mice in different groups at 24 h postinjection; **e** semiquantification of FASOC-UCNP-ICG and SOC-UCNP-ICG in the isolated organs of mice with different injection. (Reprinted with permission from ref. [244]. Copyright 2013 American Chemical Society)

positively charged naked surface at pH 6.8, significantly enhancing nanoparticles cell internalization and in vitro NIR-induced PDT efficacy [351].

Different from the methods list above, Yan et al. demonstrated an alternative use of nanoparticles to convert NIR light into UV light, thus enabling UV-light-induced photoreactions to be used to affect the structure of hydrogels. A cross-linked hybrid polyacrylamide-PEG structure is held together by photoresponsive *o*-nitrobenzyl groups. NIR irradiation of the UCNPs within this cross-linked system generates the UV light needed to cleave the *o*-nitrobenzyl groups in their typical photooxidation process, consequently triggering the release of entrapped biomacromolecules [352].

UCNPs for photothermal therapy (PTT)

PTT employs photo absorbers to generate heat from light absorption, leading to thermal ablation of cancer cells. Various nanomaterials with high NIR light absorbance such as gold and silver nanoshells, nanorods and nanocages etc. have been utilized for PTT treatment of cancer [353]. Song et al. reported the synthesis of core–shell structured hexagonal-phase $NaYF_4$:Yb^{3+},Er^{3+}@Ag nanoparticles and their unique biofunctional properties. HepG2 cells from human hepatic cancer and BCap-37 cells from human breast cancer incubated with the composite UCNPs in vitro were found to undergo photothermally induced death on exposure to 980 nm [134].

Liu and coworkers synthesized a new class of multifunctional nanoparticles consisting a UCNP particle as the core, a layer of ultra-small iron oxide nanoparticles (IONPs) as the intermediate shell, and a thin layer of gold as the outer shell. The layer of IONPs between UCNPs and the Au shell not only affords the magnetic properties but also significantly reduces the luminescence quenching effects of the gold nanostructure to UCNPs. The UCNP–IONP–Au nanoparticles are then coated with PEG to improve its biocompatibility in physiological solutions. Those multifunctional nanoparticles are used for UCL/MR multimodal imaging as well as in vitro photothermal ablation of cancer cells [16]. In the next year of 2012, they achieved highly efficient in vivo magnetically targeted PTT by using the same multifunctional nanoparticles (Fig. 9). In vivo dual modal optical/MR imaging of mice uncovers that by placing a magnet nearby the tumor, the UCNPs show high tumor accumulation after intravenous injection, which is~8 folds higher than that of without magnetic nearby. An outstanding PTT therapeutic efficacy with 100 % of tumor elimination in a murine breast cancer model is realized [354].

Most recently, Hilderbrand et al. reported the design and synthesis of $NaYF_4$:Er^{3+},Yb^{3+}@SiO_2 core-shell nanocomposites with highly absorbing NIR carbocyanine dyes in the outer silica shell for combined NIR imaging and photothermal therapy. Photo-thermal cell killing under 750 nm excitation light source demonstrated the capability of UCNPs for both diagnostic optical imaging and therapeutic thermal therapy [355].

UCNPs for radiotherapy

Radiotherapy is the controlled use of high energy X-rays to kill many different types of cancer cells by delivering therapeutic X-rays to tumor regions without surgical risks or systematic toxicity. Inaccurate tumor localization and inherent radioresistance of tumours are the two challenges for the clinical potentials of radiotherapy. Shi and coworkers developed a novel RGD-labeled $BaYbF_5$: 2 % Er^{3+} nanocube (UCA-RGD) for the first time to meet these clinical demands. These heavy metal-based nanocubes not only act as CT contrast agents for targeted tumor imaging, but also act as irradiation dose enhancers in tumors during radiotherapy, which could greatly enhance therapeutic efficacy and minimize the damage to surrounding tissues [356].

Toxicity of UCNPs

For UCNPs used for bioimaging, fully understand the toxicity for UCNPs used in vitro and in vivo biological applications is necessary and also very important. Up to now, researches on

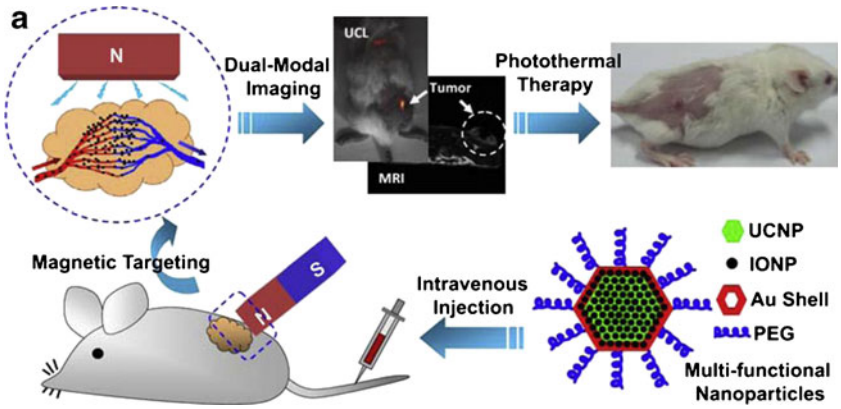

Fig. 9 A schematic illustration showing the composition of an PEG modified multifunctional nanoparticles and the concept of in vivo imaging-guided magnetically targeted PTT. The magnetic field around the tumor region induces local tumor accumulation of multifunctional nanoparticles. (Reprinted with permission from ref. [354]. Copyright 2012, Elsevier)

the toxicity of UCNPs has just begun and the data are rather few and fragmentary. Numerous cytotoxicity tests based on morphology and mitochondrial function assays have suggested the UCNPs low cell toxicity, as the most of the cell viabilities are more than 85 % when incubated with a certain range of UCNPs for more than 24 h [16, 43, 148, 185, 357, 358]. The toxicity of the UCNPs could be improved by modified with certain kinds of compounds, such as the PEG, PEI, PAA or silica etc. [112, 119, 210, 359].

Zhang and coworkers reported silica coated $NaYF_4$ nanocrystals incubated with rat skeletal myoblasts and bone marrow-derived mesenchymal stem cells and cytotoxicity was assessed by using (3-(4,5-dimethylthiazol-2-yl)-5-(3-carboxymethoxyphenyl)-2-(4-sulfophenyl)-2H-tetrazolium), sodium salts (MTS) and lactate dehydrogenase (LDH) assay. The results from this study revealed that the silica coated $NaYF_4$ UCNPs displayed good in vitro and in vivo biocompatibility, demonstrating their potential applications in both cellular and animal imaging systems [119].

Xiong et al. reported PAA coated NIR-to-NIR UCNPs of $NaYF_4$:Yb,Tm (PAA-UCNPs) for long-term in vivo distribution and toxicity studies. Biodistribution results showed that the PAA-UCNPs uptake and retention took place primarily in the liver and the spleen. Most of the PAA-UCNPs were excreted from the body of mice in a very slow manner. Up to 115 days body weight data indicated that mice intravenously injected with 15 mg·kg-1 of PAA-UCNPs didn't have any apparent adverse effects to their health. In addition, histological, hematological and biochemical analysis were used to further quantify the potential toxicity of PAA-UCNPs, and results indicated that there was no overt toxicity of PAA-UCNPs in mice at long exposure times [358] (Fig. 10).

Yan et al. reported the in vitro and in vivo toxicity assessments of water-soluble $NaYF_4$:Yb,Tm nanoparticles with HeLa cell and Caenorhabditis elegans (C. elegans) cases. $NaYF_4$:Yb,Tm nanoparticles afforded an efficient NIR image of the HeLa cells with low toxicity. Toxicity studies were further addressed with protein expression, life span, egg production, egg viability, and growth rate of the worms in comparison with those of the intact ones. The feeding of RE fluoride nanoparticles with a dose of 100 μg didn't arise obvious toxicity effect from the growth to procreation [360].

Very recently, Cui and coworkers reported the toxicity effects of UCNPs of LaF_3:Yb,Er on zebrafish. Results showed that water-soluble LaF_3:Yb, Er did not exhibit obvious toxicity to zebrafish embryos under 100 μg·mL-1, but exhibited chronic toxicities with 200 μg·mL-1 in vivo, resulting in malformations and delayed hatching rate, embryonic and larval development. The excretion channels of LaF_3:Yb,Er in adult zebrafish were primarily found in the intestine after being injected for 24 h [361].

Conclusion

This article makes a state-of-art review on recent progress in UCNPs for bioimaging, containing applications on cell imaging, biological detection and sensing, drug delivery and PPT,

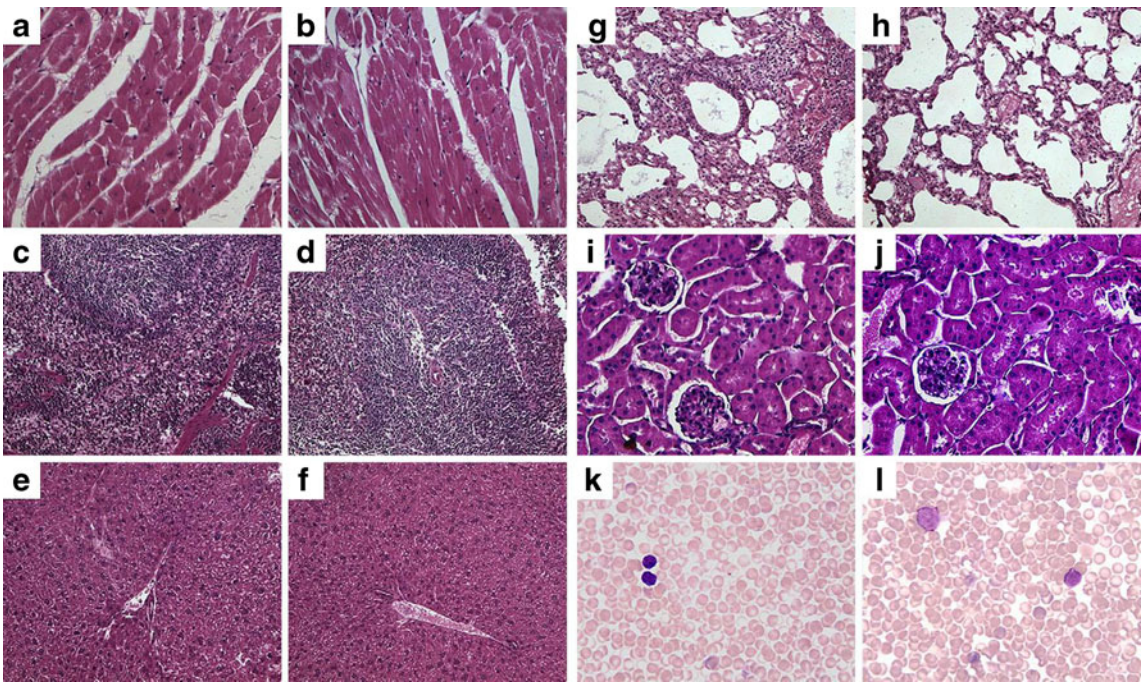

Fig. 10 H&E-stained tissue sections from mice injected with PAA-UCNPs 115 days post-injection (**a**, **c**, **e**, **g**, **i** and **k**) and mice receiving no injection (**b**, **d**, **f**, **h**, **j** and **l**). Tissues were harvested from heart (**a**, **b**), spleen (**c**, **d**), liver (**e**, **f**), lung (**g**, **h**), kidney (**i**, **j**) and blood smear (**k**, **l**). (Reprinted with permission from ref. [358]. Copyright 2010, Elsevier)

PTT and radiotherapy. Despite the tremendous number of excellent results have been made in the past few years in this region, there are still many challenges which hinder potential applications of UCNPs as therapeutic and bioimaging agents.

Firstly, the quantum yield of UCNPs is excitation power/area dependent, and a standard method of measuring absolute UCL efficiency is still required. Furthermore, the relative quantum yield of the UCNPs is still needed to be improved. As the quantum yields of the most UCNPs is usually a little more than 0.005 % but no more than 0.3 %, which significantly limiting the use of these UCNPs in optical bioimaging and PDT.

Secondly, the potential long-term toxicity study of Ln^{3+} doped UCNPs is still in its infancy. Although previous studies have shown that the UCNPs have good cell viability and have no obvious toxicity in the in vitro and in vivo toxicity assessments, the effects of UCNPs on small animals over an even longer time, the interaction between the UCNPs and the immune systems, and the effect of the UCNPs on its next generation et al. are still unknown. Much more systematic investigations are still in need.

Thirdly, both the surface modification and particle size control are still important topics. For UCNPs to be successfully used as in vivo diagnostic agents, any small changes to UCNPs shape, size, surface charge and coating will have big impacts on its behaviors toward biological systems, such as the circulation life time in vivo, drug release efficiency and the excretion rout. Coating the UCNPs with polymers or silica appear to be safer to cells and no obvious toxic to the treated small animals, but the diameter of the UCNPs will be increased from 5 nm to 50 nm or even larger. There for a facile method for synthesizing small diameters UCNPs (sub-10 nm) [64, 362] with relatively good quantum yield is in great need.

Lastly, although different kinds of multimodal UCNPs have been developed, the data based on multifunctional UCNPs for imaging, drug delivery, PDT and PTT therapeutic in vivo is still rare. More focus is needed to develop new strategies for synthesizing targeted multifunctional UCNPs which can be extended to a variety of multimodal imaging and therapies.

References

1. Dabbousi BO, Rodriguez-Viejo J, Mikulec FV, Heine JR, Mattoussi H, Ober R, Jensen KF, Bawendi MG (1997) (CdSe)ZnS Core−Shell quantum dots: synthesis and characterization of a size series of highly luminescent Nanocrystallites. J Phys Chem B 101(46): 9463–9475
2. Jaiswal JK, Mattoussi H, Mauro JM, Simon SM (2003) Long-term multiple color imaging of live cells using quantum dot bioconjugates. Nat Biotech 21(1):47–51
3. Kim S, Lim YT, Soltesz EG, De Grand AM, Lee J, Nakayama A, Parker JA, Mihaljevic T, Laurence RG, Dor DM, Cohn LH, Bawendi MG, Frangioni JV (2004) Near-infrared fluorescent type II quantum dots for sentinel lymph node mapping. Nat Biotech 22(1):93–97
4. Larson DR, Zipfel WR, Williams RM, Clark SW, Bruchez MP, Wise FW, Webb WW (2003) Water - soluble quantum dots for multiphoton fluorescence imaging in vivo. Science 300(5624): 1434–1436
5. Mattoussi H, Mauro JM, Goldman ER, Anderson GP, Sundar VC, Mikulec FV, Bawendi MG (2000) Self-assembly of CdSe−ZnS quantum dot bioconjugates using an engineered recombinant protein. J Am Chem Soc 122(49):12142–12150
6. Derfus AM, Chan WCW, Bhatia SN (2003) Probing the Cytotoxicity of Semiconductor quantum dots. Nano Lett 4(1):11–18
7. Vinegoni C, Razansky D, Hilderbrand SA, Shao FW, Ntziachristos V, Weissleder R (2009) Transillumination fluorescence imaging in mice using biocompatible upconverting nanoparticles. Opt Lett 34(17):2566–2568
8. Xu CT, Svensson N, Axelsson J, Svenmarker P, Somesfalean G, Chen GY, Liang HJ, Liu HC, Zhang ZG, Andersson-Engels S (2008) Autofluorescence insensitive imaging using upconverting nanocrystals in scattering media. Appl Phys Lett 93(17):171103–171103-3
9. Lim SF, Riehn R, Ryu WS, Khanarian N, Tung CK, Tank D, Austin RH (2006) In vivo and scanning electron microscopy imaging of upconverting nanophosphors in Caenorhabditis elegans. Nano Lett 6(2):169–174
10. Gai S, Yang P, Li C, Wang W, Dai Y, Niu N, Lin J (2010) Synthesis of Magnetic, Up-Conversion Luminescent, and Mesoporous Core–Shell-Structured Nanocomposites as Drug Carriers. Adv Funct Mater 20(7):1166–1172
11. Xing H, Bu W, Zhang S, Zheng X, Li M, Chen F, He Q, Zhou L, Peng W, Hua Y, Shi J (2012) Multifunctional nanoprobes for upconversion fluorescence, MR and CT trimodal imaging. Biomaterials 33(4):1079–1089
12. Zhou J, Yu M, Sun Y, Zhang X, Zhu X, Wu Z, Wu D, Li F (2011) Fluorine-18-labeled Gd3+/Yb3+/Er3+ co-doped NaYF4 nanophosphors for multimodality PET/MR/UCL imaging. Biomaterials 32(4):1148–1156
13. Chao Wang LC, Liu Z (2011) Drug delivery with upconversion nanoparticles for multi-functional targeted cancer cell imaging and therapy. Biomaterials 32(4):1110–1120
14. Qian HS, Guo HC, Ho PC-L, Mahendran R, Zhang Y (2009) Mesoporous-Silica-Coated Up-Conversion Fluorescent Nanoparticles for Photodynamic Therapy. Small 5(20):2285–2290
15. Wang C, Tao H, Cheng L, Liu Z (2011) Near-infrared light induced in vivo photodynamic therapy of cancer based on upconversion nanoparticles. Biomaterials 32(26):6145–6154
16. Cheng L, Yang K, Li Y, Chen J, Wang C, Shao M, Lee ST, Liu Z (2011) Facile preparation of multifunctional upconversion nanoprobes for multimodal imaging and dual-targeted photothermal therapy. Angew Chem Int Ed Engl 50(32):7385–7390
17. Mader HS, Kele P, Saleh SM, Wolfbeis OS (2010) Upconverting luminescent nanoparticles for use in bioconjugation and bioimaging. Curr Opin Chem Biol 14(5):582–596
18. Deren PJ, Strek W, Zych E, Drozdzynski J (2000) Up-conversion in elpasolite crystals doped with U3+. Chem Phys Lett 332(3):308–312
19. Stump NA, Murray GM, Delcul GD, Haire RG, Peterson JR (1993) Stokes and anti-stokes luminescence from the Trihalides of CM-248. Radiochim Acta 61(3–4):129–136
20. Auzel F (2003) Upconversion and anti-stokes processes with f and d ions in solids. Chem Rev 104(1):139–174
21. Chen G, Ohulchanskyy TY, Kumar R, Agren H, Prasad PN (2010) Ultrasmall monodisperse NaYF(4):Yb(3+)/Tm(3+) nanocrystals

with enhanced near-infrared to near-infrared upconversion photoluminescence. ACS Nano 4(6):3163–3168
22. Dou Q, Zhang Y (2011) Tuning of the structure and emission spectra of upconversion nanocrystals by alkali ion doping. Langmuir 27(21):13236–13241
23. Patra A, Friend CS, Kapoor R, Prasad PN (2002) Upconversion in Er3+:ZrO2 Nanocrystals. J Phys Chem B 106(8):1909–1912
24. Yi GS, Chow GM (2006) Synthesis of Hexagonal-Phase NaYF4: Yb, Er and NaYF4:Yb, Tm Nanocrystals with Efficient Up-Conversion Fluorescence. Adv Funct Mater 16(18):2324–2329
25. Ang LY, Lim ME, Ong LC, Zhang Y (2011) Applications of upconversion nanoparticles in imaging, detection and therapy. Nanomedicine-UK 6(7):1273–1288
26. Suyver JF, Grimm J, Krämer KW, Güdel HU (2005) Highly efficient near-infrared to visible up-conversion process in. J Lumin 114(1):53–59
27. Babu S, Cho J-H, Dowding JM, Heckert E, Komanski C, Das S, Colon J, Baker CH, Bass M, Self WT, Seal S (2010) Multicolored redox active upconverter cerium oxide nanoparticle for bio-imaging and therapeutics. Chem Commun 46(37):6915–6917
28. Cho JH, Bass M, Babu S, Dowding JM, Self WT, Seal S (2012) Up conversion luminescence of Yb3+-Er3+ codoped CeO2 nanocrystals with imaging applications. J Lumin 132(3):743–749
29. Lopez-Luke T, de la Rosa E, Gonzalez-Yebra AL, Gonzalez-Yebra B, Angeles-Chavez C, Solis D, Salas P, Saldana C, Meza O (2010) Synthesis and characterization of up-conversion emission on lanthanides doped ZrO(2) nanocrystals coated with SiO(2) for biological applications. In: Achilefu S, Raghavachari R (eds) Reporters, Markers, Dyes, Nanoparticles, and Molecular Probes for Biomedical Applications Ii, vol 7576. Proceedings of SPIE-The International Society for Optical Engineering. Spie-Int Soc Optical Engineering, Bellingham. doi:10.1117/12.842993
30. Yang DM, Dai YL, Ma PA, Kang XJ, Shang MM, Cheng ZY, Li CX, Lin J (2012) Synthesis of Li1-xNaxYF4:Yb3+/Ln(3+) (0<= x <= 0.3, Ln=Er, Tm, Ho) nanocrystals with multicolor upconversion luminescence properties for in vitro cell imaging. J Mater Chem 22(38):20618–20625
31. Islangulov RR, Castellano FN (2006) Photochemical Upconversion: Anthracene Dimerization Sensitized to Visible Light by a RuII Chromophore. Angew Chem Int Ed 45(36): 5957–5959
32. Ji S, Guo H, Wu W, Wu W, Zhao J (2011) Ruthenium(II) Polyimine–Coumarin Dyad with Non-emissive 3IL Excited State as Sensitizer for Triplet–Triplet Annihilation Based Upconversion. Angew Chem Int Ed 50(36):8283–8286
33. Khnayzer RS, Blumhoff J, Harrington JA, Haefele A, Deng F, Castellano FN (2012) Upconversion- powered photoelectrochemistry. Chem Commun 48(2):209–211
34. Singh-Rachford TN, Castellano FN (2008) Pd(II) Phthalocyanine-Sensitized Triplet−Triplet Annihilation from Rubrene. J Phys Chem A 112(16):3550–3556
35. Singh-Rachford TN, Haefele A, Ziessel R, Castellano FN (2008) Boron dipyrromethene chromophores: next generation triplet acceptors/annihilators for low power upconversion schemes. J Am Chem Soc 130(48):16164–16165
36. Islangulov RR, Lott J, Weder C, Castellano FN (2007) Noncoherent Low-Power Upconversion in Solid Polymer Films. J Am Chem Soc 129(42):12652–12653
37. Singh-Rachford TN, Lott J, Weder C, Castellano FN (2009) Influence of Temperature on Low-Power Upconversion in Rubbery Polymer Blends. J Am Chem Soc 131(33):12007–12014
38. Liu Q, Yang T, Feng W, Li F (2012) Blue-emissive upconversion nanoparticles for low-power-excited bioimaging in vivo. J Am Chem Soc 134(11):5390–5397
39. Liu Q, Yin B, Yang T, Yang Y, Shen Z, Yao P, Li F (2013) A general strategy for biocompatible, high-effective upconversion nanocapsules based on triplet–triplet annihilation. J Am Chem Soc 135(13):5029–5037
40. Pelle F, Dhaouadi M, Michely L, Aschehoug P, Toncelli A, Veronesi S, Tonelli M (2011) Spectroscopic properties and upconversion in Pr3+:YF3 nanoparticles. PCCP 13(39):17453–17460
41. Qin F, Zheng Y, Yu Y, Zheng C, Tayebi PS, Zhang Z, Cao W (2011) Ultraviolet upconversion luminescence of Gd3+ from Ho3+ and Gd3+ codoped oxide ceramic induced by 532-nm CW laser excitation. Opt Commun 284(12):3114–3117
42. Nadort A, Sreenivasan VKA, Song Z, Grebenik EA, Nechaev AV, Semchishen VA, Panchenko VY, Zvyagin AV (2013) Quantitative imaging of single upconversion nanoparticles in biological tissue. PLos One 8(5):263292
43. Chatterjee DK, Rufaihah AJ, Zhang Y (2008) Upconversion fluorescence imaging of cells and small animals using lanthanide doped nanocrystals. Biomaterials 29(7):937–943
44. Nam SH, Bae YM, Park YI, Kim JH, Kim HM, Choi JS, Lee KT, Hyeon T, Suh YD (2011) Long-term real-time tracking of lanthanide ion doped upconverting nanoparticles in living cells. Angew Chem Int Ed 50(27):6093–6097
45. Park YI, Kim JH, Lee KT, Jeon K-S, Na HB, Yu JH, Kim HM, Lee N, Choi SH, Baik S-I, Kim H, Park SP, Park B-J, Kim YW, Lee SH, Yoon S-Y, Song IC, Moon WK, Suh YD, Hyeon T (2009) Nonblinking and nonbleaching upconverting nanoparticles as an optical imaging nanoprobe and T1 magnetic resonance imaging contrast agent. Adv Mater 21(44):4467–4471
46. Dong B, Cao B, He Y, Liu Z, Li Z, Feng Z (2012) Temperature sensing and in vivo imaging by molybdenum sensitized visible upconversion luminescence of rare-earth oxides. Adv Mater 24(15):1987–1993
47. Patra A, Friend CS, Kapoor R, Prasad PN (2003) Fluorescence upconversion properties of Er3+-Doped TiO2 and BaTiO3 nanocrystallites. Chem Mater 15(19):3650–3655
48. Wang X, Kong XG, Shan GY, Yu Y, Sun YJ, Feng LY, Chao KF, Lu SZ, Li YJ (2004) Luminescence spectroscopy and visible upconversion properties of Er3+ in ZnO nanocrystals. J Phys Chem B 108(48):18408–18413
49. Venkatramu V, Falcomer D, Speghini A, Bettinelli M, Jayasankar CK (2008) Synthesis and luminescence properties of Er3+-doped Lu3Ga5O12 nanocrystals. J Lumin 128(5–6):811–813
50. Venkatramu V, Leon-Luis SF, Rodriguez-Mendoza UR, Monteseguro V, Manjon FJ, Lozano-Gorrin AD, Valiente R, Navarro-Urrios D, Jayasankar CK, Munoz A, Lavin V (2012) Synthesis, structure and luminescence of Er3+-doped Y3Ga5O12 nano-garnets. J Mater Chem 22(27):13788–13799
51. Kumar KU, Vijaya N, Oliva J, Jacinto C, de La Rosa E, Jayasankar CK (2012) Multicolor upconversion emission and color tunability in Tm3+/Er3+/Yb3+ Tr-Doped NaNbO3 Nanocrystals. Materials Express 2(4):294–302
52. Guo H, Dong N, Yin M, Zhang WP, Lou LR, Xia SD (2004) Visible upconversion in rare earth ion-doped Gd2O3 nanocrystals. J Phys Chem B 108(50):19205–19209
53. Rai M, Mishra K, Singh SK, Verma RK, Rai SB (2012) Infrared to visible upconversion in Ho3+/Yb3+ co-doped Y2O3 phosphor: Effect of laser input power and external temperature. Spectrochim Acta A 97:825–829
54. Li DY, Wang YX, Zhang XR, Shi G, Liu G, Song YL (2013) White upconversion emission in Yb3+/Tm3+/Ho3+ doped SrMoO4 nanocrystals by high excited state energy transfer. J Alloys Compd 550:509–513
55. Stouwdam JW, van Veggel FCJM (2002) Near-infrared Emission of Redispersible Er3+, Nd3+, and Ho3+ Doped LaF3 Nanoparticles. Nano Lett 2(7):733–737
56. Yi G-S, Chow G-M (2005) Colloidal LaF3:Yb, Er, LaF3:Yb, Ho and LaF3:Yb, Tm nanocrystals with multicolor upconversion fluorescence. J Mater Chem 15(41):4460–4464

57. Heer S, Kömpe K, Güdel HU, Haase M (2004) Highly efficient multicolour upconversion emission in transparent colloids of lanthanide-doped NaYF4 Nanocrystals. Adv Mater 16(23–24): 2102–2105
58. Heer S, Lehmann O, Haase M, Güdel H-U (2003) Blue, green, and red upconversion emission from lanthanide-doped LuPO4 and YbPO4 nanocrystals in a transparent colloidal solution. Angew Chem Int Ed 42(27):3179–3182
59. Yi G, Lu H, Zhao S, Ge Y, Yang W, Chen D, Guo L-H (2004) Synthesis, characterization, and biological application of size-controlled nanocrystalline NaYF4:Yb, Er Infrared-to-visible up-conversion phosphors. Nano Lett 4(11):2191–2196
60. Zhang Y-W, Sun X, Si R, You L-P, Yan C-H (2005) Single-crystalline and monodisperse LaF3 triangular nanoplates from a single-source precursor. J Am Chem Soc 127(10):3260–3261
61. Yin A, Zhang Y, Sun L, Yan C (2010) Colloidal synthesis and blue based multicolor upconversion emissions of size and composition controlled monodisperse hexagonal NaYF4: Yb, Tm nanocrystals. Nanoscale 2(6):953–959
62. Mai H-X, Zhang Y-W, Si R, Yan Z-G, L-d S, You L-P, Yan C-H (2006) High-quality sodium rare-earth fluoride nanocrystals: controlled synthesis and optical properties. J Am Chem Soc 128(19): 6426–6436
63. Mai H-X, Zhang Y-W, Sun L-D, Yan C-H (2007) Highly Efficient Multicolor Up-Conversion Emissions and Their Mechanisms of Monodisperse NaYF4:Yb, Er Core and Core/Shell-Structured Nanocrystals. J Phys Chem C 111(37):13721–13729
64. Liu Q, Sun Y, Yang T, Feng W, Li C, Li F (2011) Sub-10 nm hexagonal lanthanide-doped NaLuF4 upconversion nanocrystals for sensitive bioimaging in vivo. J Am Chem Soc 133(43):17122–17125
65. Boyer J-C, Vetrone F, Cuccia LA, Capobianco JA (2006) Synthesis of Colloidal Upconverting NaYF4 Nanocrystals Doped with Er3+, Yb3+ and Tm3+, Yb3+ via Thermal Decomposition of Lanthanide Trifluoroacetate Precursors. J Am Chem Soc 128(23):7444–7445
66. Boyer J-C, Cuccia LA, Capobianco JA (2007) Synthesis of Colloidal Upconverting NaYF4: Er3+/Yb3+ and Tm3+/Yb3+ Monodisperse Nanocrystals. Nano Lett 7(3):847–852
67. Naccache R, Vetrone F, Mahalingam V, Cuccia LA, Capobianco JA (2009) Controlled synthesis and water dispersibility of hexagonal Phase NaGdF4:Ho3+/Yb3+ nanoparticles. Chem Mater 21(4):717–723
68. Vetrone F, Mahalingam V, Capobianco JA (2009) Near-Infrared-to-blue upconversion in colloidal BaYF5:Tm3+, Yb3+ nanocrystals. Chem Mater 21(9):1847–1851
69. Vetrone F, Naccache R, Mahalingam V, Morgan CG, Capobianco JA (2009) The active -core/active-shell approach: a strategy to enhance the upconversion luminescence in lanthanide-doped nanoparticles. Adv Funct Mater 19(18):2924–2929
70. He M, Huang P, Zhang CL, Hu HY, Bao CC, Gao G, He R, Cui DX (2011) Dual phase-controlled synthesis of uniform lanthanide-doped NaGdF4 upconversion nanocrystals Via an OA/Ionic liquid two-phase system for in vivo dual-modality imaging. Adv Funct Mater 21(23):4470–4477
71. Huang WJ, Ding MY, Huang HM, Jiang CF, Song Y, Ni YR, Lu CH, Xu ZZ (2013) Uniform NaYF4N:Yb, Tm hexagonal submicroplates: controlled synthesis and enhanced UV and blue upconversion luminescence. Mater Res Bull 48(2):300–304
72. Huang WJ, Lu CH, Song Y, Huang HM, Wang YQ, Ni YR, Xu ZZ (2012) Controlled Synthesis and Upconversion Luminescence Properties of Yb3+-Tm3+ codoped NaYF4 Hexagonal Submicroplates. In: Kao JCM, Hou M, Chen R (eds) Frontier of Nanoscience and Technology Ii, vol 528, Advanced Materials Research. Trans Tech Publications Ltd, Stafa-Zurich, pp 117–120
73. Karvianto CGM (2011) The effects of surface and surface coatings on fluorescence properties of hollow NaYF4:Yb, Er upconversion nanoparticles. J Mater Res 26(1):70–81
74. Liu Q, Chen M, Sun Y, Chen G, Yang T, Gao Y, Zhang X, Li F (2011) Multifunctional rare-earth self-assembled nanosystem for tri-modal upconversion luminescence/fluorescence/positron emission tomography imaging. Biomaterials 32(32):8243–8253
75. Pires AM, Serra OA, Heer S, Gudel HU (2005) Low-temperature upconversion spectroscopy of nanosized Y2O3 : Er,Yb phosphor. J Appl Phys 98(6):063529–063529-7
76. Yang D, Li C, Li G, Shang M, Kang X, Lin J (2011) Colloidal synthesis and remarkable enhancement of the upconversion luminescence of BaGdF5:Yb3+/Er3+ nanoparticles by active-shell modification. J Mater Chem 21(16):5923–5927
77. Wei Y, Lu FQ, Zhang XR, Chen DP (2008) Polyol-mediated synthesis and luminescence of lanthanide-doped NaYF4 nanocrystal upconversion phosphors. J Alloys Compd 455(1–2):376–384
78. Wang L, Li Y (2007) Controlled Synthesis and Luminescence of Lanthanide Doped NaYF4 Nanocrystals. Chem Mater 19(4):727–734
79. Zhang F, Wan Y, Yu T, Zhang F, Shi Y, Xie S, Li Y, Xu L, Tu B, Zhao D (2007) Uniform nanostructured arrays of sodium rare-earth fluorides for highly efficient multicolor upconversion luminescence. Angew Chem Int Ed 46(42):7976–7979
80. Jin J, Gu YJ, Man CW, Cheng J, Xu Z, Zhang Y, Wang H, Lee VH, Cheng SH, Wong WT (2011) Polymer-coated NaYF(4):Yb(3)(+), Er(3)(+) upconversion nanoparticles for charge-dependent cellular imaging. ACS Nano 5(10):7838–7847
81. Yang D, Kang X, Ma P, Dai Y, Hou Z, Cheng Z, Li C, Lin J (2013) Hollow structured upconversion luminescent NaYF(4):Yb(3)(+), Er(3)(+) nanospheres for cell imaging and targeted anti-cancer drug delivery. Biomaterials 34(5):1601–1612
82. Zhao JW, Liu XM, Cui D, Sun YJ, Yu Y, Yang YF, Du C, Wang Y, Song K, Liu K, Lu SZ, Kong XG, Zhang H (2010) A Facile Approach to Fabrication of Hexagonal-Phase NaYF4:Yb3+, Er3+ Hollow nanospheres: formation mechanism and upconversion luminescence. Eur J Inorg Chem 12:1813–1819
83. Liang YJ, Chui PF, Sun XN, Zhao Y, Cheng FM, Sun KN (2013) Hydrothermal synthesis and upconversion luminescent properties of YVO4:Yb3+, Er3+ nanoparticles. J Alloys Compd 552:289–293
84. Gao G, Zhang CL, Zhou ZJ, Zhang X, Ma JB, Li C, Jin WL, Cui DX (2013) One-pot hydrothermal synthesis of lanthanide ions doped one-dimensional upconversion submicrocrystals and their potential application in vivo CT imaging. Nanoscale 5(1):351–362
85. Liu Z, Sun LN, Li FY, Liu Q, Shi LY, Zhang DS, Yuan S, Liu T, Qiu YN (2011) One-pot self-assembly of multifunctional mesoporous nanoprobes with magnetic nanoparticles and hydrophobic upconversion nanocrystals. J Mater Chem 21(44):17615–17618
86. Wong H-T, Tsang M-K, Chan C-F, Wong K-L, Fei B, Hao J (2013) In vitro cell imaging using multifunctional small sized KGdF4: Yb3+, Er3+ upconverting nanoparticles synthesized by a one-pot solvothermal process. Nanoscale 5(8):3465–3473
87. Wang J, Bo S, Song L, Hu J, Liu X, Zhen Z (2007) One-step synthesis of highly water-soluble LaF 3:Ln 3+ nanocrystals in methanol without using any ligands. Nanotechnology 18(46): 465606
88. Wei Y, Lu FQ, Zhang XR, Chen DP (2007) Polyol-mediated synthesis of water-soluble LaF3: Yb, Er upconversion fluorescent nanocrystals. Mater Lett 61(6):1337–1340
89. Hu D, Chen M, Gao Y, Li F, Wu L (2011) A facile method to synthesize superparamagnetic and up-conversion luminescent NaYF4:Yb, Er/Tm@SiO2@Fe3O4 nanocomposite particles and their bioapplication. J Mater Chem 21(30):11276–11282
90. Lu H, Yi G, Zhao S, Chen D, Guo L-H, Cheng J (2004) Synthesis and characterization of multi-functional nanoparticles possessing magnetic, up-conversion fluorescence and bio-affinity properties. J Mater Chem 14(8):1336–1341
91. Zeng JH, Li ZH, Su J, Wang L, Yan R, Li Y (2006) Synthesis of complex rare earth fluoride nanocrystal phosphors. Nanotechnology 17(14):3549–3555

92. Zeng JH, Su J, Li ZH, Yan RX, Li YD (2005) Synthesis and upconversion luminescence of hexagonal-phase NaYF4:Yb, Er3+ Phosphors of controlled size and morphology. Adv Mater 17(17): 2119–2123
93. Ghosh P, de la Rosa E, Oliva J, Solis D, Kar A, Patra A (2009) Influence of surface coating on the upconversion emission properties of LaPO4:Yb/Tm core-shell nanorods. J Appl Phys 105(11): 113532–113535
94. Li C, Quan Z, Yang J, Yang P, Lin J (2007) Highly Uniform and Monodisperse β-NaYF4:Ln3+ (Ln=Eu, Tb, Yb/Er, and Yb/Tm) Hexagonal Microprism Crystals: Hydrothermal Synthesis and Luminescent Properties. Inorg Chem 46(16):6329–6337
95. Ma DK, Huang SM, Yu YY, Xu YF, Dong YQ (2009) Rare-earth-ion-doped hexagonal-phase NaYF4 nanowires: controlled synthesis and luminescent properties. J Phys Chem C 113(19):8136–8142
96. Wang ZL, Hao JH, Chan HLW (2010) Down- and up-conversion photoluminescence, cathodolu- minescence and paramagnetic properties of NaGdF4: Yb3+, Er3+ submicron disks assembled from primary nanocrystals. J Mater Chem 20(16):3178–3185
97. Zhao J, Sun Y, Kong X, Tian L, Wang Y, Tu L, Zhao J, Zhang H (2008) Controlled synthesis, formation mechanism, and great enhancement of red upconversion luminescence of NaYF4:Yb3+, Er3+ nanocrystals/submicroplates at low doping level. J Phys Chem B 112(49):15666–15672
98. Yang D, Dai Y, Ma P, Kang X, Cheng Z, Li C, Lin J (2013) One-Step Synthesis of Small-Sized and Water-Soluble NaREF(4) upconversion nanoparticles for in vitro cell imaging and drug delivery. Chem-Eur J 19(8):2685–2694
99. Sikora B, Fronc K, Kaminska I, Koper K, Szewczyk S, Paterczyk B, Wojciechowski T, Sobczak K, Minikayev R, Paszkowicz W, Stepien P, Elbaum D (2013) Transport of NaYF4:Er3+, Yb3+ upconverting nanoparticles into HeLa cells. Nanotechnology 24(23): 235702
100. Yang J, Shen D, Li X, Li W, Fang Y, Wei Y, Yao C, Tu B, Zhang F, Zhao D (2012) One-step hydrothermal synthesis of carboxyl-functionalized upconversion phosphors for bioapplications. Chem-Eur J 18(43):13642–13650
101. Wang ZL, Hao J, Chan HLW, Law GL, Wong WT, Wong KL, Murphy MB, Su T, Zhang ZH, Zeng SQ (2011) Simultaneous synthesis and functionalization of water-soluble up-conversion nanoparticles for in-vitro cell and nude mouse imaging. Nanoscale 3(5):2175–2181
102. Gao Y, Cao TY, Li FY (2012) Water-soluble upconversion nanophosphors with cooperative ligands for in vivo lymph node imaging. Chinese J Inorg Chem 28(10):2043–2048
103. Wang M, Mi CC, Liu JL, Wu XL, Zhang YX, Hou W, Li F, Xu SK (2009) One-step synthesis and characterization of water-soluble NaYF4:Yb, Er/Polymer nanoparticles with efficient up-conversion fluorescence. J Alloys Compd 485(1–2):L24–L27
104. Wang Z, Liu CH, Chang LJ, Li ZP (2012) One-pot synthesis of water-soluble and carboxyl- functionalized beta-NaYF4:Yb, Er(Tm) upconversion nanocrystals and their application for bioimaging. J Mater Chem 22(24):12186–12192
105. Cao T, Yang Y, Gao Y, Zhou J, Li Z, Li F (2011) High-quality water-soluble and surface-functionalized upconversion nanocrystals as luminescent probes for bioimaging. Biomaterials 32(11):2959–2968
106. Chen C, Sun LD, Li ZX, Li LL, Zhang J, Zhang YW, Yan CH (2010) Ionic liquid-based route to spherical NaYF4 nanoclusters with the assistance of microwave radiation and their multicolor upconversion luminescence. Langmuir 26(11):8797–8803
107. Liu X, Zhao J, Sun Y, Song K, Yu Y, Du C, Kong X, Zhang H (2009) Ionothermal synthesis of hexagonal-phase NaYF(4):Yb(3+), Er(3+)/Tm(3+) upconversion nanophosphors. Chem Commun 43: 6628–6630
108. Chen Z, Chen H, Hu H, Yu M, Li F, Zhang Q, Zhou Z, Yi T, Huang C (2008) Versatile synthesis strategy for carboxylic acid − functionalized upconverting nanophosphors as biological labels. J Am Chem Soc 130(10):3023–3029
109. Hu H, Yu M, Li F, Chen Z, Gao X, Xiong L, Huang C (2008) Facile epoxidation strategy for producing amphiphilic up-converting rare-earth nanophosphors as biological labels. Chem Mater 20(22): 7003–7009
110. Chen K, Huang X, Wei H, Tang X (2013) Fabrication of core/shell structured NaYF4:Yb3+, Er3+/polyphosphazene upconversion nanophosphors functionalized with abundant active amino groups. Mater Lett 101(15):54–56
111. Gao X, Cui Y, Levenson RM, Chung LWK, Nie S (2004) In vivo cancer targeting and imaging with semiconductor quantum dots. Nat Biotech 22(8):969–976
112. Jingning Shan JC, Juan M, Josh C, Wole S (2008) Biofunctionalization, cytotoxicity, and cell uptake of lanthanide doped hydrophobically ligated NaYF4 upconversion nanophosphors. J Appl Phys 104(9):094308–094308-7
113. Luccardini C, Tribet C, Vial F, Marchi-Artzner V, Dahan M (2006) Size, charge, and interactions with giant lipid vesicles of quantum dots coated with an amphiphilic macromolecule. Langmuir 22(5): 2304–2310
114. Decher G (1997) Fuzzy nanoassemblies: toward layered polymeric multicomposites. Science 277(5330):1232–1237
115. Hong X, Li J, Wang M, Xu J, Guo W, Li J, Bai Y, Li T (2004) Fabrication of magnetic luminescent nanocomposites by a layer-by-layer self-assembly approach. Chem Mater 16(21):4022–4027
116. Wang D, Rogach AL, Caruso F (2002) Semiconductor quantum dot-labeled microsphere bioconjugates prepared by stepwise self-assembly. Nano Lett 2(8):857–861
117. Wang L, Yan R, Huo Z, Wang L, Zeng J, Bao J, Wang X, Peng Q, Li Y (2005) Fluorescence resonant energy transfer biosensor based on upconversion-luminescent nanoparticles. Angew Chem Int Ed 44(37):6054–6057
118. Zhang P, Rogelj S, Nguyen K, Wheeler D (2006) Design of a highly sensitive and specific nucleotide sensor based on photon upconverting particles. J Am Chem Soc 128(38):12410–12411
119. Abdul Jalil R, Zhang Y (2008) Biocompatibility of silica coated NaYF(4) upconversion fluorescent nanocrystals. Biomaterials 29(30):4122–4128
120. Das GK, Tan TTY (2008) Rare-earth-doped and codoped Y 2O 3 nanomaterials as potential bioimaging probes. J Phys Chem C 112(30):11211–11217
121. Mader HS, Link M, Achatz DE, Uhlmann K, Li X, Wolfbeis OS (2010) Surface-modified upconverting microparticles and nanoparticles for use in click chemistries. Chem-Eur J 16(18):5416–5424. doi:10.1002/chem.201000117
122. Sivakumar S, Diamente PR, van Veggel FCJM (2006) Silica-coated Ln3+-Doped LaF3 nanoparticles as robust down- and upconverting biolabels. Chem-Eur J 12(22):5878–5884
123. Sisi C, Haiyan C, Yueqing G (2011) Comparison of two strategies for the synthesis of upconverting nanoparticles as biological labels. J Phys Conf Ser 277(1):012006
124. Zhang QB, Song K, Zhao JW, Kong XG, Sun YJ, Liu XM, Zhang YL, Zeng QH, Zhang H (2009) Hexanedioic acid mediated surface-ligand-exchange process for transferring NaYF4:Yb/Er (or Yb/Tm) up-converting nanoparticles from hydrophobic to hydrophilic. J Colloid Interface Sci 336(1):171–175
125. Kumar R, Nyk M, Ohulchanskyy TY, Flask CA, Prasad PN (2009) Combined optical and MR bioimaging using rare earth ion doped NaYF4 nanocrystals. Adv Funct Mater 19(6):853–859
126. Nyk M, Kumar R, Ohulchanskyy TY, Bergey EJ, Prasad PN (2008) High contrast in vitro and in vivo photoluminescence bioimaging using near infrared to near infrared up-conversion in Tm3+ and Yb3+ Doped Fluoride Nanophosphors. Nano Lett 8(11):3834–3838

127. Chen Q, Wang X, Chen F, Zhang Q, Dong B, Yang H, Liu G, Zhu Y (2011) Functionalization of upconverted luminescent NaYF4: Yb/Er nanocrystals by folic acid-chitosan conjugates for targeted lung cancer cell imaging. J Mater Chem 21(21): 7661–7667
128. Wu ZN, Guo CR, Liang S, Zhang H, Wang LP, Sun HC, Yang B (2012) A pluronic F127 coating strategy to produce stable up-conversion NaYF4:Yb, Er(Tm) nanoparticles in culture media for bioimaging. J Mater Chem 22(35):18596–18602
129. Zhan Q, Qian J, Liang H, Somesfalean G, Wang D, He S, Zhang Z, Andersson-Engels S (2011) Using 915 nm laser excited Tm(3)+/Er(3)+/Ho(3)+- doped NaYbF4 upconversion nanoparticles for in vitro and deeper in vivo bioimaging without overheating irradiation. ACS Nano 5(5):3744–3757
130. Tianye Cao TY, Gao Y, Yang Y, He H, Li F (2010) Water-soluble NaYF4:Yb/Er upconver- sion nanophosphors: synthesis, characteristics and application in bioimaging. Inorg Chem Commun 13(3): 392–394
131. Wu S, Han G, Milliron DJ, Aloni S, Altoe V, Talapin DV, Cohen BE, Schuck PJ (2009) Non-blinking and photostable upconverted luminescence from single lanthanide-doped nanocrystals. Proc Natl Acad Sci U S A 106(27):10917–10921
132. Bogdan N, Vetrone F, Roy R, Capobianco JA (2010) Carbohydrate-coated lanthanide-doped upconverting nanoparticles for lectin recognition. J Mater Chem 20(35):7543–7550
133. Yi G, Peng Y, Gao Z (2011) Strong Red-Emitting near-Infrared-to-Visible upconversion fluorescent nanoparticles. Chem Mater 23(11):2729–2734
134. Dong B, Xu S, Sun J, Bi S, Li D, Bai X, Wang Y, Wang L, Song H (2011) Multifunctional NaYF4: Yb3+, Er3+@Ag core/shell nanocomposites: integration of upconversion imaging and photothermal therapy. J Mater Chem 21(17):6193–6200
135. Li D, Dong B, Bai X, Wang Y, Song H (2010) Influence of the TGA modification on upconversion luminescence of hexagonal-phase NaYF4:Yb3+, Er3+ Nanoparticles. J Phys Chem C 114(18):8219–8226
136. Liebherr RB, Soukka T, Wolfbeis OS, Gorris HH (2012) Maleimide activation of photon upconverting nanoparticles for bioconjugation. Nanotechnology 23(48):485103
137. Dong A, Ye X, Chen J, Kang Y, Gordon T, Kikkawa JM, Murray CB (2011) A generalized ligand-exchange strategy enabling sequential surface functionalization of colloidal nanocrystals. J Am Chem Soc 133(4):998–1006
138. Esipova TV, Ye XC, Collins JE, Sakadzic S, Mandeville ET, Murray CB, Vinogradov SA (2012) Dendritic upconverting nanoparticles enable in vivo multiphoton microscopy with low-power continuous wave sources. Proc Natl Acad Sci U S A 109(51): 20826–20831
139. Zhou H-P, Xu C-H, Sun W, Yan C-H (2009) Clean and Flexible Modification Strategy for Carboxyl/Aldehyde-Functionalized Upconversion Nanoparticles and Their Optical Applications. Adv Funct Mater 19(24):3892–3900
140. Cheng L, Yang K, Chen Q, Liu Z (2012) Organic stealth nanoparticles for highly effective in vivo near-infrared photothermal therapy of cancer. ACS Nano 6(6):5605–5613
141. Liu Q, Li C, Yang T, Yi T, Li F (2010) "Drawing" upconversion nanophosphors into water through host-guest interaction. Chem Commun 46(30):5551–5553
142. Wang M, Liu JL, Zhang YX, Hou W, Wu XL, Xu SK (2009) Two-phase solvothermal synthesis of rare-earth doped NaYF4 upconversion fluorescent nanocrystals. Mater Lett 63(2):325–327
143. Bogdan N, Vetrone F, Ozin GA, Capobianco JA (2011) Synthesis of ligand-free colloidally stable water dispersible brightly luminescent lanthanide-doped upconverting nanoparticles. Nano Lett 11(2): 835–840
144. Yi GS, Chow GM (2006) Water-Soluble NaYF4:Yb, Er(Tm)/NaYF4/Polymer core/shell/shell nanopartic- les with Significant Enhancement of Upconversion Fluorescence. Chem Mater 19(3):341–343
145. Budijono SJ, Shan J, Yao N, Miura Y, Hoye T, Austin RH, Ju Y, Prud'homme RK (2009) Synthesis of Stable Block-Copolymer-Protected NaYF4:Yb3+, Er3+ Up-Converting Phosphor Nanoparticles. Chem Mater 22(2):311–318
146. Shan J, Budijono SJ, Hu G, Yao N, Kang Y, Ju Y, Prud'homme RK (2011) Pegylated composite nanoparticles containing upconverting phosphors and meso-tetraphenyl porphine (TPP) for Photodynamic Therapy. Adv Funct Mater 21(13):2488–2495
147. Cheng L, Yang K, Zhang S, Shao M, Lee S, Liu Z (2010) Highly-sensitive multiplexed in vivo imaging using pegylated upconversion nanoparticles. Nano Res 3(10):722–732
148. Kobayashi H, Kosaka N, Ogawa M, Morgan NY, Smith PD, Murray CB, Ye X, Collins J, Kumar GA, Bell H, Choyke PL (2009) In vivo multiple color lymphatic imaging using upconverting nanocrystals. J Mater Chem 19(36):6481–6484
149. Li Z, Zhang Y (2006) Monodisperse Silica-Coated Polyvinylpyrrolidone/NaYF4 Nanocrystals with Multicolor upconversion fluorescence emission. Angew Chem Int Ed 45(46):7732–7735
150. Zako T, Nagata H, Terada N, Utsumi A, Sakono M, Yohda M, Ueda H, Soga K, Maeda M (2009) Cyclic RGD peptide-labeled upconversion nanophosphors for tumor cell-targeted imaging. Biochem Biophys Res Commun 381(1):54–58
151. Hu H, Xiong L, Zhou J, Li F, Cao T, Huang C (2009) Multimodal-luminescence core–shell nanocomposites for targeted imaging of tumor cells. Chem-Eur J 15(14):3577–3584
152. Wilhelm S, Hirsch T, Patterson WM, Scheucher E, Mayr T, Wolfbeis OS (2013) Multicolor upconversion nanoparticles for protein conjugation. Theranostics 3(4):239–248
153. Li F, Li C, Liu X, Bai T, Dong W, Zhang X, Shi Z, Feng S (2013) Microwave-assisted synthesis and up–down conversion luminescent properties of multicolor hydrophilic LaF3:Ln3+ nanocrystals. Dalton Trans 42 (6):2015–2022
154. Murugana AV, Viswanath AK, Ravi V, Kakade A, Saaminathan V (2006) Photoluminescence studies of Eu3+ doped Y2O3 nanophosphor prepared by microwave hydrothermal method. Appl Phys Lett 89(12):123120
155. Patra CR, Alexandra G, Patra S, Jacob DS, Gedanken A, Landau A, Gofer Y (2005) Microwave approach for the synthesis of rhabdophane-type lanthanide orthophosphate (Ln=La, Ce, Nd, Sm, Eu, Gd and Tb) nanorods under solvothermal conditions. New J Chem 29(5):733–739
156. Qin X, Yokomori T, Ju YG (2007) Flame synthesis and characterization of rare-earth (Er3+, Ho3+, and Tm3+) doped upconversion nanophosphors. Appl Phys Lett 90(7):073104
157. Ehlert O, Thomann R, Darbandi M, Nann T (2008) A four-color colloidal multiplexing nanoparticle System. ACS Nano 2(1):120–124
158. Gorris HH, Wolfbeis OS (2013) Photon-upconverting nanoparticles for optical encoding and multiplexing of cells, biomolecules, and microspheres. Angew Chem Int Ed 52(13): 3584–3600
159. Wang F, Han Y, Lim CS, Lu Y, Wang J, Xu J, Chen H, Zhang C, Hong M, Liu X (2010) Simultaneous phase and size control of upconversion nanocrystals through lanthanide doping. Nature 463(7284):1061–1065
160. Vetrone F, Boyer JC, Capobianco JA, Speghini A, Bettinelli M (2004) Significance of Yb3+ concentration on the upconversion mechanisms in codoped Y2O3: Er3+, Yb3+ nanocrystals. J Appl Phys 96(1):661–667
161. Wang F, Liu X (2008) Upconversion multicolor fine-tuning: visible to near-infrared emission from lanthanide-doped NaYF4 nanoparticles. J Am Chem Soc 130(17):5642–5643

162. Gorris HH, Ali R, Saleh SM, Wolfbeis OS (2011) Tuning the dual emission of photon- upconverting nanoparticles for ratiometric multiplexed encoding. Adv Mater 23(14):1652–1655
163. Bai X, Song H, Pan G, Lei Y, Wang T, Ren X, Lu S, Dong B, Dai Q, Fan L (2007) Size-dependent upconversion luminescence in Er3+/Yb3+-codoped nanocrystalline Yttria: saturation and thermal effects. J Phys Chem C 111(36):13611–13617
164. Dou Q, Idris NM, Zhang Y (2013) Sandwich-structured upconversion nanoparticles with tunable color for multiplexed cell labeling. Biomaterials 34(6):1722–1731
165. Gainer CF, Joshua GS, Romanowski M (2012) Toward the Use of Two-Color Emission Control in Upconverting NaYF4:Er3+, Yb3+ Nanoparticles for Biomedical Imaging. In: Cartwright AN, Nicolau DV (eds) Nanoscale Imaging, Sensing, and Actuation for Biomedical Applications Viii, vol 8231. Proceedings of SPIE. Spie-Int Soc Optical Engineering, Bellingham
166. Saleh SM, Ali R, Wolfbeis OS (2011) Quenching of the luminescence of upconverting luminescent nanoparticles by heavy metal ions. Chem-Eur J 17(51):14611–14617
167. Chen G, Ohulchanskyy TY, Kachynski A, Agren H, Prasad PN (2011) Intense visible and near-infrared upconversion photoluminescence in colloidal LiYF(4):Er(3)+nanocrystals under excitation at 1490 nm. ACS Nano 5(6):4981–4986
168. Vetrone F, Boyer JC, Capobianco JA, Speghini A, Bettinelli M (2003) Effect of Yb3+ codoping on the upconversion emission in nanocrystalline Y2O3:Er3+. J Phys Chem B 107(5):1107–1112
169. Yin W, Zhao L, Zhou L, Gu Z, Liu X, Tian G, Jin S, Yan L, Ren W, Xing G, Zhao Y (2012) Enhanced red emission from GdF3:Yb3+, Er3+ upconversion nanocrystals by Li+doping and their application for bioimaging. Chem-Eur J 18(30):9239–9245
170. Wang F, Wang J, Liu X (2010) Direct evidence of a surface quenching effect on size-dependent luminescence of upconversion nanoparticles. Angew Chem Int Ed 49(41):7456–7460
171. Hai G, Zhengquan L, Haisheng Q, Yong H, Idris Niagara M (2010) Seed-mediated synthesis of NaY F 4:Y b, Er/NaGdF 4 nanocrystals with improved upconversion fluorescence and MR relaxivity. Nanotechnology 21(12):125602
172. Liu C, Wang H, Li X, Chen D (2009) Monodisperse, size-tunable and highly efficient [small beta]-NaYF4:Yb, Er(Tm) up-conversion luminescent nanospheres: controllable synthesis and their surface modifications. J Mater Chem 19(21):3546–3553
173. Qian HS, Zhang Y (2008) Synthesis of hexagonal-phase core-shell NaYF4 nanocrystals with tunable upconversion fluorescence. Langmuir 24(21):12123–12125
174. Schäfer H, Ptacek P, Zerzouf O, Haase M (2008) Synthesis and Optical Properties of KYF4/Yb, Er Nanocrystals, and their Surface Modification with Undoped KYF4. Adv Funct Mater 18(19):2913–2918
175. Su Q, Han S, Xie X, Zhu H, Chen H, Chen CK, Liu RS, Chen X, Wang F, Liu X (2012) The effect of surface coating on energy migration-mediated upconversion. J Am Chem Soc 134(51):20849–20857
176. Wang Y, Tu L, Zhao J, Sun Y, Kong X, Zhang H (2009) Upconversion luminescence of β-NaYF4: Yb3+, Er3+@β-NaYF4 Core/Shell nanoparticles: excitation power density and surface dependence. J Phys Chem C 113(17):7164–7169
177. Zhang F, Che R, Li X, Yao C, Yang J, Shen D, Hu P, Li W, Zhao D (2012) Direct imaging the upconversion nanocrystal core/shell structure at the subnanometer level: shell thickness dependence in upconverting optical properties. Nano Lett 12(6):2852–2858
178. Chen G, Shen J, Ohulchanskyy TY, Patel NJ, Kutikov A, Li Z, Song J, Pandey RK, Agren H, Prasad PN, Han G (2012) (alpha-NaYbF4:Tm(3+))/CaF2 core/shell nanoparticles with efficient near-infrared to near-infrared upconversion for high-contrast deep tissue bioimaging. ACS Nano 6(9):8280–8287
179. Feng W, Sun LD, Yan CH (2009) Ag nanowires enhanced upconversion emission of NaYF4:Yb, Er nanocrystals via a direct assembly method. Chem Commun 29:4393–4395
180. Schietinger S, Aichele T, Wang HQ, Nann T, Benson O (2010) Plasmon-enhanced upconversion in single NaYF4:Yb3+/Er3+ codoped nanocrystals. Nano Lett 10(1):134–138
181. Sudheendra L, Ortalan V, Dey S, Browning ND, Kennedy IM (2011) Plasmonic Enhanced Emissions from Cubic NaYF4:Yb:Er/Tm Nanophosphors. Chem Mater 23(11):2987–2993
182. Yuan P, Lee YH, Gnanasammandhan MK, Guan Z, Zhang Y, Xu QH (2012) Plasmon enhanced upconversion luminescence of NaYF4:Yb, Er@SiO2@Ag core-shell nanocomposites for cell imaging. Nanoscale 4(16):5132–5137
183. Zhang F, Braun GB, Shi Y, Zhang Y, Sun X, Reich NO, Zhao D, Stucky G (2010) Fabrication of Ag@SiO(2)@Y(2)O(3):Er nanostructures for bioimaging: tuning of the upconversion fluorescence with silver nanoparticles. J Am Chem Soc 132(9):2850–2851
184. Xiao QB, Zhu HM, Tu DT, Ma E, Chen XY (2013) Near-Infrared-to-Near-Infrared Downshifting and Near-Infrared-to-Visible Upconverting Luminescence of Er3+-Doped In2O3 Nanocrystals. J Phys Chem C 117(20):10834–10841
185. Zhou J, Sun Y, Du X, Xiong L, Hu H, Li F (2010) Dual-modality in vivo imaging using rare-earth nanocrystals with near-infrared to near-infrared (NIR-to-NIR) upconversion luminescence and magnetic resonance properties. Biomaterials 31(12):3287–3295
186. Wang YF, Liu GY, Sun LD, Xiao JW, Zhou JC, Yan CH (2013) Nd3+-Sensitized upconversion nanophosphors: efficient In vivo bioimaging probes with minimized heating effect. ACS Nano. doi: 10.1021/nn402601d
187. Alexis F, Pridgen E, Molnar LK, Farokhzad OC (2008) Factors affecting the clearance and biodistribution of polymeric nanoparticles. Mol Pharm 5(4):505–515
188. Fang C, Shi B, Pei Y-Y, Hong M-H, Wu J, Chen H-Z (2006) In vivo tumor targeting of tumor necrosis factor-α-loaded stealth nanoparticles: Effect of MePEG molecular weight and particle size. Eur J Pharm Sci 27(1):27–36
189. Hobbs SK, Monsky WL, Yuan F, Roberts WG, Griffith L, Torchilin VP, Jain RK (1998) Regulation of transport pathways in tumor vessels: role of tumor type and microenvironment. Proc Natl Acad Sci U S A 95(8):4607–4612
190. Dass CR, Su T (2001) Particle-mediated intravascular delivery of oligonucleotides to tumors: associated biology and lessons from genotherapy. Drug Deliv 8(4):191–213
191. Davis ME (2009) The first targeted delivery of siRNA in humans via a self-assembling, Cyclodextrin polymer-based nanoparticle: from concept to clinic. Mol Pharm 6(3):659–668
192. Davis ME, Chen Z, Shin DM (2008) Nanoparticle therapeutics: an emerging treatment modality for cancer. Nat Rev Drug Discov 7(9):771–782
193. Xiao K, Li YP, Luo JT, Lee JS, Xiao WW, Gonik AM, Agarwal RG, Lam KS (2011) The effect of surface charge on in vivo biodistribution of PEG-oligocholic acid based micellar nanoparticles. Biomaterials 32(13):3435–3446
194. Goodman CM, McCusker CD, Yilmaz T, Rotello VM (2004) Toxicity of gold nanoparticles functionalized with cationic and anionic side chains. Bioconj Chem 15(4):897–900
195. Nel AE, Madler L, Velegol D, Xia T, Hoek EMV, Somasundaran P, Klaessig F, Castranova V, Thompson M (2009) Understanding biophysicochemical interactions at the nano-bio interface. Nat Mater 8(7):543–557
196. Xia T, Kovochich M, Liong M, Zink JI, Nel AE (2007) Cationic Polystyrene Nanosphere Toxicity Depends on Cell-Specific Endocytic and Mitochondrial Injury Pathways. ACS Nano 2(1):85–96
197. Jiang S, Zhang Y (2008) IR-to-visible Upconversion Nanoparticles for in Vitro Fluorescent Imaging. In: AbuOsman NA, Ibrahim F, WanAbas WAB, AbdulRahman HS, Ting HN (eds) 4th Kuala

Lumpur International Conference on Biomedical Engineering 2008, Vols 1 and 2, vol 21, IFMBE Proceedings, vol 1-2. Springer, New York, pp 330–332
198. Knop K, Hoogenboom R, Fischer D, Schubert US (2010) Poly(ethylene glycol) in drug delivery: Pros and cons as well as potential alternatives. Angew Chem Int Ed 49(36):6288–6308
199. Nie G, Hah HJ, Kim G, Lee YE, Qin M, Ratani TS, Fotiadis P, Miller A, Kochi A, Gao D, Chen T, Orringer DA, Sagher O, Philbert MA, Kopelman R (2012) Hydrogel nanoparticles with covalently linked coomassie blue for brain tumor delineation visible to the surgeon. Small 8(6):884–891
200. Peppas NA, Keys KB, Torres-Lugo M, Lowman AM (1999) Poly(ethylene glycol)-containing hydrogels in drug delivery. J Controlled Release 62(1–2):81–87
201. Wang S, Kim G, Lee YE, Hah HJ, Ethirajan M, Pandey RK, Kopelman R (2012) Multifunctional biodegradable polyacrylamide nanocarriers for cancer theranostics–a "see and treat" strategy. ACS Nano 6(8):6843–6851
202. Wenger Y, Schneider RJ 2nd, Reddy GR, Kopelman R, Jolliet O, Philbert MA (2011) Tissue distribution and pharmacokinetics of stable polyacrylamide nanoparticles following intravenous injection in the rat. Toxicol Appl Pharmacol 251(3):181–190
203. Wang C, Cheng L, Xu H, Liu Z (2012) Towards whole-body imaging at the single cell level using ultra-sensitive stem cell labeling with oligo-arginine modified upconversion nanoparticles. Biomaterials 33(19):4872–4881
204. Boyer J-C, Manseau M-P, Murray JI, van Veggel FCJM (2009) Surface Modification of Upconverting NaYF4 Nanoparticles with PEG−Phosphate Ligands for NIR (800 nm) biolabeling within the biological window. Langmuir 26(2):1157–1164
205. Kamimura M, Miyamoto D, Saito Y, Soga K, Nagasaki Y (2008) Design of poly(ethylene glycol)/streptavidin coimmobilized upconversion nanophosphors and their application to fluorescence biolabeling. Langmuir 24(16):8864–8870
206. Kamimura M, Miyamoto D, Saito Y, Soga K, Nagasaki Y (2008) Preparation of PEG and protein co-immobilized upconversion nanophosphors as near-infrared biolabeling materials. J Photopolym Sci Technol 21(2):183–187
207. Konishi T, Yamada M, Soga K, Matsuura D, Nagasaki Y (2006) PEG-based surface modification on upconversion nanophosphors for bio-imaging under IR excitation. J Photopolym Sci Technol 19(2):145–149
208. Zako T, Nagata H, Terada N, Sakono M, Soga K, Maeda M (2008) Improvement of dispersion stability and characterization of upconversion nanophosphors covalently modified with PEG as a fluorescence bioimaging probe. J Mater Sci 43(15):5325–5330
209. Zeng S, Tsang MK, Chan CF, Wong KL, Hao J (2012) PEG modified BaGdF(5):Yb/Er nanoprobes for multi-modal upconversion fluorescent, in vivo X-ray computed tomography and biomagnetic imaging. Biomaterials 33(36):9232–9238
210. Cheng L, Yang K, Shao M, Lu X, Liu Z (2011) In vivo pharmacokinetics, long-term biodistribution and toxicology study of functionalized upconversion nanoparticles in mice. Nanomedicine-UK 6(8): 1327–1340
211. Wang Y, Wu Z, Liu Z (2013) Upconversion fluorescence resonance energy transfer biosensor with aromatic polymer nanospheres as the lable-free energy acceptor. Anal Chem 85(1):258–264
212. Xu H, Cheng L, Wang C, Ma X, Li Y, Liu Z (2011) Polymer encapsulated upconversion nanoparticle/iron oxide nanocomposites for multimodal imaging and magnetic targeted drug delivery. Biomaterials 32(35):9364–9373
213. Lee J, Lee TS, Ryu J, Hong S, Kang M, Im K, Kang JH, Lim SM, Park S, Song R (2013) RGD peptide-conjugated multimodal NaGdF4:Yb3+/Er3+ nanophosphors for upconversion luminescence, MR, and PET imaging of tumor angiogenesis. J Nucl Med 54(1):96–103
214. Naczynski DJ, Andelman T, Pal D, Chen S, Riman RE, Roth CM, Moghe PV (2010) Albumin Nanoshell Encapsulation of Near-Infrared-Excitable Rare-Earth Nanoparticles Enhances Biocompatibility and Enables Targeted Cell Imaging. Small 6(15): 1631–1640
215. Xiong L, Chen Z, Tian Q, Cao T, Xu C, Li F (2009) High contrast upconversion luminescence targeted imaging in vivo using peptide-labeled nanophosphors. Anal Chem 81(21):8687–8694
216. Zhou A, Wei Y, Wu B, Chen Q, Xing D (2012) Pyropheophorbide A and c(RGDyK) comodified chitosan-wrapped upconversion nanoparticle for targeted near-infrared photodynamic therapy. Mol Pharm 9(6):1580–1589
217. Bogdan N, Rodriguez EM, Sanz-Rodriguez F, de la Cruz MCI, Juarranz A, Jaque D, Sole JG, Capobianco JA (2012) Bio-functionalization of ligand-free upconverting lanthanide doped nanoparticles for bio-imaging and cell targeting. Nanoscale 4(12): 3647–3650
218. Hischemoller A, Walter C, Weiler V, Hummel H, Thepen T, Huhn M, Barth S, Hoheisel W, Kohler K, Dimova-Landen D, Bremer C, Haase M, Waldeck J (2012) Labeling of Anti-MUC-1 Binding Single Chain Fv Fragments to Surface Modified Upconversion Nanoparticles for an Initial in vivo Molecular Imaging Proof of Principle Approach. Int J Mol Sci 13(4):4153–4167
219. Huang Z, Wu S, Duan N, Hua D, Hu Y, Wang Z (2012) Sensitive detection of carcinoembryonic antigen with magnetic nano-bead and upconversion nanoparticles-based immunoassay. J Pharm Biomed Anal 66:225–231
220. Kamimura M, Miyamoto D, Saito Y, Soga K, Nagasaki Y (2008) Preparation of PEGylated upconversion nanophosphors with high dispersion stability under physiological conditions for near-infrared bioimaging, vol 33. Transactions of the Materials Research Society of Japan, 33(3), 3. Materials Research Society Japan-Mrs-J, Tokyo
221. Kong X, Zhang H, Sun Y, Zhao Z, Qu Y, Wang Y, Aalders M (2008) Luminescent upconversion nanoparticle (ULNP) with photosensitizing functions to be used for the diagnosis and therapy of cancer. Luminescence 23(2):77–77
222. Liu CH, Wang Z, Wang XK, Li ZP (2011) Surface modification of hydrophobic NaYF4:Yb, Er upconversion nanophosphors and their applications for immunoassay. Science China-Chemistry 54(8): 1292–1297
223. Mi C, Tian Z, Cao C, Wang Z, Mao C, Xu S (2011) Novel microwave-assisted solvothermal synthesis of NaYF4:Yb, Er upconversion nanoparticles and their application in cancer cell imaging. Langmuir 27(23):14632–14637
224. Nagarajan S, Li Z, Marchi-Artzner V, Grasset F, Zhang Y (2010) Imaging gap junctions with silica-coated upconversion nanoparticles. Med Biol Eng Comput 48(10):1033–1041
225. Pakkila H, Yliharsila M, Lahtinen S, Hattara L, Salminen N, Arppe R, Lastusaari M, Saviranta P, Soukka T (2012) Quantitative multianalyte microarray immunoassay utilizing upconverting phosphor technology. Anal Chem 84(20):8628–8634
226. Shan J, Yong Z, Kian Meng L, Eugene KWS, Lei Y (2009) NIR-to-visible upconversion nanoparticles for fluorescent labeling and targeted delivery of siRNA. Nanotechnology 20(15):155101
227. Song K, Ran YY, Kong XG (2011) Homogeneous immunoassay technology based on near infrared upconversion fluorescence resonance energy transfer. Guang Pu Xue Yu Guang Pu Fen Xi 31(1):86–90
228. Song K, Tian LJ, Kong XG, Liu K, Zhang QB, Du C, Zeng QH, Sun YJ, Liu XM (2010) Preparation, characterization and specific biological labeling of silica coated upconversion fluorescent nanocrystals. Guang Pu Xue Yu Guang Pu Fen Xi 30(1):133–136
229. Wang M, Hou W, Mi C-C, Wang W-X, Xu Z-R, Teng H-H, Mao C-B, Xu S-K (2009) Immunoassay of goat antihuman immunoglobulin g antibody based on luminescence resonance energy transfer

between near-infrared responsive NaYF4:Yb, Er Upconversion fluorescent nanoparticles and gold nanoparticles. Anal Chem 81(21):8783–8789
230. Wang M, Mi C-C, Wang W-X, Liu C-H, Wu Y-F, Xu Z-R, Mao C-B, Xu S-K (2009) Immunolabeling and NIR-Excited Fluorescent Imaging of HeLa Cells by Using NaYF4:Yb, Er Upconversion Nanoparticles. ACS Nano 3(6):1580–1586
231. Wang M, Mi C, Zhang Y, Liu J, Li F, Mao C, Xu S (2009) NIR-responsive silica-coated NaYbF(4):Er/Tm/Ho upconversion fluorescent nanoparticles with tunable emission colors and their applications in immunolabeling and fluorescent imaging of cancer cells. J Phys Chem C Nanomater Interfaces 113(44):19021–19027
232. Liu JN, Bu W, Pan LM, Zhang S, Chen F, Zhou L, Zhao KL, Peng W, Shi J (2012) Simultaneous nuclear imaging and intranuclear drug delivery by nuclear-targeted multifunctional upconversion nanoprobes. Biomaterials 33(29):7282–7290
233. Yu XF, Sun Z, Li M, Xiang Y, Wang QQ, Tang F, Wu Y, Cao Z, Li W (2010) Neurotoxin-conjugated upconversion nanoprobes for direct visualization of tumors under near-infrared irradiation. Biomaterials 31(33):8724–8731
234. Chen H-Q, Yuan F, Wang S-Z, Xu J, Zhang Y-Y, Wang L (2013) Near-infrared to near-infrared upconverting NaYF4:Yb3+, Tm3+ nanoparticles-aptamer-Au nanorods light resonance energy transfer system for the detection of mercuric(ii) ions in solution. Analyst 138(8):2392–2397
235. Chen H, Yuan F, Wang S, Xu J, Zhang Y, Wang L (2013) Aptamer-based sensing for thrombin in red region via fluorescence resonant energy transfer between NaYF4:Yb, Er upconversion nanoparticles and gold nanorods. Biosensors Bioelectron 48:19–25
236. Duan N, Wu S, Zhu C, Ma X, Wang Z, Yu Y, Jiang Y (2012) Dual-color upconversion fluorescence and aptamer-functionalized magnetic nanoparticles-based bioassay for the simultaneous detection of Salmonella Typhimurium and Staphylococcus aureus. Anal Chim Acta 723:1–6
237. Li L-L, Wu P, Hwang K, Lu Y (2013) An Exceptionally Simple Strategy for DNA-Functionalized Up-Conversion Nanoparticles as Biocompatible Agents for Nanoassembly, DNA Delivery, and Imaging. J Am Chem Soc 135(7):2411–2414
238. Liu J, Cheng J, Zhang Y (2012) Upconversion nanoparticle based LRET system for sensitive detection of MRSA DNA sequence. Biosens Bioelectron 43C:252–256
239. Rubner MM, Achatz DE, Mader HS, Stolwijk JA, Wegener J, Harms GS, Wolfbeis OS, Wagenknecht HA (2012) DNA "Nanolamps": "Clicked" DNA Conjugates with Photon Upconverting Nanoparticles as Highly Emissive Biomaterial. Chempluschem 77(2):129–134
240. Song K, Kong X, Liu X, Zhang Y, Zeng Q, Tu L, Shi Z, Zhang H (2012) Aptamer optical biosensor without bio-breakage using upconversion nanoparticles as donors. Chem Commun 48(8): 1156–1158
241. Song K, Kong XG (2011) A new optical switch using upconversion nanoparticles conjugated aptamer. Spectrosc Spectr Anal 31(3): 844–848
242. Wu S, Duan N, Wang Z, Wang H (2011) Aptamer-functionalized magnetic nanoparticle-based bioassay for the detection of ochratoxin A using upconversion nanoparticles as labels. Analyst 136(11): 2306–2314
243. Yliharsila M, Valta T, Karp M, Hattara L, Harju E, Holsa J, Saviranta P, Waris M, Soukka T (2011) Oligonucleotide Array-in-well platform for detection and genotyping human adenoviruses by utilizing upconverting phosphor label technology. Anal Chem 83(4):1456–1461
244. Cui S, Yin D, Chen Y, Di Y, Chen H, Ma Y, Achilefu S, Gu Y (2013) In vivo targeted deep-tissue photodynamic therapy based on near-infrared light triggered upconversion nanoconstruct. ACS nano 7(1):676–688
245. Lee KY, Seow E, Zhang Y, Lim YC (2013) Targeting CCL21–folic acid–upconversion nanoparticles conjugates to folate receptor-α expressing tumor cells in an endothelial-tumor cell bilayer model. Biomaterials 34(20):4860–4871
246. Ma J, Huang P, He M, Pan L, Zhou Z, Feng L, Gao G, Cui D (2012) Folic acid-conjugated LaF3:Yb, Tm@SiO2 nanoprobes for targeting dual-modality imaging of upconversion luminescence and X-ray computed tomography. J Phys Chem B 116(48):14062–14070
247. Xiong LQ, Chen ZG, Yu MX, Li FY, Liu C, Huang CH (2009) Synthesis, characterization, and in vivo targeted imaging of amine-functionalized rare-earth up-converting nanophosphors. Biomaterials 30(29):5592–5600
248. Achatz DE, Meier RJ, Fischer LH, Wolfbeis OS (2011) Luminescent sensing of oxygen using a quenchable probe and upconverting nanoparticles. Angew Chem Int Ed 50(1):260–263
249. Mader HS, Wolfbeis OS (2010) Optical ammonia sensor based on upconverting luminescent nanoparticles. Anal Chem 82(12):5002–5004
250. Sun LN, Peng H, Stich MIJ, Achatz D, Wolfbeis OS (2009) pH sensor based on upconverting luminescent lanthanide nanorods. Chem Commun 33:5000–5002
251. Ali R, Saleh SM, Meier RJ, Azab HA, Abdelgawad II, Wolfbeis OS (2010) Upconverting nanoparticle based optical sensor for carbon dioxide. Sensor Actuat B-Chem 150(1):126–131
252. Li C, Liu J, Alonso S, Li F, Zhang Y (2012) Upconversion nanoparticles for sensitive and in-depth detection of Cu2+ ions. Nanoscale 4(19):6065–6071
253. Liu J, Liu Y, Liu Q, Li C, Sun L, Li F (2011) Iridium(III) complex-coated nanosystem for ratiometric upconversion luminescence bioimaging of cyanide anions. J Am Chem Soc 133(39):15276–15279
254. Liu Q, Peng J, Sun L, Li F (2011) High-efficiency upconversion luminescent sensing and bioimaging of Hg(II) by chromophoric ruthenium complex-assembled nanophosphors. ACS Nano 5(10): 8040–8048
255. Weissleder R, Kelly K, Sun EY, Shtatland T, Josephson L (2005) Cell-specific targeting of nanoparticles by multivalent attachment of small molecules. Nat Biotech 23(11):1418–1423
256. Yang Y, Shao Q, Deng R, Wang C, Teng X, Cheng K, Cheng Z, Huang L, Liu Z, Liu X, Xing B (2012) In vitro and in vivo uncaging and bioluminescence imaging by using photocaged upconversion nanoparticles. Angew Chem Int Ed Engl 51(13):3125–3129
257. Liu Y, Chen M, Cao T, Sun Y, Li C, Liu Q, Yang T, Yao L, Feng W, Li F (2013) A Cyanine-Modified Nanosystem for in vivo Upconversion Luminescence Bioimaging of Methylmercury. J Am Chem Soc 135(26):9869–9876
258. Wei YC, Chen Q, Wu BY, Zhou AG, Xing D (2012) High-sensitivity in vivo imaging for tumors using a spectral up-conversion nanoparticle NaYF4:Yb3+, Er3+ in cooperation with a microtubulin inhibitor. Nanoscale 4(13):3901–3909
259. Deng M, Ma Y, Huang S, Hu G, Wang L (2011) Monodisperse upconversion NaYF4 nanocrystals: syntheses and bioapplications. Nano Res 4(7):685–694
260. Jeong S, Won N, Lee J, Bang J, Yoo J, Kim SG, Chang JA, Kim J, Kim S (2011) Multiplexed near-infrared in vivo imaging complementarily using quantum dots and upconverting NaYF4:Yb3+, Tm3+ nanoparticles. Chem Commun 47(28):8022–8024
261. Ryu J, Park H-Y, Kim K, Kim H, Yoo JH, Kang M, Im K, Grailhe R, Song R (2010) Facile synthesis of ultrasmall and Hexagonal NaGdF4: Yb3+, Er3+ Nanoparticles with magnetic and upconversion imaging properties. J Phys Chem C 114(49):21077–21082
262. Salthouse C, Hildebrand S, Weissleder R, Mahmood U (2008) Design and demonstration of a small-animal up-conversion imager. Opt Express 16(26):21731–21737

263. Vetrone F, Naccache R, de la Fuente AJ, Sanz-Rodriguez F, Blazquez-Castro A, Rodriguez EM, Jaque D, Sole JG, Capobianco JA (2010) Intracellular imaging of HeLa cells by non-functionalized NaYF4: Er3+, Yb3+ upconverting nanoparticles. Nanoscale 2(4):495–498
264. Yu MX, Li FY, Chen ZG, Hu H, Zhan C, Yang H, Huang CH (2009) Laser Scanning Up-Conversion Luminescence Microscopy for Imaging Cells Labeled with Rare-Earth Nanophosphors. Anal Chem 81(3):930–935
265. Xia A, Gao Y, Zhou J, Li C, Yang T, Wu D, Wu L, Li F (2011) Core-shell NaYF4:Yb3+, Tm3+@FexOy nanocrystals for dual-modality T2-enhanced magnetic resonance and NIR-to-NIR upconversion luminescent imaging of small-animal lymphatic node. Biomaterials 32(29):7200–7208
266. Yang T, Sun Y, Liu Q, Feng W, Yang P, Li F (2012) Cubic sub-20 nm NaLuF(4)-based upconversion nanophosphors for high-contrast bioimaging in different animal species. Biomaterials 33(14):3733–3742
267. Zhou J, Zhu X, Chen M, Sun Y, Li F (2012) Water-stable NaLuF4-based upconversion nanophosphors with long-term validity for multimodal lymphatic imaging. Biomaterials 33(26):6201–6210
268. Idris NM, Li Z, Ye L, Sim EK, Mahendran R, Ho PC, Zhang Y (2009) Tracking transplanted cells in live animal using upconversion fluorescent nanoparticles. Biomaterials 30(28): 5104–5113
269. Li LL, Zhang R, Yin L, Zheng K, Qin W, Selvin PR, Lu Y (2012) Biomimetic surface engineering of lanthanide-doped upconversion nanoparticles as versatile bioprobes. Angew Chem Int Ed Engl 51(25):6121–6125
270. Nagarajan S, Zhang Y (2011) Upconversion fluorescent nanoparticles as a potential tool for in-depth imaging. Nanotechnology 22(39):395101
271. Chen DQ, Yu YL, Huang F, Yang AP, Wang YS (2011) Lanthanide activator doped NaYb(1-x)Gd(x)F4 nanocrystals with tunable down-, up-conversion luminescence and paramagnetic properties. J Mater Chem 21(17):6186–6192
272. Chen F, Zhang S, Bu W, Liu X, Chen Y, He Q, Zhu M, Zhang L, Zhou L, Peng W, Shi J (2010) A "Neck-Formation" Strategy for an Antiquenching Magnetic/Upconversion Fluorescent Bimodal Cancer Probe. Chem-Eur J 16(37):11254–11260
273. Chen H, Qi B, Moore T, Colvin DC, Crawford T, Gore JC, Alexis F, Mefford OT, Anker JN (2013) Synthesis of brightly PEGylated luminescent magnetic upconversion nanophosphors for deep tissue and dual MRI imaging. Small. doi:10.1002/smll.201300828
274. Das GK, Heng BC, Ng S-C, White T, Loo JSC, D'Silva L, Padmanabhan P, Bhakoo KK, Selvan ST, Tan TTY (2010) Gadolinium oxide ultranarrow nanorods as multimodal contrast agents for optical and magnetic resonance imaging. Langmuir 26(11):8959–8965
275. Debasu ML, Ananias D, Pinho SLC, Geraldes C, Carlos LD, Rocha J (2012) (Gd, Yb, Tb)PO4 up-conversion nanocrystals for bimodal luminescence-MR imaging. Nanoscale 4(16):5154–5162
276. Hou Y, Yin ZF, Xin HL, Su YH, Yang HG (2012) Fe3O4 modified up-conversion luminescent nanocrystals for biological applications. Chin J Chem 30(12):2774–2778
277. Li FF, Li CG, Liu XM, Chen Y, Bai TY, Wang L, Shi Z, Feng SH (2012) Hydrophilic, upconverting, multicolor, lanthanide-doped NaGdF4 Nanocrystals as Potential multifunctional bioprobes. Chem-Eur J 18(37):11641–11646
278. Liu C, Gao Z, Zeng J, Hou Y, Fang F, Li Y, Qiao R, Shen L, Lei H, Yang W, Gao M (2013) Magnetic/upconversion fluorescent NaGdF4:Yb, Er Nanoparticle-Based Dual-Modal molecular probes for imaging tiny tumors in vivo. ACS Nano. doi:10.1021/nn4030898
279. Lu Q, Wei DX, Cheng JJ, Xu JR, Zhu J (2012) A novel contrast agent with rare earth-doped up-conversion luminescence and Gd-DTPA magnetic resonance properties. J Solid State Chem 192:75–80
280. Mi CC, Zhang JP, Gao HY, Wu XL, Wang M, Wu YF, Di YQ, Xu ZR, Mao CB, Xu SK (2010) Multifunctional nanocomposites of superparamagnetic (Fe3O4) and NIR-responsive rare earth-doped up-conversion fluorescent (NaYF4: Yb, Er) nanoparticles and their applications in biolabeling and fluorescent imaging of cancer cells. Nanoscale 2(7):1141–1148
281. Paik T, Gordon TR, Prantner AM, Yun H, Murray CB (2013) Designing tripodal and triangular gadolinium oxide nanoplates and self-assembled nanofibrils as potential multimodal bioimaging probes. ACS Nano 7(3):2850–2859
282. Wang Y, Ji L, Zhang BB, Yin PH, Qiu YY, Song DQ, Zhou JY, Li Q (2013) Upconverting rare-earth nanoparticles with a paramagnetic lanthanide complex shell for upconversion fluorescent and magnetic resonance dual-modality imaging. Nanotechnology 24(17):175101
283. Wilhelm S, Hirsch T, Scheucher E, Mayr T, Wolfbeis OS (2011) Magnetic nanosensor particles in luminescence upconversion capability. Angew Chem Int Ed Engl 50(37):A59–62
284. Wong HT, Vetrone F, Naccache R, Chan HLW, Hao JH, Capobianco JA (2011) Water dispersible ultra-small multifunctional KGdF4: Tm3+, Yb3+ nanoparticles with near-infrared to near-infrared upconversion. J Mater Chem 21(41):16589–16596
285. Zeng S, Tsang MK, Chan CF, Wong KL, Fei B, Hao J (2012) Dual-modal fluorescent/magnetic bioprobes based on small sized upconversion nanoparticles of amine-functionalized BaGdF5:Yb/Er. Nanoscale 4(16):5118–5124
286. Chen G, Ohulchanskyy TY, Law WC, Agren H, Prasad PN (2011) Monodisperse NaYbF4:Tm3+/NaGdF4 core/shell nanocrystals with near-infrared to near-infrared upconversion photoluminescence and magnetic resonance properties. Nanoscale 3(5):2003–2008
287. Shen J, Sun L-D, Zhang Y-W, Yan C-H (2010) Superparamagnetic and upconversion emitting Fe3O4/NaYF4: Yb, Er heteronanoparticles via a crosslinker anchoring strategy. Chem Commun 46(31):5731–5733
288. Zhang L, Wang YS, Yang Y, Zhang F, Dong WF, Zhou SY, Pei WH, Chen HD, Sun HB (2012) Magnetic/upconversion luminescent mesoparticles of Fe3O4@LaF3:Yb3+, Er3+ for dual-modal bioimaging. Chem Commun 48(91):11238–11240
289. Xiao Q, Bu W, Ren Q, Zhang S, Xing H, Chen F, Li M, Zheng X, Hua Y, Zhou L, Peng W, Qu H, Wang Z, Zhao K, Shi J (2012) Radiopaque fluorescence-transparent TaOx decorated upconversion nanophosphors for in vivo CT/MR/UCL trimodal imaging. Biomaterials 33(30):7530–7539
290. Xing HY, Bu WB, Ren QG, Zheng XP, Li M, Zhang SJ, Qu HY, Wang Z, Hua YQ, Zhao KL, Zhou LP, Peng WJ, Shi JL (2012) A NaYbF4: Tm3+ nanoprobe for CT and NIR-to-NIR fluorescent bimodal imaging. Biomaterials 33(21):5384–5393
291. Zhang G, Liu Y, Yuan Q, Zong C, Liu J, Lu L (2011) Dual modal in vivo imaging using upconversion luminescence and enhanced computed tomography properties. Nanoscale 3(10):4365–4371
292. Liu Z, Li Z, Liu J, Gu S, Yuan Q, Ren J, Qu X (2012) Long-circulating Er3+-doped Yb2O3 up-conversion nanoparticle as an in vivo X-Ray CT imaging contrast agent. Biomaterials 33(28): 6748–6757
293. Liu FY, He XX, Liu L, You HP, Zhang HM, Wang ZX (2013) Conjugation of NaGdF4 upconverting nanoparticles on silica nanospheres as contrast agents for multi-modality imaging. Biomaterials 34(21):5218–5225
294. Xia A, Chen M, Gao Y, Wu D, Feng W, Li F (2012) Gd3+ complex-modified NaLuF4-based upconversion nanophosphors for trimodality imaging of NIR-to-NIR upconversion luminescence, X-Ray computed tomography and magnetic resonance. Biomaterials 33(21):5394–5405

295. Zhu X, Zhou J, Chen M, Shi M, Feng W, Li F (2012) Core-shell Fe3O4@NaLuF4:Yb, Er/Tm nanostructure for MRI, CT and upconversion luminescence tri-modality imaging. Biomaterials 33(18):4618–4627
296. Liu Z, Pu F, Huang S, Yuan QH, Ren JS, Qu XG (2013) Long-circulating Gd2O3:Yb3+, Er3+ up-conversion nanoprobes as high-performance contrast agents for multi-modality imaging. Biomaterials 34(6):1712–1721
297. Sun Y, Yu M, Liang S, Zhang Y, Li C, Mou T, Yang W, Zhang X, Li B, Huang C, Li F (2011) Fluorine-18 labeled rare-earth nanoparticles for positron emission tomography (PET) imaging of sentinel lymph node. Biomaterials 32(11):2999–3007
298. Liu Q, Sun Y, Li C, Zhou J, Li C, Yang T, Zhang X, Yi T, Wu D, Li F (2011) 18 F-Labeled magnetic-upconversion nanophosphors via rare-Earth cation-assisted ligand assembly. ACS Nano 5(4):3146–3157
299. Sun Y, Liu Q, Peng J, Feng W, Zhang Y, Yang P, Li F (2013) Radioisotope post-labeling upconversion nanophosphors for in vivo quantitative tracking. Biomaterials 34(9):2289–2295
300. Achatz D, Ali R, Wolfbeis O (2011) Luminescent Chemical Sensing, Biosensing, and Screening Using Upconverting Nanoparticles. In: Prodi L, Montalti M, Zaccheroni N (eds) Luminescence Applied in Sensor Science, vol 300. Topics in Current Chemistry. Springer Berlin Heidelberg, pp 29–50
301. Deng R, Xie X, Vendrell M, Chang YT, Liu X (2011) Intracellular glutathione detection using MnO(2)-nanosheet-modified upconversion nanoparticles. J Am Chem Soc 133(50):20168–20171
302. Corstjens P, Zuiderwijk M, Nilsson M, Feindt H, Niedbala RS, Tanke HJ (2003) Lateral-flow and up-converting phosphor reporters to detect single-stranded nucleic acids in a sandwich-hybridization assay. Anal Biochem 312(2):191–200
303. van de Rijke F, Zijlmans H, Li S, Vail T, Raap AK, Niedbala RS, Tanke HJ (2001) Up-converting phosphor reporters for nucleic acid microarrays. Nat Biotechnol 19(3):273–276
304. Wu S, Duan N, Zhu C, Ma X, Wang M, Wang Z (2011) Magnetic nanobead-based immunoassay for the simultaneous detection of aflatoxin B1 and ochratoxin A using upconversion nanoparticles as multicolor labels. Biosens Bioelectron 30(1):35–42
305. Liu C, Wang Z, Jia H, Li Z (2011) Efficient fluorescence resonance energy transfer between upconversion nanophosphors and graphene oxide: a highly sensitive biosensing platform. Chem Commun 47(16):4661–4663
306. Kumar M, Zhang P (2009) Highly Sensitive and Selective Label-Free Optical Detection of DNA Hybridization Based on Photon Upconverting Nanoparticles. Langmuir 25(11):6024–6027
307. Wang L, Li Y (2006) Green upconversion nanocrystals for DNA detection. Chem Commun 24:2557–2559
308. Zhang F, Shi Q, Zhang Y, Shi Y, Ding K, Zhao D, Stucky GD (2011) Fluorescence Upconversion Microbarcodes for Multiplexed Biological Detection: Nucleic Acid Encoding. Adv Mater 23(33): 3775–3779
309. Jiang S, Zhang Y (2010) Upconversion nanoparticle-based FRET system for study of siRNA in live cells. Langmuir 26(9):6689–6694
310. Wang Y, Shen P, Li C, Wang Y, Liu Z (2012) Upconversion fluorescence resonance energy transfer based biosensor for ultra-sensitive detection of matrix metalloproteinase-2 in blood. Anal Chem 84(3):1466–1473
311. Kuningas K, Ukonaho T, Pakkila H, Rantanen T, Rosenberg J, Lovgren T, Soukka T (2006) Upconversion fluorescence resonance energy transfer in a homogeneous immunoassay for estradiol. Anal Chem 78(13):4690–4696
312. Tian G, Gu Z, Zhou L, Yin W, Liu X, Yan L, Jin S, Ren W, Xing G, Li S, Zhao Y (2012) Mn2+ dopant-controlled synthesis of NaYF4: Yb/Er upconversion nanoparticles for in vivo imaging and drug delivery. Adv Mater 24(9):1226–1231
313. Guo H, Hao R, Qian H, Sun S, Sun D, Yin H, Liu Z, Liu X (2012) Upconversion nanoparticles modified with aminosilanes as carriers of DNA vaccine for foot-and-mouth disease. Appl Microbiol Biotechnol 95(5):1253–1263
314. Zhang F, Braun GB, Pallaoro A, Zhang Y, Shi Y, Cui D, Moskovits M, Zhao D, Stucky GD (2012) Mesoporous multifunctional upconversion luminescent and magnetic "nanorattle" materials for targeted chemotherapy. Nano Lett 12(1):61–67
315. Xu Z, Li C, Pa M, Hou Z, Yang D, Kang X, Lin J (2011) Facile synthesis of an up-conversion luminescent and mesoporous Gd2O3: Er3+@nSiO2@mSiO2 nanocomposite as a drug carrier. Nanoscale 3(2):661–667
316. Li C, Yang D, Pa M, Chen Y, Wu Y, Hou Z, Dai Y, Zhao J, Sui C, Lin J (2013) Multifunctional Upconversion Mesoporous Silica Nanostructures for Dual Modal Imaging and In vivo Drug Delivery. Small. doi:10.1002/smll.201301093
317. Hou Z, Li C, Ma P, Li G, Cheng Z, Peng C, Yang D, Yang P, Lin J (2011) Electrospinning Preparation and Drug-Delivery Properties of an Up-conversion Luminescent Porous NaYF4:Yb3+, Er3+ @Silica Fiber Nanocomposite. Adv Funct Mater 21(12):2356–2365
318. Hou Z, Li X, Li C, Dai Y, Pa M, Zhang X, Kang X, Cheng Z, Lin J (2013) Electrospun Upconversion Composite Fibers as Dual Drugs Delivery System with Individual Release Properties. Langmuir 29(30):9473–9482
319. Kang X, Cheng Z, Li C, Yang D, Shang M, Pa M, Li G, Liu N, Lin J (2011) Core–Shell Structured Up-Conversion Luminescent and Mesoporous NaYF4:Yb3+/Er3+@nSiO2@mSiO2 Nanospheres as Carriers for Drug Delivery. J Phys Chem C 115(32):15801–15811
320. Dai YL, Ma PA, Cheng ZY, Kang XJ, Zhang X, Hou ZY, Li CX, Yang DM, Zhai XF, Lin J (2012) Up-Conversion Cell Imaging and pH-Induced Thermally Controlled Drug Release from NaYF4: Yb3+/Er3+@Hydrogel Core-Shell Hybrid Microspheres. ACS Nano 6(4):3327–3338
321. Hou ZY, Li CX, Ma PA, Cheng ZY, Li XJ, Zhang X, Dai YL, Yang DM, Lian HZ, Lin J (2012) Up-Conversion Luminescent and Porous NaYF4:Yb3+, Er3+@SiO2 Nanocomposite Fibers for Anti-Cancer Drug Delivery and Cell Imaging. Adv Funct Mater 22(13):2713–2722
322. Dai YL, Kang XJ, Yang DM, Li XJ, Zhang X, Li CX, Hou ZY, Cheng ZY, Ma PA, Lin J (2013) Platinum (IV) Pro-Drug Conjugated NaYF4:Yb3+/Er3+Nanoparticles for Targeted Drug Delivery and Up-Conversion Cell Imaging. Advanced Healthcare Materials 2(4):562–567
323. Liu J, Bu W, Zhang S, Chen F, Xing H, Pan L, Zhou L, Peng W, Shi J (2012) Controlled synthesis of uniform and monodisperse upconversion core/mesoporous silica shell nanocomposites for bi-modal imaging. Chem-Eur J 18(8):2335–2341
324. Pa M, Xiao H, Li X, Li C, Dai Y, Cheng Z, Jing X, Lin J (2013) Rational Design of Multifunctional Upconversion Nanocrystals/ Polymer Nanocomposites for Cisplatin (IV) Delivery and Biomedical Imaging. Adv Mater:n/a-n/a. doi:10.1002/adma.201301713
325. Kang XJ, Yang DM, Dai YL, Shang MM, Cheng ZY, Zhang X, Lian HZ, Ma PA, Lin J (2013) Poly(acrylic acid) modified lanthanide-doped GdVO4 hollow spheres for up-conversion cell imaging, MRI and pH-dependent drug release. Nanoscale 5(1):253–261
326. Dong L, An D, Gong M, Lu Y, Gao H-L, Xu Y-J, Yu S-H (2013) PEGylated Upconverting Luminescent Hollow Nanospheres for Drug Delivery and In vivo Imaging. Small. doi:10.1002/smll.201300433
327. Yang Y, Velmurugan B, Liu X, Xing B (2013) NIR Photoresponsive Crosslinked Upconverting Nanocarriers Toward Selective Intracellular Drug Release. Small. doi:10.1002/smll.201201765
328. Cheng Z, Chai R, Ma P, Dai Y, Kang X, Lian H, Hou Z, Li C, Lin J (2013) Multiwalled carbon nanotubes and NaYF4:Yb3+/Er3+ Nanoparticle-Doped Bilayer hydrogel for concurrent nir-triggered drug release and up-conversion luminescence tagging. Langmuir 29(30):9573–9580

329. Yang Y, Liu F, Liu X, Xing B (2013) NIR light controlled photorelease of siRNA and its targeted intracellular delivery based on upconversion nanoparticles. Nanoscale 5(1):231–238
330. Koo YE, Fan W, Hah H, Xu H, Orringer D, Ross B, Rehemtulla A, Philbert MA, Kopelman R (2007) Photonic explorers based on multifunctional nanoplatforms for biosensing and photodynamic therapy. Appl Opt 46(10):1924–1930
331. Lee YE, Kopelman R (2011) Polymeric nanoparticles for photodynamic therapy. Methods Mol Biol 726:151–178
332. Reddy GR, Bhojani MS, McConville P, Moody J, Moffat BA, Hall DE, Kim G, Koo YE, Woolliscroft MJ, Sugai JV, Johnson TD, Philbert MA, Kopelman R, Rehemtulla A, Ross BD (2006) Vascular targeted nanoparticles for imaging and treatment of brain tumors. Clin Cancer Res 12(22):6677–6686
333. Gupta A, Wang S, Pera P, Rao KV, Patel N, Ohulchanskyy TY, Missert J, Morgan J, Koo-Lee YE, Kopelman R, Pandey RK (2012) Multifunctional nanoplatforms for fluorescence imaging and photodynamic therapy developed by post-loading photosensitizer and fluorophore to polyacrylamide nanoparticles. Nanomedicine-UK 8(6):941–950
334. Wang S, Fan W, Kim G, Hah HJ, Lee YE, Kopelman R, Ethirajan M, Gupta A, Goswami LN, Pera P, Morgan J, Pandey RK (2011) Novel methods to incorporate photosensitizers into nanocarriers for cancer treatment by photodynamic therapy. Lasers Surg Med 43(7):686–695
335. Zhang P, Steelant W, Kumar M, Scholfield M (2007) Versatile Photosensitizers for Photodynamic Therapy at Infrared Excitation. J Am Chem Soc 129(15):4526–4527
336. Carling C-J, Nourmohammadian F, Boyer J-C, Branda NR (2010) Remote-Control Photorelease of Caged Compounds Using Near-Infrared Light and Upconverting Nanoparticles. Angew Chem Int Ed 49(22):3782–3785
337. Chen F, Zhang S, Bu W, Chen Y, Xiao Q, Liu J, Xing H, Zhou L, Peng W, Shi J (2012) A uniform sub-50 nm-sized magnetic/upconversion fluorescent bimodal imaging agent capable of generating singlet oxygen by using a 980 nm laser. Chem-Eur J 18(23):7082–7090
338. Wang FF, Yang XJ, Ma L, Huang BR, Na N, Ying CE, He DC, Ouyang J (2012) Multifunctional up-converting nanocomposites with multimodal imaging and photosensitization at near-infrared excitation. J Mater Chem 22(47):24597–24604
339. Zhao ZX, Han YN, Lin CH, Hu D, Wang F, Chen XL, Chen Z, Zheng NF (2012) Multifunctional Core-Shell Upconverting Nanoparticles for Imaging and Photodynamic Therapy of Liver Cancer Cells. Chem-Asian J 7(4):830–837
340. Tian G, Ren WL, Yan L, Jian S, Gu ZJ, Zhou LJ, Jin S, Yin WY, Li SJ, Zhao YL (2013) Red-Emitting upconverting nanoparticles for photodynamic therapy in cancer cells under near-infrared excitation. Small 9(11):1929–1938
341. Il Park Y, Kim HM, Kim JH, Moon KC, Yoo B, Lee KT, Yoon SY, Suh YD, Lee SH, Hyeon T (2012) Luminescence/magnetic resonance imaging and photodynamic therapy based on upconverting nanoparticles. In: Choi SH, Choy JH, Lee U, Varadan VK (eds) Nanosystems in Engineering and Medicine, vol 8548. Proceedings of SPIE. Spie-Int Soc Optical Engineering, Bellingham. doi:10.1117/12.999411
342. Lim ME, Lee YL, Zhang Y, Chu JJ (2012) Photodynamic inactivation of viruses using upconversion nanoparticles. Biomaterials 33(6):1912–1920
343. Chatterjee DK, Yong Z (2008) Upconverting nanoparticles as nanotransducers for photodynamic therapy in cancer cells. Nanomedicine-UK 3(1):73–82
344. Guo H, Qian H, Idris NM, Zhang Y (2010) Singlet oxygen-induced apoptosis of cancer cells using upconversion fluorescent nanoparticles as a carrier of photosensitizer. Nanomedicine-UK 6(3):486–495
345. Idris NM, Gnanasammandhan MK, Zhang J, Ho PC, Mahendran R, Zhang Y (2012) In vivo photodynamic therapy using upconversion nanoparticles as remote-controlled nanotransducers. Nat Med 18(10):1580–1585
346. Ungun B, Prud'homme RK, Budijon SJ, Shan J, Lim SF, Ju Y, Austin R (2009) Nanofabricated upconversion nanoparticles for photodynamic therapy. Opt Express 17(1):80–86
347. Hah HJ, Kim G, Lee YE, Orringer DA, Sagher O, Philbert MA, Kopelman R (2011) Methylene blue-conjugated hydrogel nanoparticles and tumor-cell targeted photodynamic therapy. Macromol Biosci 11(1):90–99
348. Qin M, Hah HJ, Kim G, Nie G, Lee YE, Kopelman R (2011) Methylene blue covalently loaded polyacrylamide nanoparticles for enhanced tumor-targeted photodynamic therapy. Photochem Photobiol Sci 10(5):832–841
349. Tang W, Xu H, Kopelman R, Philbert MA (2005) Photodynamic characterization and in vitro application of methylene blue-containing nanoparticle platforms. Photochem Photobiol 81(2):242–249
350. Tang W, Xu H, Park EJ, Philbert MA, Kopelman R (2008) Encapsulation of methylene blue in polyacrylamide nanoparticle platforms protects its photodynamic effectiveness. Biochem Biophys Res Commun 369(2):579–583
351. Wang C, Cheng L, Liu Y, Wang X, Ma X, Deng Z, Li Y, Liu Z (2013) Imaging-Guided pH-Sensitive Photodynamic Therapy Using Charge Reversible Upconversion Nanoparticles under Near-Infrared Light. Adv Funct Mater 23(24):3077–3086
352. Yan B, Boyer JC, Habault D, Branda NR, Zhao Y (2012) Near infrared light triggered release of biomacromolecules from hydrogels loaded with upconversion nanoparticles. J Am Chem Soc 134(40):16558–16561
353. Huang X, El-Sayed IH, Qian W, El-Sayed MA (2006) Cancer Cell Imaging and Photothermal Therapy in the Near-Infrared Region by Using Gold Nanorods. J Am Chem Soc 128(6):2115–2120
354. Cheng L, Yang K, Li Y, Zeng X, Shao M, Lee ST, Liu Z (2012) Multifunctional nanoparticles for upconversion luminescence/MR multimodal imaging and magnetically targeted photothermal therapy. Biomaterials 33(7):2215–2222
355. Shan GB, Weissleder R, Hilderbrand SA (2013) Upconverting Organic Dye Doped Core-Shell Nano-Composites for Dual-Modality NIR Imaging and Photo-Thermal Therapy. Theranostics 3(4):267–274
356. Xing HY, Zheng XP, Ren QG, Bu WB, Ge WQ, Xiao QF, Zhang SJ, Wei CY, Qu HY, Wang Z, Hua YQ, Zhou LP, Peng WJ, Zhao KL, Shi JL (2013) Computed tomography imaging-guided radiotherapy by targeting upconversion nanocubes with significant imaging and radiosensitization enhancements. Scientific Reports 3:1751
357. Hilderbrand SA, Shao F, Salthouse C, Mahmood U, Weissleder R (2009) Upconverting luminescent nanomaterials: application to in vivo bioimaging. Chem Commun 28:4188–4190
358. Xiong L, Yang T, Yang Y, Xu C, Li F (2010) Long-term in vivo biodistribution imaging and toxicity of polyacrylic acid-coated upconversion nanophosphors. Biomaterials 31(27):7078–7085
359. Bae YM, Park YI, Nam SH, Kim JH, Lee K, Kim HM, Yoo B, Choi JS, Lee KT, Hyeon T, Suh YD (2012) Endocytosis, intracellular transport, and exocytosis of lanthanide-doped upconverting nanoparticles in single living cells. Biomaterials 33(35):9080–9086
360. Zhou JC, Yang ZL, Dong W, Tang RJ, Sun LD, Yan CH (2011) Bioimaging and toxicity assessments of near-infrared upconversion luminescent NaYF4:Yb, Tm nanocrystals. Biomaterials 32(34):9059–9067
361. Wang K, Ma JB, He M, Gao G, Xu H, Sang J, Wang YX, Zhao BQ, Cui DX (2013) Toxicity Assessments of Near-infrared Upconversion Luminescent LaF3:Yb, Er in Early Development of Zebrafish Embryos. Theranostics 3(4):258–266
362. Ostrowski AD, Chan EM, Gargas DJ, Katz EM, Han G, Schuck PJ, Milliron DJ, Cohen BE (2012) Controlled synthesis and single-particle imaging of bright, Sub-10 nm Lanthanide-Doped upconverting nanocrystals. ACS Nano 6(3):2686–2692